A THEORETICAL STUDY OF PHOTON FIELDS NEAR SURFACES WITH APPLICATION TO PHOTOEMISSION

A Thesis
Submitted to the University of North Bengal
For the
Degree of Doctor of Philosophy in Science

Ram Kumar Thapa
Department of Physics
North Bengal University
Darjeeling Pin - 734430
West Bengal INDIA
November 1993

ACKNOWLEDGEMENTS

The author would first of all like to thank his research supervisor Dr. Nikhiles Kar, Department of Physics, North Bengal University, Darjeeling (India) for his patient guidance, tolerance and constant encouragement throughout the works related to this thesis. He also takes this opportunity to thank the faculty members of the Department of Physics, North Bengal University, Darjeeling for being always kind and hospitable. He acknowledges also the help of Miss Pranati Das, Research Scholar, Department of Physics, North Bengal University in setting up the part of the computer programs.

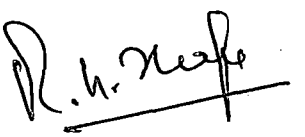

(Ram Kumar Thapa)

Dated: 23-11-1993

Department of Physics

North Bengal University

To my

Wife Kamala, Son and Daughter

CONTENTS

LIST OF FIGURES

CHAPTER I

INTRODUCTION

Photoemission spectroscopy is now widely used as an investigative method for the electronic states of the surface and the bulk of a solid. The high absorption coefficient of ultraviolet radiation and the small escape depth of the electrons photoemitted from solid gives the ultraviolet photoemission spectroscopy a big advantage over the other methods of investigating the electronic states on the surface of solids. Angle resolved ultraviolet photoemission spectroscopy (ARUPS) allows the determination of the energy and the momentum of the photoemitted electrons and can be used to reveal the electronic structure of the surface and the bulk of the crystal. In the ultraviolet (UV) photoemission experiments, ultraviolet radiation in the range of 10 to about 300 eV excites electrons of which those within the escape depth, which may be a few to about a hundred layers, can get out of the solid. The small value of the escape depth in the region of 10 - 100 eV makes photoemission an useful technique for surface studies. In addition, variation of the photon energy leads to a variation in escape depth whereby the relative importance of the surface and the bulk features can be varied.

To measure the energy distribution of the photoemitted electrons, two kinds of the energy analyzer are usually used. In one method, electrons emitted in all angles are collected in a hemispherical analyser. This is known as angle-integrated ultraviolet photoemission spectroscopy. The other one can analyse the energy of the electrons emitted at a prescribed angle giving the angle resolved energy distribution curves (AREDC). Knowing the kinetic energy and the direction of the photoemitted electrons, one can determine the momentum of the electrons creating the maximum on the ARDEC and establish the energy-momentum dependence corresponding to the band creating this maximum. Measuring the shift in energy positions of the maxima on the AREDC's with the change of momentum obtained by varying the angle of the analyser or the energy $\hbar\omega$ of the UV radiation, the energy-wave vector relationship can be determined. Knowing the kinetic energy of the electron one can determine the absolute value of the momentum K of the electron in vacuum from the relation $E=\hbar^2K^2/2m$. In Fig. (1.1), the method of ARUPS is illustrated. The incoming UV radiation is incident on the sample at an angle of 45^o with respect to the normal. The angle θ of the electron analyser can be varied between 0 and 90^o. The azimuthal angle can be set to any desired value. One can determine the energy and angular distributions of the photoemitted electrons as a function of

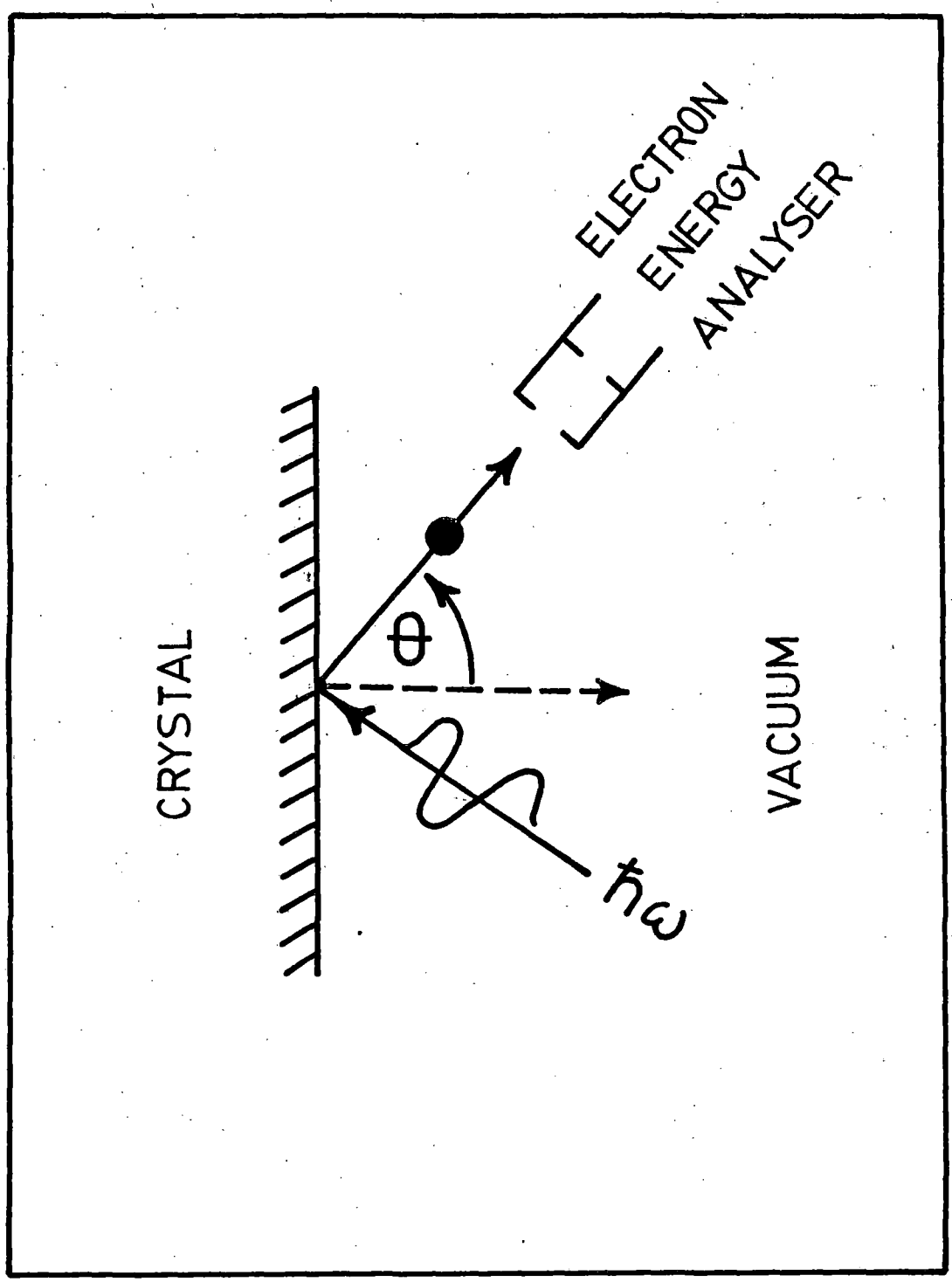

Figure 1.1

the energy, polarization and angle of incidence of the applied radiation. The theoretical explanation of such data clearly requires a detailed knowledge of both the electronic structure of the photoemitting substance and its interaction with the radiation.

There had been a great deal of interest in photoemission as a probe of bonding of atoms which lie in the outermost layers of a solid. But the detailed interpretation of the photoemission (PE) data requires the use of a theory of PE which should in its simplest form be able to calculate the initial and final state electron wavefunctions as well as the spatial form of the vector potential which is involved in the photoemission matrix element. Considerable progress have been made in the past for calculating the self-consistent wavefunctions corresponding to electron states below the vacuum level for semi-infinite solids[1,2]. Reliable techniques have been developed for the calculation of electron wavefunctions at energies 30 - 300 eV above the vacuum level. But the same cannot be said for calculation of the electromagnetic fields which excites photoelectrons especially from the surface of the solid where the electrons have a very short mean free path. For consistency one should include the variation of the electromagnetic field in the presence of the surface. The calculation of the vector potential is an extremely difficult

problem in the general case. In most of the calculations therefore, one proceeds with the assumptions of spatially constant vector potential for computational simplicity. However in certain situations one has to include the photon field variation to get even qualitative agreement with the experimental value.

A simple calculation of photocurrent involves the evaluation of the matrix element $\langle\psi_f|H'|\psi_i\rangle$ where ψ_i and ψ_f are the initial and final one electron states whose energies are connected by $E_f=E_i-\hbar\omega$. The perturbation in the hamiltonian responsible for the photo excitation of the electron is given by

$$H' = \frac{e}{2mc}\,(\vec{p}.\vec{A}+\vec{A}.\vec{p}) \qquad (1.1)$$

where $\vec{p}$ is the one electron momentum operator and $\vec{A}$ is the vector potential. In the standard photoemission calculation, the one electron states are calculated with a high degree of accuracy but the variation of the photon field is generally neglected. In the case where one looks at the photoemission current as a function of the photon energy with the constant initial state, the photon field variation in the surface region needs to be considered more carefully. A first principle calculation of the electromagnetic field in the presence of the surface is an extremely complex problem. The calculation of the vector potential in the surface region therefore needs a

detailed microscopic analysis of the surface in terms of the dielectric response function. This is because the usual theory of refraction breaks down at a microscopic level which therefore calls for the consideration of the factors like surface discontinuity, non-locality etc.

The photocurrent arising from the interaction of the electromagnetic field with the solid has been derived by a number of authors[3-6]. The current density may be written with the help of golden rule expression[7] as

$$\frac{dj(E)}{d\Omega} = \frac{2\pi}{\hbar} \sum_f |\langle \psi_f | H' | \psi_i \rangle|^2 \delta(E-E_f)\delta(E_f-E_i-\hbar\omega) f_o(E-\hbar\omega)[1-f_o(E)] \qquad (1.2)$$

In Eq. (1.2), $E_i(E_f)$ is the initial (final) state energy and f_o is the Fermi occupation function. δ - function describes the energy conservation. Thus we see that the calculation of the photocurrent density is based on the evaluation of the matrix element $\langle \psi_f | H' | \psi_i \rangle$.

Several authors have done the photocurrent calculations by using various approaches. For example, Endriz[8] has used the modified form of the Mitchell-Makinson time dependent perturbation calculation of the surface photoeffect. He calculated the photocurrent by using the hydrodynamic approximation and applied it to the case of aluminium and other

alkali metals where the results for photon energy at plasmon energy($\hbar\omega_p$) agreed with the experimental data. However the model of Endriz did not reproduce the experimental data of Petersen and Hagstrom[9] which showed a maximum at 12 eV in photoemission cross-section. Schaich and Ashcroft[4] had also developed a model theory of photoemission on the basis of quadratic response and independent particle formalism but had not assumed any detailed model of the dielectric response function for the surface. They used a computationally simple model to study the electronic structure in solids and surfaces to understand photoemission.. To incorporate band structure effects, the model of Kronig-Penney was used. In this model spatial dependence of the vector potential was neglected and throughout the calculation it was assumed to be a constant. The approach of Mahan[3] was to extend the wave mechanical scattering theory originally proposed by Adawi[10] which regards the emitted electron wavefunction as equivalent to the time reversed form of an incident electron along with the scattered part.

The evaluation of the matrix element $\langle\psi_f|\vec{A}.\vec{p}+\vec{p}.\vec{A}|\psi_i\rangle$ involves the knowledge of ψ_i and ψ_f. Leibsch[11], Pendry[12] and others have recognised that the calculation of ψ_i and ψ_f was similar in principle to Low Energy Electron Diffraction calculation. Their approach was to consider the solid to be a

stack of identical layers terminated at the surface. The final state, which had an electron going into the detector, was shown to be a time-reversed LEED state. The initial state can also be constructed similarly. Pendry[12], for example, has given a detailed method of calculation using these ideas and has also developed a detailed program for application to real system with notable success. In his calculations, the initial and final states are computed quite accurately but the vector potential is taken to be a constant. Although Pendry recognised the fact that the vector potential would vary in the surface region, to take exact account of that was too complex a problem. Also taking $\vec{A}$ to be constant simplified the calculation of the matrix element by using certain commutation relations and choosing a convenient gauge for $\vec{A}$. This method of calculation has been quite successful in different cases. However for the case of photocurrent against photon energy from a constant initial state, this method does not give the right behaviour, especially near the plasmon energy.

Feibelman[13] thought that if the theory of surface electromagnetic field is to be used to interpret the results of the photoemission experiments that probe the outer few layers of a solid, one should use a scheme of calculations to get the correct responses of the external field even in the presence of the surface. This was the motivation which led

Feibelman to envisage the concept of Random Phase Approximation (RPA) dielectric tensor to study the plasmon dispersion and the microscopic refraction problem. In RPA calculation, the surface is smooth and the dielectric response naturally includes the effect of the electron spill-out in the region of the dipolar layer. The only inputs are the electron radius (r_s) and the single-electron surface potential barrier. The potential barrier completely determines the electronic structure of the surface. This can be taken to be output of a self-consistent jellium ground state calculation. But it can also be varied at will to test the similarity of the aspects of the surface responses to various features of the ground state. The RPA is exact for the bulk high density electron gas ($r_s \to 0$) where it is assumed that the single-electron wavefunction and the energies are based on a Hartee-Fock type calculation. None of these conditions apply to the RPA description of the surface dielectric response. Here the electron gas is not infinite, therefore RPA is not only not exact but it is also not clear how one might write down the first correction to it. The importance of RPA model lies in the fact that it incorporates many electron features that are expected to be important. The RPA dielectric function ε is non-local and interpolates smoothly from 1 in the vacuum to ε_B in the bulk. It includes the single-electron excitation spectrum and it gives rise to

bulk and surface plasma oscillations and satisfies the requirement of charge conservation. Also the prediction of RPA agree remarkably well with photoemission experiments that tests the nature of the electromagnetic field in the case of free-electron metal surfaces. Feibelman assumed that spatial variation parallel to the surface is negligible compared to those perpendicular to the surface. He evaluated A_z within the RPA using $r_s=2$ and incorporated this to the calculation of photoexcitation matrix element using the Lang-Kohn potential for the initial and final state. It was found that his calculated data of jellium was in good agreement with the measured data of Levinson et al[14]. However the calculations of Feibelman which has the most accurate description of the field variation could be applied only to metals which may be represented by jellium model. Mukhopadhayay and Lundqvist[15] and Bagchi[16] have also developed similar methods for calculating the electromagnetic fields near the surfaces.

The semi-classical infinite barrier (SCIB) model of Kliewer[17] considers a sharp surface but it does take into consideration the particle-hole and plasmon excitation. The SCIB model apparently violates the nature of the surface from its very assumption as the infinite barrier is not an accurate approximation to the potential existing at the surface. In this model the electron cannot tunnel out of the solid; therefore,

SCIB power absorptance is assumed to represent the photocurrent emitted. For example, the photocurrent is larger above the plasmon energy $\hbar\omega_p$ and below it is completely in disagreement with the experimental data of Levinson et al[14].

The hydrodynamical model of Forstman and Stenschke[18] takes into account the electron-hole spectrum and the dielectric function used is a very simple one from which one can very easily evaluate the photon field $\vec{A}$. Kempa and Forstman[19] have performed the detailed calculations of the electromagnetic field using the hydrodynamical model and had incorporated the field to calculations of the photoyield. This was applied to the case of aluminium and was found that the frequency dependence of the surface photoemission yield is due to the behaviour of the electric field and does not depend very much on the initial and final state wavefunction. Photoyield results obtained by them showed similar experimental behavior as found by Levinson et al[14]. Barberan and Inglesfield[20] have also done a detailed calculations on photoemission using the hydrodynamical screening of the photon field. They had shown that both the uniform vector potential and the Fresnel field are inadequate description of the screened electromagnetic field inside the metal to explain the photoemission results. They found that below ω_z, A_z rises rapidly near the surface due to polarization charge but at ω_p, the rise becomes less rapid

and above ω_p there are plasma oscillations. But A_z is almost zero inside the metal at ω_p. This follows as a result of matching the normal component of P which is zero at $\hbar\omega=\hbar\omega_p$ and hence $P_z=0$. It means that E_z is zero inside the metal. This results of Barberan and Inglesfield[20] for the case of aluminium is in good agreement with the microscopic calculation of Feibelman[13] apart from the oscillations in A_z below ω_p. This had been attributed to the excitations in A_z below ω_p which has arisen due to Friedel type of oscillations from the electron-hole excitations which were not included in the hydrodynamic calculation. Maniv and Metiv[6] have achieved also a considerable progress in the calculation of the electromagnetic field in the metal-vacuum interfacial region. They primarily considered the near fields in the immediate vicinity of the interface. They developed a scheme for a more general solution of the Feibelman's model[13] and were thus able to determine a dielectric response function which in contrast to more conventional models is continuous across the interfacial region. The plot of the photoyield versus the photon energy did not show the behavior as obtained by Feibelman[13] and Levinson et al[14] in the case of aluminium. They found that the model was true for photon energy larger than plasmon energy and was applicable to only free electron type of solids.

We find therefore that no such calculations have been done

in photoemisssion which considered simultaneously the photon field variation as well as the LEED type states in the matrix. Also not much attention have been paid to the calculation of the fields in the surface region for transition metals and semiconductor. In this thesis we shall at first calculate the spatial variation of the photon field and apply it to the case of a number of elements. The dielectric model of Bagchi and Kar[21] will be used to calculate the photon field. The field calculation will also include the solids like aluminium, silver, rhodium, molybdenum, palladium and semiconductor silicon. The field variations so calculated will be incorporated to the matrix element $\langle\psi_f|\vec{A}.\vec{p}+\vec{p}.\vec{A}|\psi_i\rangle$ in Eq. (1.1) for calculating photoemission cross-sections. We first used free electron type wavefunctions for the initial and final states and applied this model to aluminium with the appropriate parameters. The calculated photocurrent in aluminium showed a qualitative features in agreement with the experimental data of Levinson et al[14]. To incorporate band structure effects, we used a simple model given first by Kronig and Penney. With the initial state calculated with this model we used the field derived from the experimentally determined dielectric functions of a number of materials and analysed our results.

The material in this thesis is arranged as follows. In

chapter II, we shall discuss the model theory of dielectric response function used for the calculations of the electromagnetic field (vector potential) for the vacuum, surface and bulk region of the solids. In chapter III, photoemission calculations using the free electron model of the solid will be discussed. This will be applied to the case of aluminium as it is a weakly s-p bonded metal where free electron theory is applicable. In chapter IV, we shall discuss the general formulation of the initial state wavefunction ψ_i by using the Kronig-Penney model and discuss a number of applications.

CHAPTER II

CALCULATION OF ELECTROMAGNETIC FIELDS

(A) Dielectric model and Electromagnetic Field:

In this chapter, we shall discuss the calculation of the electromagnetic field in a solid when electromagnetic radiation is incident on it. This is an extremely complex problem and ab initio calculations have been done only for jellium in the presence of a surface. However, these calculations have not been extended to other metals where the jellium model is not applicable. Consequently, if one wants to consider the field variation in the presence of the surface for metals e.g., transition metals like tungsten, molybdenum, palladium, chromium etc, one has to consider simpler models. Such a model used by Bagchi, Barrera and Kar[21,22] for tungsten has been adopted for the calculation of the electromagnetic field in the surface region. Although this model involving a linear interpolation in the surface region between the experimentally determined bulk dielectric function and the vacuum value, has some shortcomings, perhaps the most important being that it is a local response function, it has the virtue of being tractable and as evidenced by the application to tungsten[21] and aluminium[23,24], it also gives reasonably good

results. Since the input required for this model is experimentally obtained[25] bulk dielectric value, the field calculation can also be extended to the case of semiconductors. In the following, we briefly describe the model and the calculation of the electromagnetic fields from it. We shall then discuss the application of this model to a number of cases.

The dielectric model used is the one given by Bagchi and Kar[21] which is shown in Fig. (2.1). The metal is assumed to occupy the space to the left of $z=0$ plane which is the nominal surface plane. In the region $-a/2 \leq z \leq a/2$, the dielectric constant is chosen to be a local function which interpolates linearly between the bulk value inside the metal and the vacuum value (unity) outside. The model frequency dependent dielectric function is:

$$\varepsilon(\omega,z) = \begin{cases} \varepsilon(\omega) = \varepsilon_1(\omega) + i\varepsilon_2(\omega), & z \leq -a/2 \\ \frac{1}{2}\left[1 + \varepsilon(\omega)\right] + \left[1 - \varepsilon(\omega)\right]\frac{z}{a}, & -a/2 \leq z \leq a/2 \\ 1, & z \geq a/2 \end{cases} \qquad (2.1)$$

The incident radiation was taken to be p - polarised of frequency ω. It was incident on the surface defined by x-y plane at an angle of incidence θ_i. A gauge was chosen in which the scalar potential is set equal to zero and the

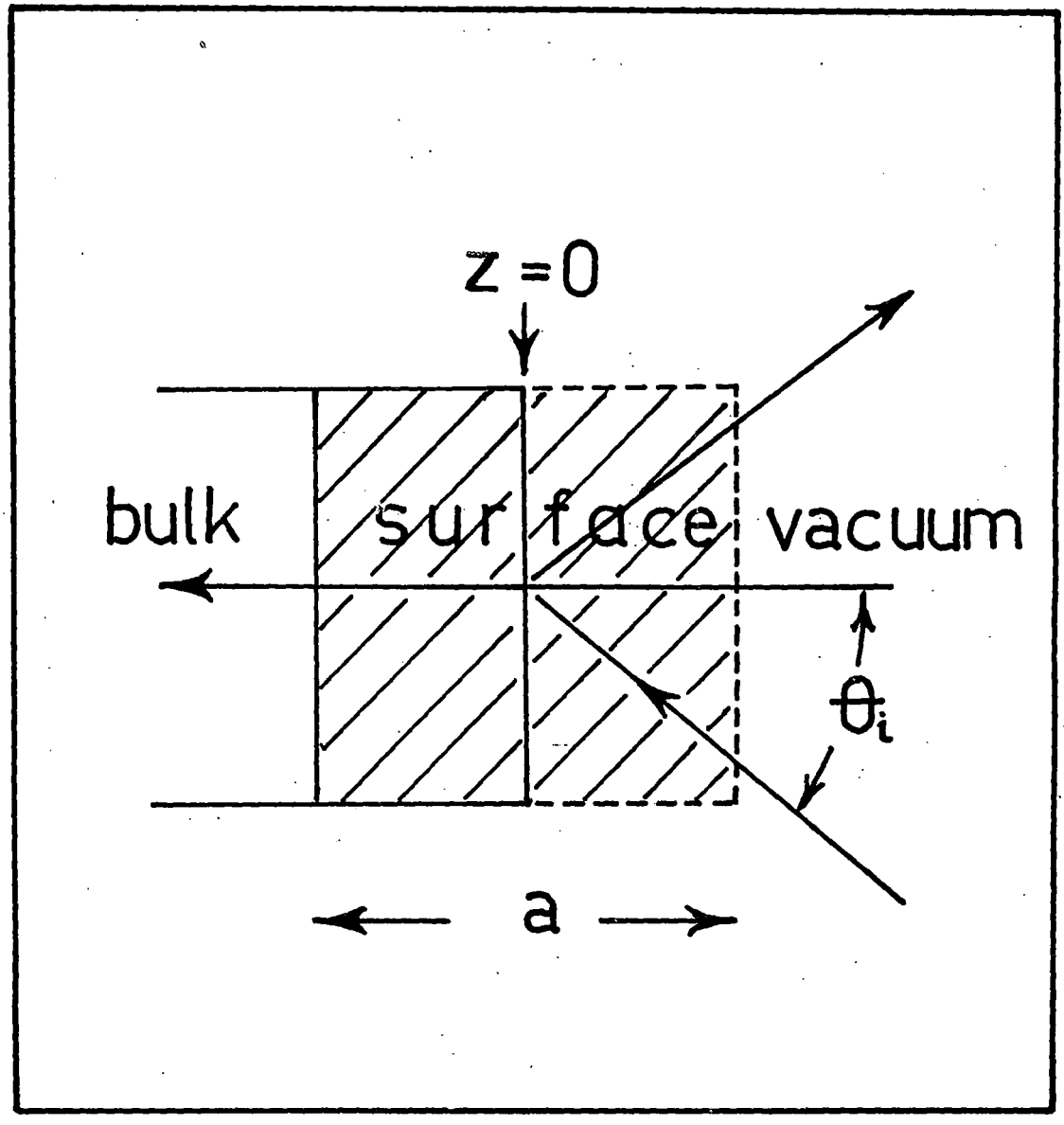

Figure 2.1

electromagnetic field $\vec{E}(\vec{Q},\omega;z)$ is expressed in terms of vector potential $\vec{A}(\vec{Q},\omega,z)$ as

$$\vec{E}(\vec{Q},\omega;z) = \frac{i\omega}{c}\vec{A}(\vec{Q},\omega;z)$$

where $Q = (\omega/c)\sin\theta_i$. The magnetic field $B(z)=B(\vec{Q},\omega;z)$ points in the y- direction and it obeys the following equation:

$$\frac{d}{dz}\left(\frac{1}{\varepsilon}\frac{dB}{dz}\right) + \left(\frac{\omega^2}{c^2} - \frac{Q^2}{\varepsilon}\right) B = 0 \qquad (2.2)$$

where $\varepsilon = \varepsilon(\omega;z)$. The electric field components can be obtained from the magnetic field as

$$E^x(\vec{Q},\omega;z) = \frac{c}{i\omega\varepsilon}\frac{dB}{dz}$$

$$E^z(\vec{Q},\omega;z) = -\frac{\sin\theta_i}{\varepsilon} B \qquad (2.3)$$

To solve Eq. (2.2), a new variable $u(z)$ was introduced according to prescription of Landau and Lifshitz which is given by $B(z) = u(z)\sqrt{\varepsilon}$. $u(z)$ then satisfies the equation

$$\frac{d^2u}{dz^2} + \frac{\omega^2}{c^2}(\varepsilon - \sin^2\theta_i)u + \left[\frac{1}{2\varepsilon}\frac{d^2\varepsilon}{dz^2} - \frac{3}{4}\frac{1}{\varepsilon^2}\left(\frac{d\varepsilon}{dz}\right)^2\right]u = 0 \qquad (2.4)$$

For the dielectric model used, $d\varepsilon/dz$ is finite only in the

region $-a/2 \leq z \leq a/2$ and $d^2\varepsilon/dz^2$ vanishes everywhere except for singularities at $z=\pm a/2$. Matching the fields at the boundary points, the magnetic and electric fields were obtained. The normal component of the electric field in the long wavelength limit as deduced by Bagchi and Kar[21] is:

$$\tilde{A}_{\omega}(z) = \frac{E^{z}_{\omega}(z)}{E_{o}} =$$

$$\begin{cases} -\dfrac{\sin 2\theta_i}{[\varepsilon(\omega) - \sin^2\theta_i]^{1/2} + \varepsilon(\omega)\cos\theta_i}, & z \leq -a/2 \\[2ex] -\dfrac{\sin 2\theta_i}{\frac{z}{a} + \frac{1}{2}\left[\frac{1+\varepsilon(\omega)}{1+\varepsilon(\omega)}\right]} \cdot \dfrac{\varepsilon(\omega)/[1-\varepsilon(\omega)]}{[\varepsilon(\omega) - \sin^2\theta_i]^{1/2} + \varepsilon(\omega)\cos\theta_i}, & -a/2 \leq z \leq a/2 \\[2ex] -\dfrac{\varepsilon(\omega)\sin 2\theta_i}{[\varepsilon(\omega) - \sin^2\theta_i]^{1/2} + \varepsilon(\omega)\cos\theta_i}, & z \geq a/2 \end{cases}$$

(2.5)

The electromagnetic fields had been calculated for photon energy below and above the plasmon energy of the metals. We take the plasmon energy to be the energy at which the real part of the dielectric constant of the solids i.e., $\varepsilon_1 \rightarrow 0$. In calculating the electromagnetic field, the value of the dielectric constant $\varepsilon(\omega)$ is unity for vacuum region. For the

bulk and the surface region, we have used the experimental data for $\varepsilon(\omega)$ as given by Weaver[25] and have calculated the frequency dependence of the magnitude of $\tilde{A}_\omega(z)$ and $|\tilde{A}_\omega(z)|^2$ for a number of cases. $|\tilde{A}_\omega(z)|^2$ was calculated as the photoemission cross-section is a quadratic function of $\tilde{A}_\omega(z)$. The solids whose dielectric functions were used are the free electron metal (aluminium), noble metal (silver) and transition metals like rhodium, molybdenum and palladium as well as silicon. $|\tilde{A}_\omega(z)|^2$ has been plotted against photon energy ($\hbar\omega$) for different planes in the surface region,i.e., for a number of values of z/a. Real and imaginary parts of $\tilde{A}_\omega(z)$ have been plotted for aluminium against z for different values of photon energy. The thickness of the surface is a parameter in our calculation. However it has been found by Appelbaum[26] that for most metals, a $\sim$ 15 Å with respect to the last plane of the atoms beyond which the electronic properties are independent of the presence of the surface and we have taken the value of a $\sim$ 10 Å.

(B) Evaluation of the electromagnetic fields:

In this section, we shall present the electromagnetic fields calculated by using the formula in Eq. (2.5) for aluminium, silver, rhodium, molybdenum, palladium and silicon. We have plotted $|\tilde{A}_\omega(z)|$ as a function of photon energy ($\hbar\omega$) and the distance (z) from the surface of the solids.

(i) Aluminium:

Fig. (2.2) shows the plot of $|\tilde{A}_\omega(z)|^2$ against the photon energy for various positions of the surface planes located at z/a=0.5 (vacuum), 0.0 (surface) and -0.5 (bulk). Here 'a' is the thickness of the surface. For regions at the surface and the bulk of the solids, we find that the graph peaks at around 11 eV and again shows a minimum at 15 eV (the plasmon energy of aluminium is taken as 15.75 eV). Also the experimental photocurrent data of Levinson et al[14] showed a peak at 11 eV and a minimum at 16 eV for the surface region of aluminium. For regions in the vacuum side, we find that in the case of aluminium, the graph shows a small peak at photon energy larger than the plasmon energy. The detailed photoemission cross-section calculation in the case of aluminium will be discussed in chapter III.

Figures (2.3) and (2.4) shows the plot of the field against distance from the surface of aluminium calculated by Thapa[27] using the dielectric function as given by jellium model:

$$\varepsilon(\omega) = 1 - \frac{\omega_p^2}{\omega^2}$$

where ω_p is the plasmon frequency of the solid. In Fig. (2.3) we show the plot of $Re\tilde{A}_\omega(z)$ and $Im\tilde{A}_\omega(z)$ for $\hbar\omega$=7.87 eV and

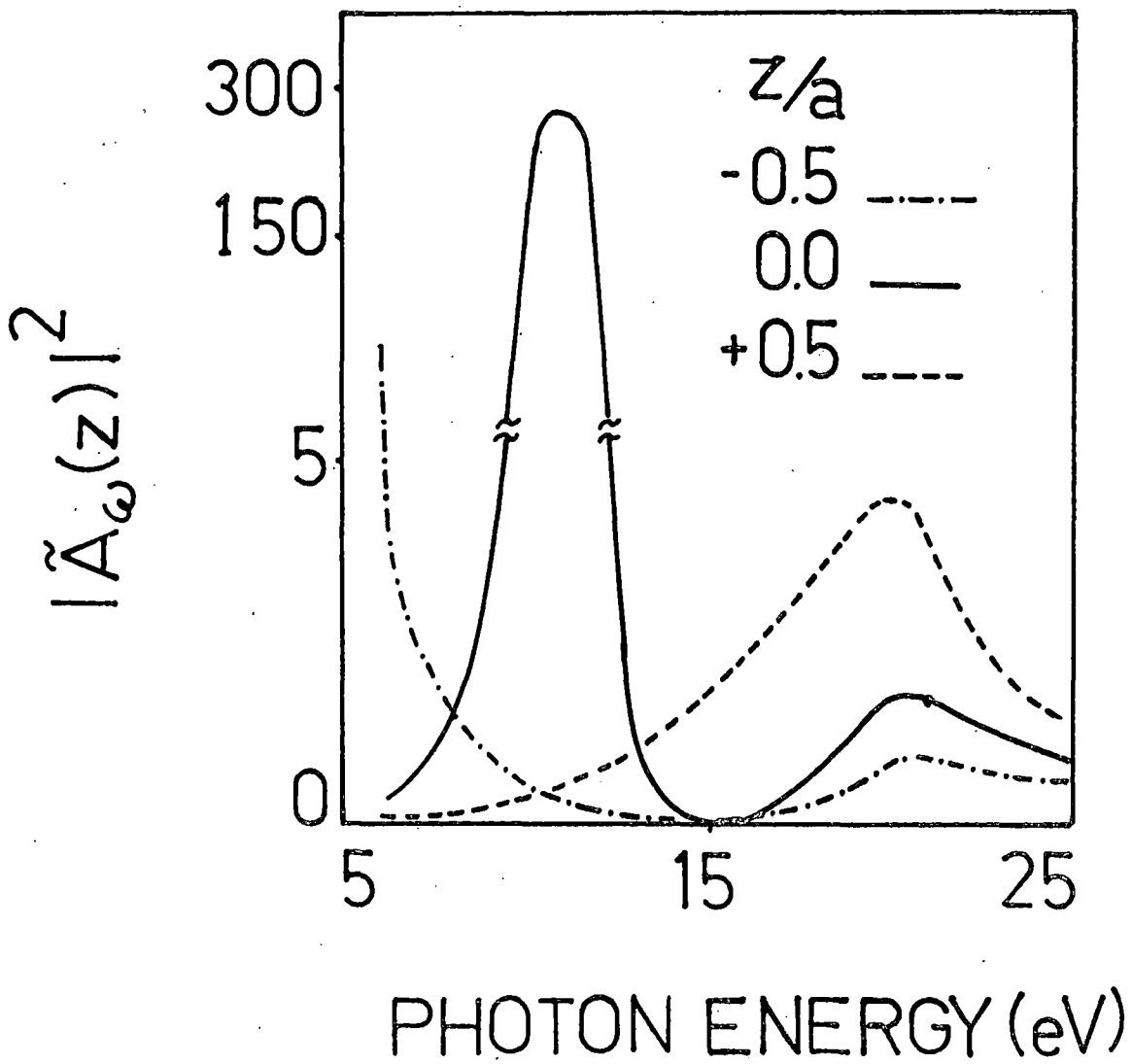

Figure 2.2

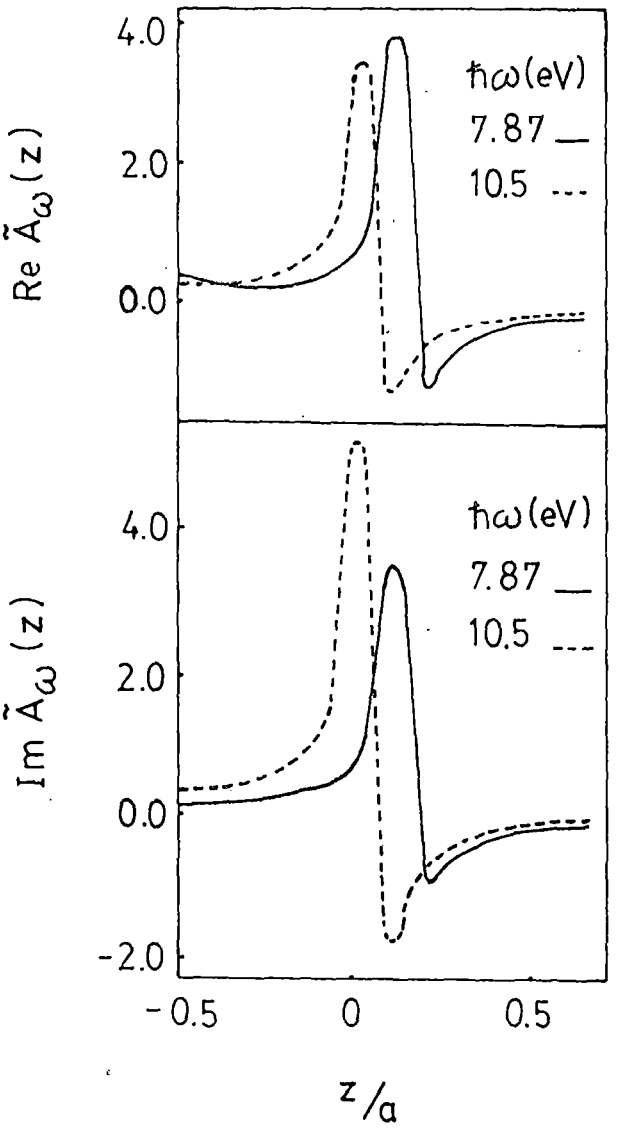
4.0
2.0
0.0
Re $\tilde{A}_\omega(z)$
$\hbar\omega$(eV)
7.87
10.5
4.0
2.0
0.0
-2.0
Im $\tilde{A}_\omega(z)$
$\hbar\omega$(eV)
7.87
10.5
-0.5
0
0.5
z/a

Figure 2.3

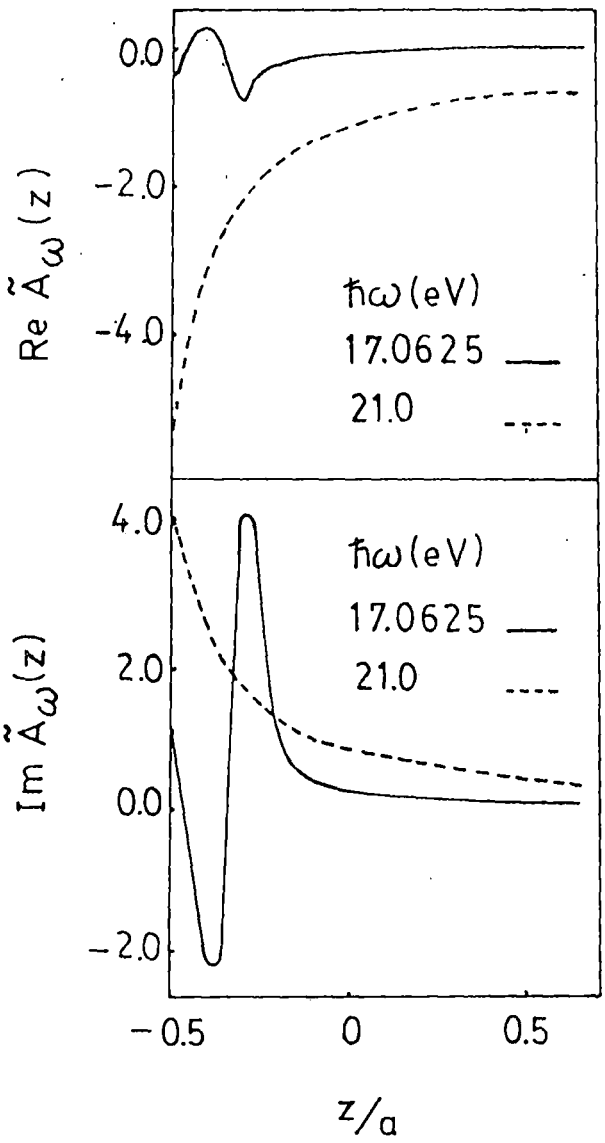
0.0
-2.0
-4.0
Re $\tilde{A}_\omega(z)$
$\hbar\omega$(eV)
17.0625
21.0
4.0
2.0
0.0
-2.0
Im $\tilde{A}_\omega(z)$
$\hbar\omega$(eV)
17.0625
21.0
-0.5
0
0.5
z/a

Figure 2.4

10.5 eV. Similarly in Fig. (2.4), the plot of $Re\tilde{A}_\omega(z)$ and $Im\tilde{A}_\omega(z)$ for photon energies at 17.065 eV and 21 eV is shown.

The behaviour of $|\tilde{A}_\omega(z)|$ as calculated by using the model of Bagchi and Kar[21] has same qualitative features like the experimental results of Levinson et al[14] but there are some differences with the data of Feibelman[13]. For example, at photon energy $\hbar\omega$ = 17.0625 eV, $Re\tilde{A}_\omega(z)$ and $Im\tilde{A}_\omega(z)$ fluctuates in the surface region in the vacuum side but decays exponentially towards the bulk region[27]. Below the plasmon energy, the real and imaginary parts of $\tilde{A}_\omega(z)$ peaks around the surface region but towards the bulk decreases exponentially. The fact that the peak is localised at the surface means that photoemission is a surface related phenomena. Moreover the magnitude of the peak height in $Im\tilde{A}_\omega(z)$ is more than that of $Re\tilde{A}_\omega(z)$ which implies that the surface phenomena is associated with the power absorption. This appears to be in agreement with the data of Feibelman[13] with the only difference that Friedel type oscillations is not exhibited towards the bulk region. This may be attributed to the locality assumption of the dielectric function in the model of Bagchi and Kar[21].

(ii) Silver:

In Fig. (2.5), we show the plot of variation of $|\tilde{A}_\omega(z)|^2$ against the photon energy for the values of z= -a/2, 0.0, and

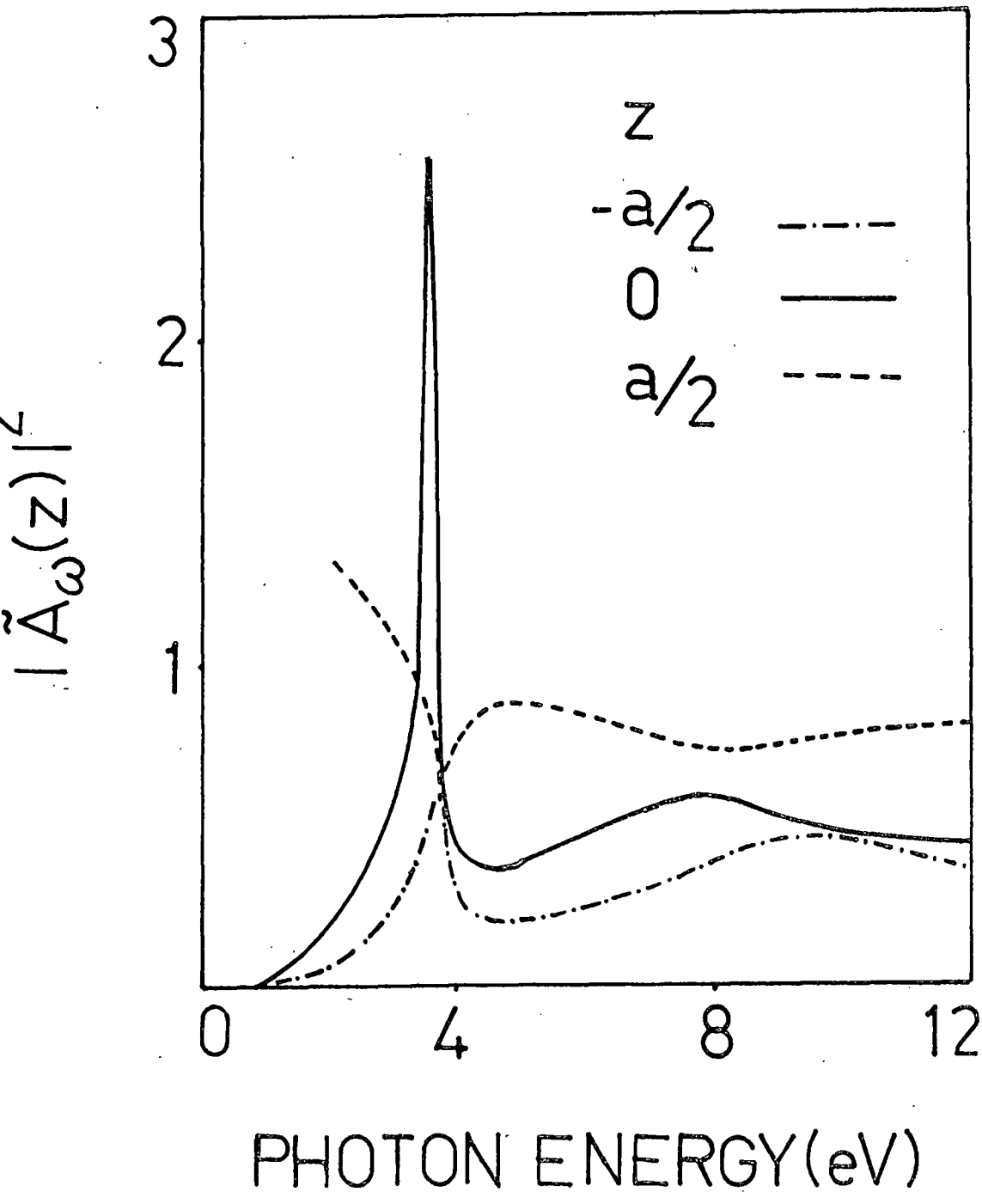

Figure 2.5

+a/2. We note that there is a sharp peak in the curve corresponding to z= 0.0 at 3.6 eV followed by a minimum at 3.9 eV which is due to surface effect. This can be concluded from the plot of $|\tilde{A}_\omega(z)|$ as a function of z for $\hbar\omega$=3.6 eV (Fig. 2.6). The peak in $|\tilde{A}_\omega(z)|$ is much weaker as we move away from 3.6 eV and at 4 eV for example, there is no peak in the surface region. Since we are using the experimentally measured dielectric function as input in our calculations, it is not possible to attribute any physical fact related to this peak. However from experimental photoemission data of Berguland and Spicer[29], it had been found that the photoemission yield is minimum at $\hbar\omega$=3.9 eV. He argued further that such phenomena is attributed to the fact that the incident photon energy near the plasmon energy have been absorbed in exciting the plasma oscillations thus not directly producing the photoelectrons.

(iii) Rhodium:

In Fig. (2.7), we are showing the plot of $|\tilde{A}_\omega(z)|^2$ as a function of the photon energy for three locations of the surface planes at z= a/2(surface), 0.0(middle of the surface) and -a/2 (bulk). The curve for z= 0.0 shows a peak at 8 eV and then has a minimum at 14 eV but increases[28] subsequently above 14 eV. If we look at $|\tilde{A}_\omega(z)|$ as a function of z for $\hbar\omega$ = 8 eV (Fig. 2.8), we see that there is a peak at z=+0.27a while for $\hbar\omega$ =14 eV, there is no peak in the surface region. So we may

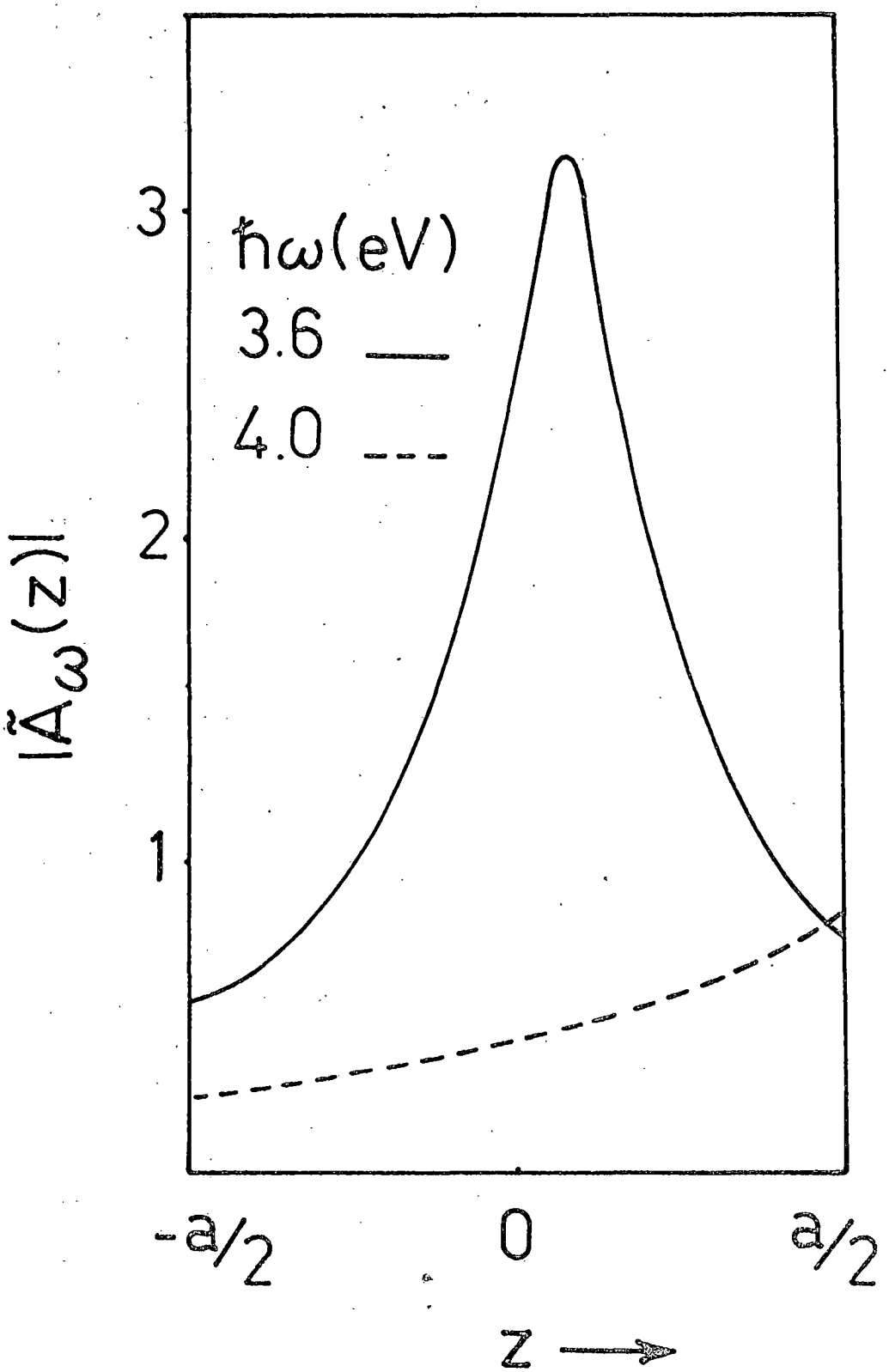

Figure 2.6

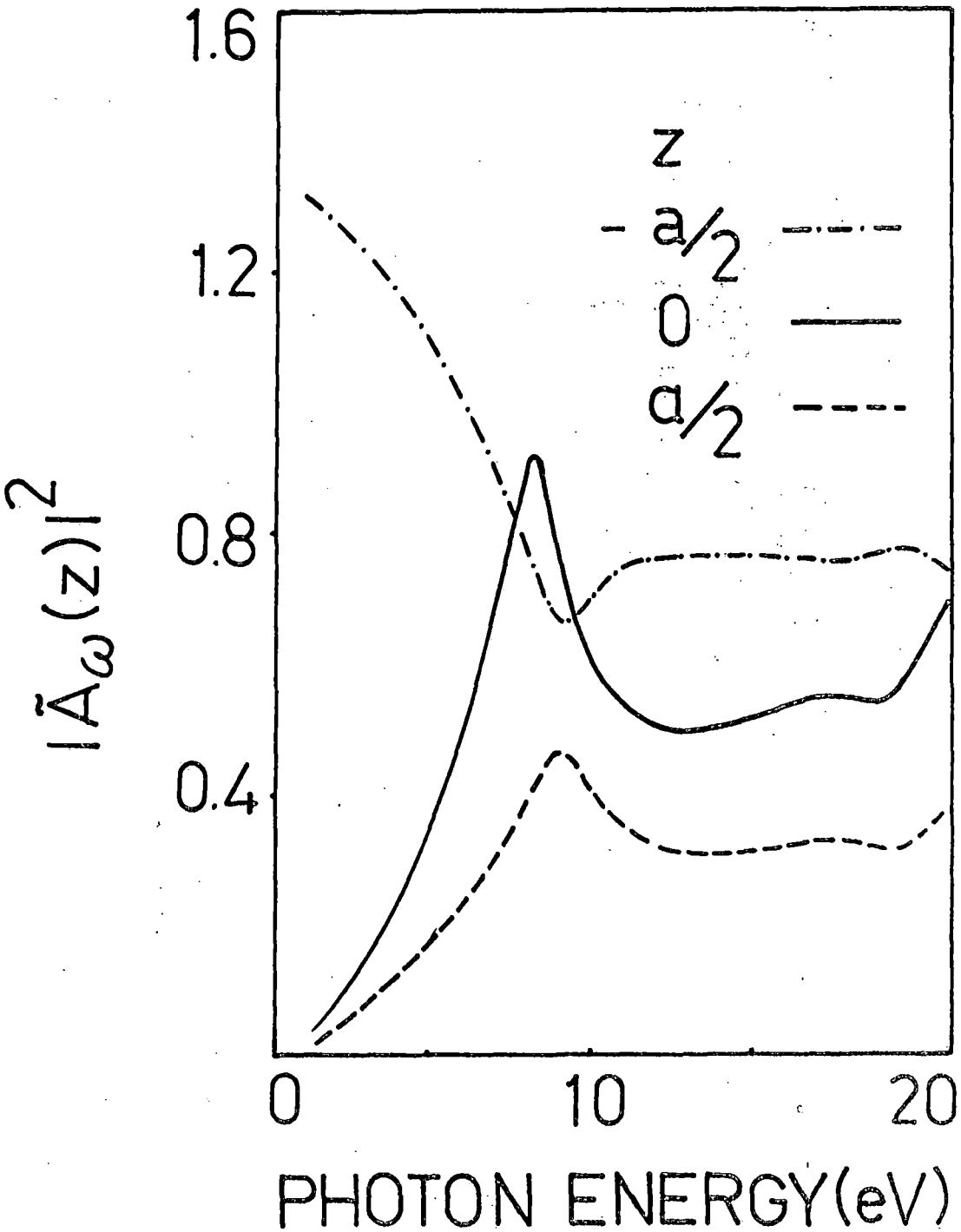

Figure 2.7

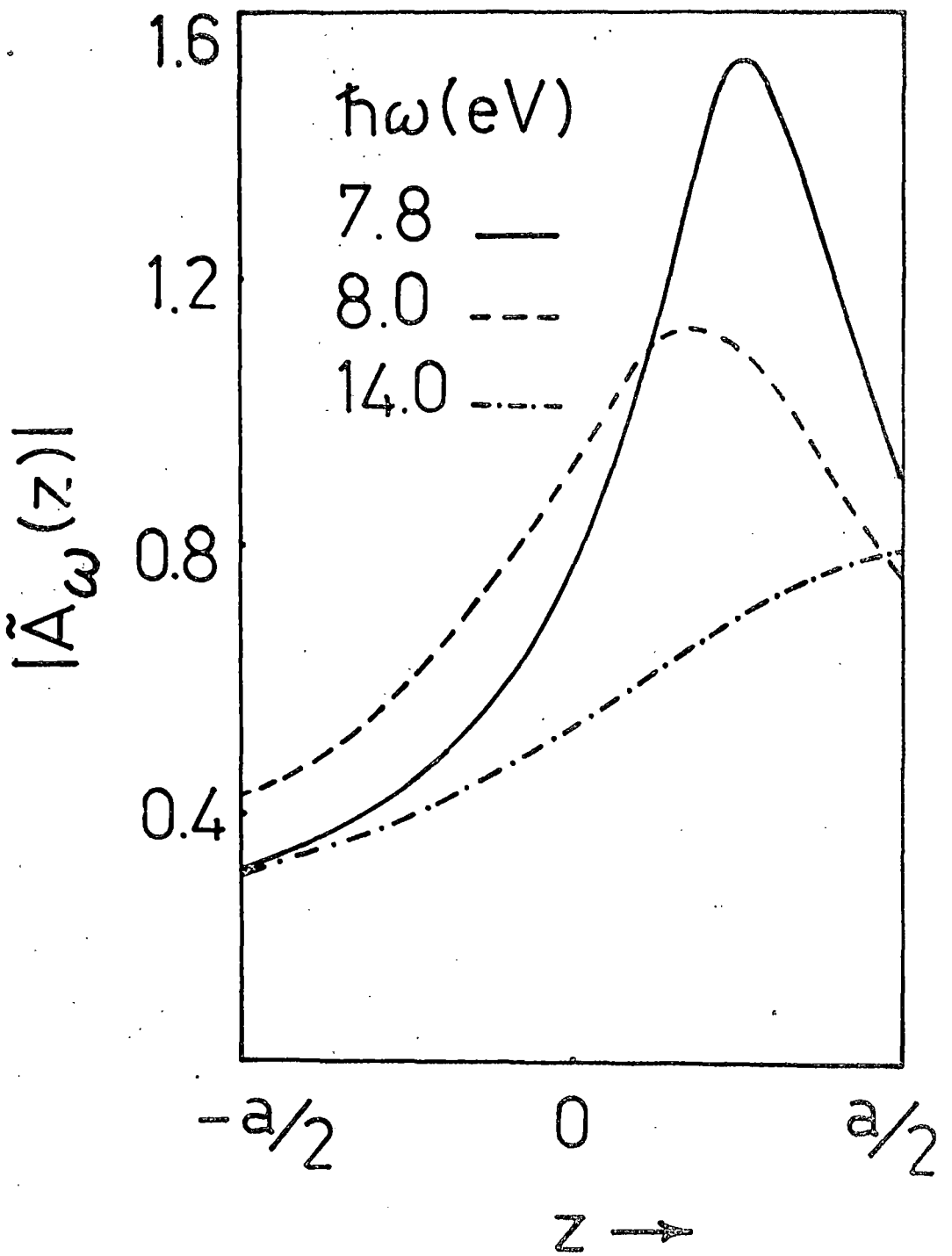

Figure 2.8

conclude that if we look at the normal photoemission there would be a peak[28] at around 8 eV which has its origin in the variation of the field in the surface region.

(iv) Molybdenum:

Fig. (2.9) shows the variation of $|\tilde{A}_\omega(z)|^2$ against photon energy for three locations of the planes at z= a/2 (vacuum - surface region interface), 0 (middle of the surface region) and -a/2 (bulk - surface region interface). The figure has a lot of structures[28] in the curves. The plot for z=0.0 shows two prominent peaks at photon energies 9.2 eV and 20 eV. Fig. (2.10) shows the plot of $|\tilde{A}_\omega(z)|$ as a function of z for photon energies 9 eV, 9.2 eV and 9.6 eV. We found that for each of these energies, there is a peak in the surface region. Also there is a peak in the surface region for energies at 19.6 eV, 20 eV and 20.6 eV as shown in (Fig.2.11). But in contrast there is no peak at 25 eV in the surface region. The photon energy dependence of $|\tilde{A}_\omega(z)|$ and $|\tilde{A}_\omega(z)|^2$ on both the sides of the interface (z=a/2 and -a/2) is quite revealing. Our calculated data of molybdenum showed qualitative features with the experimental data of Weng et al[30] who had also calculated the photon energy dependence of the field. They found that the field just outside the surface has a minimum near 25 eV and inside the surface it has a maximum at around 27 eV. For photon energy greater than 27 eV, it decreases rapidly (slowly)

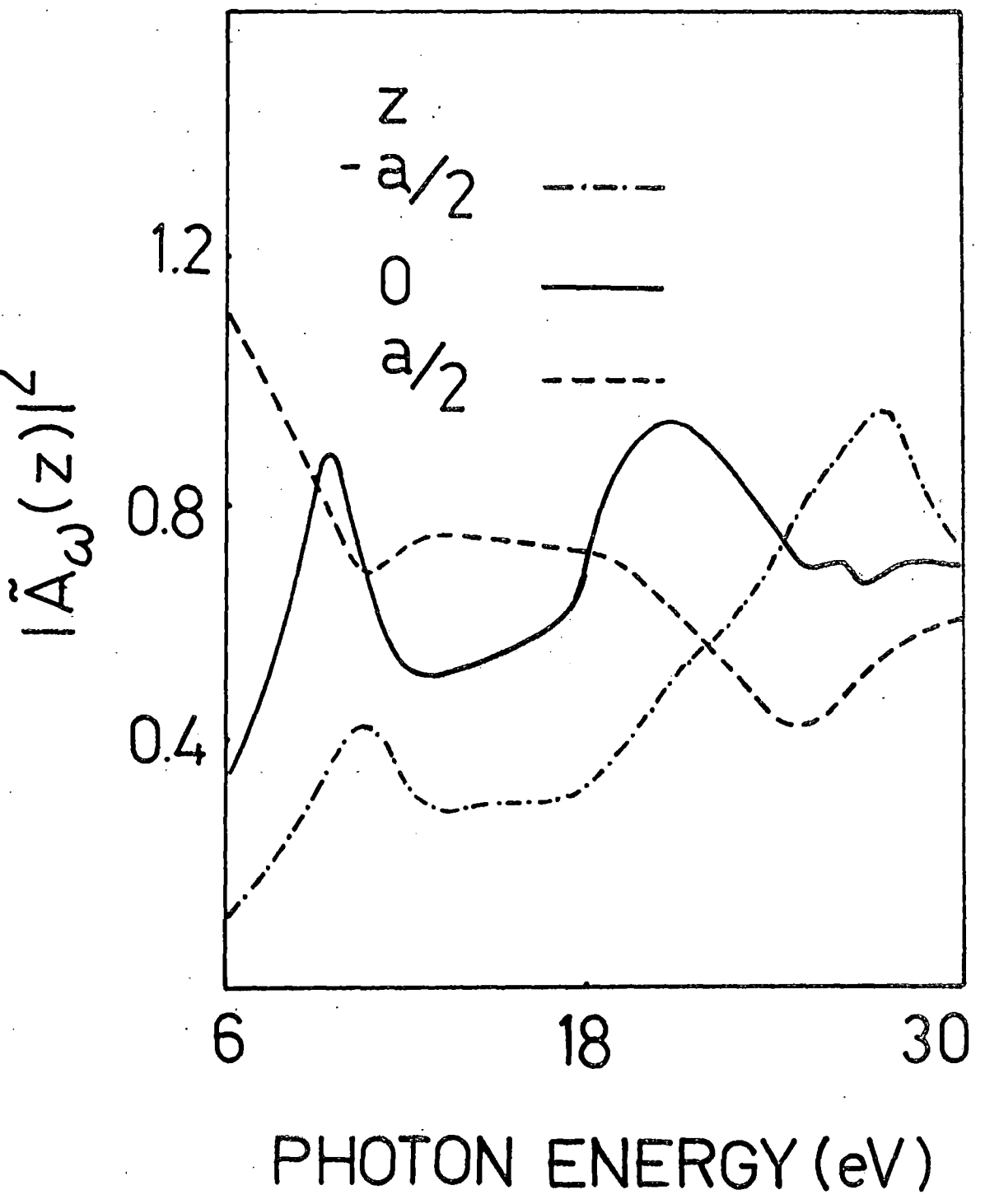

Figure 2.9

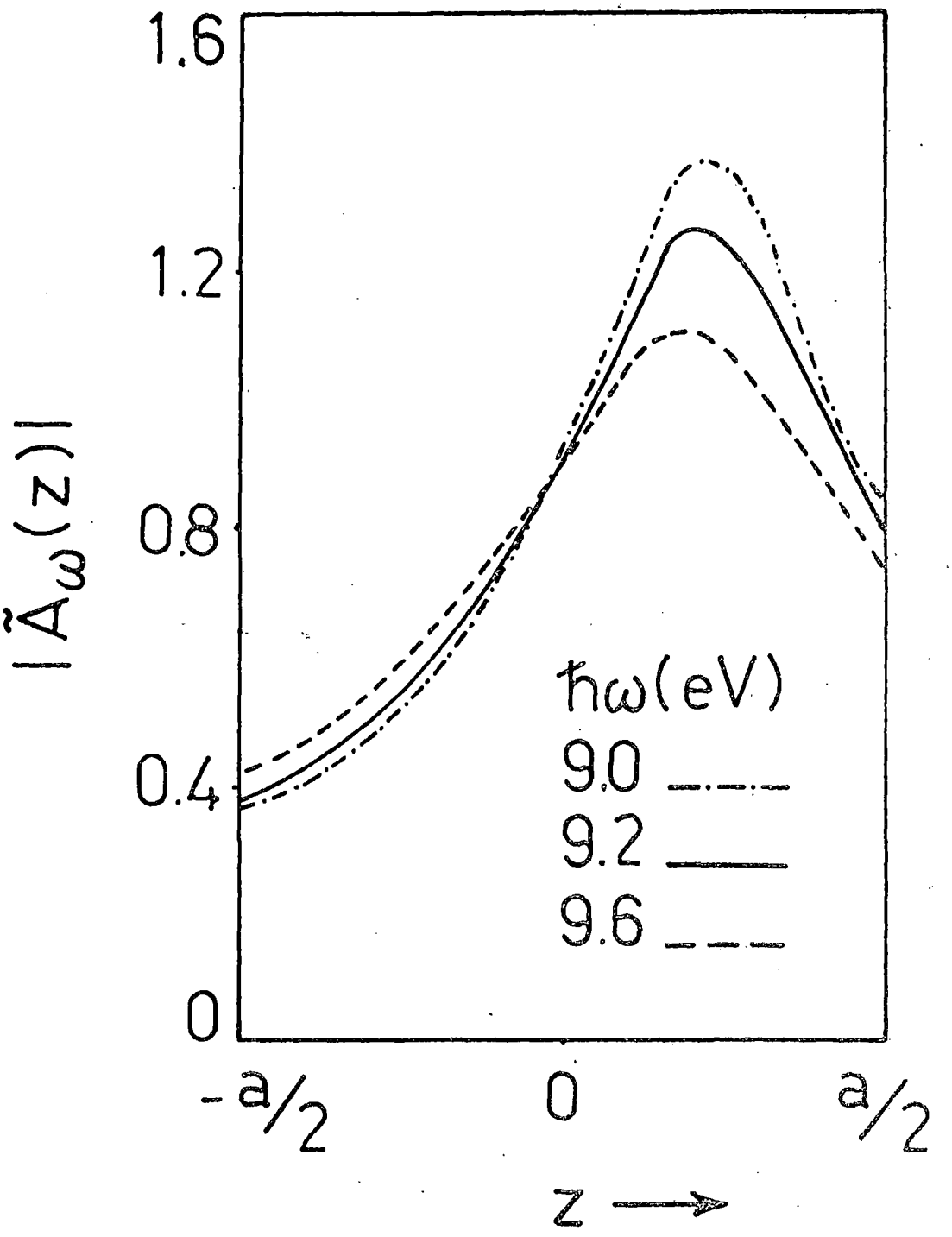

Figure 2.10

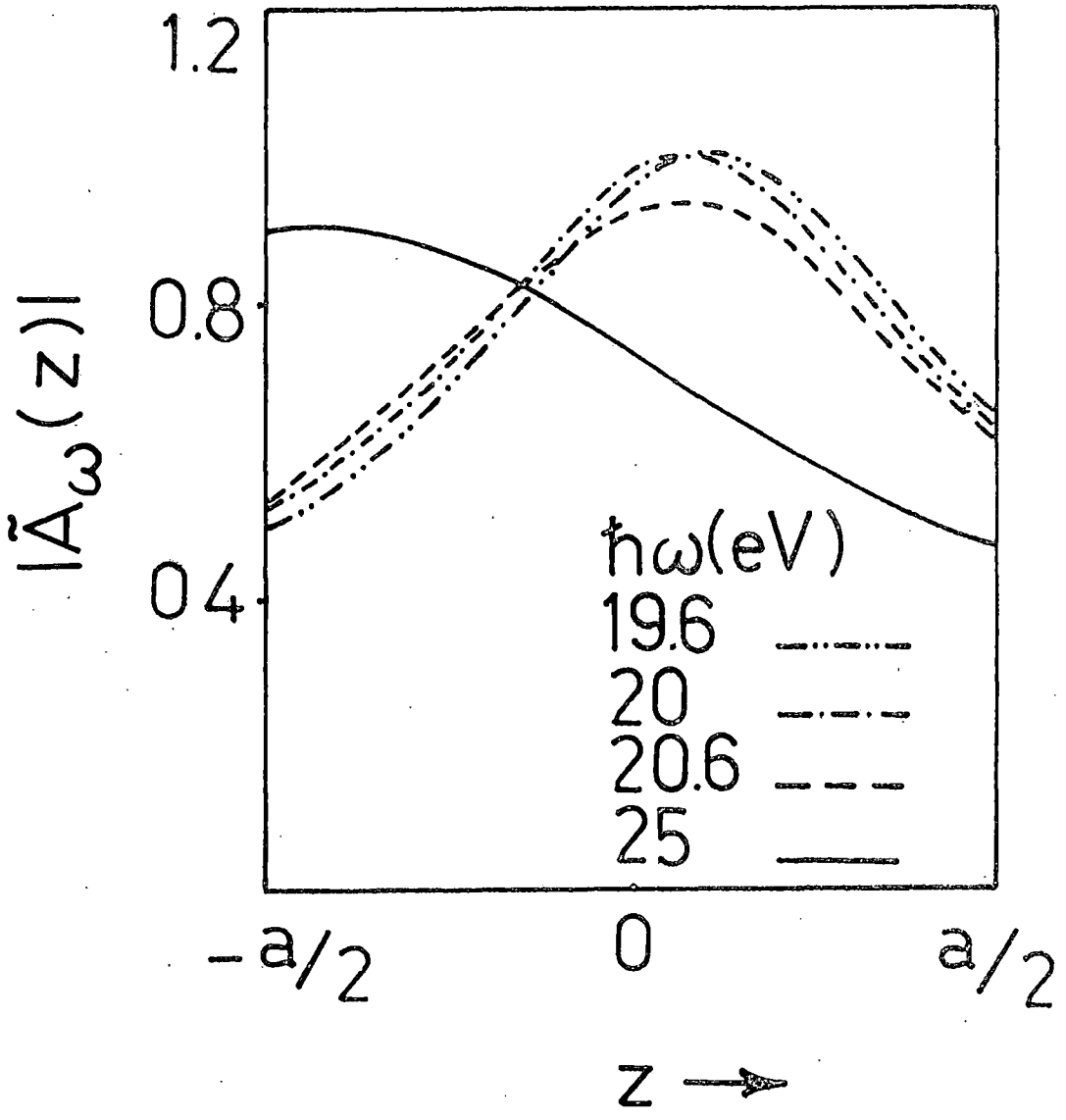

Figure 2.11

towards the low (high) photon energy side. Similar feature had been exhibited by our calculated data of field in molybdenum for region within and outside the surface (Fig. 2.9). It is found that there are two peaks at 9.5 eV and 20 eV for z = 0.0. This may be correlated to the two peaks observed in the photoemission calculation of high lying resonance for molybdenum as obtained by Weng et al[30].

(v) Palladium:

The plots of $|\tilde{A}_{\omega}(z)|^2$ against the photon energy for three location of the parallel planes at z= a/2(vacuum - surface region interface), 0.0(middle of the surface region) and -a/2(bulk - surface region interface) in case of palladium is shown in Fig. (2.12). It is found that the graph shows a minimum at photon energy 12 eV and has a peak at 7 eV. The field calculation for palladium had been reported by the author elsewhere[31]. The photon energy at 12 eV corresponds to the plasmon energy of palladium at which $\varepsilon_1 \to 0$. The calculated data of field in palladium also showed features as exhibited by other metals like aluminium, tungsten, silver etc. There is a peak in the curve at photon energy less than the plasmon energy whereas another peak smaller in height was found for photon energy greater than plasmon energy.

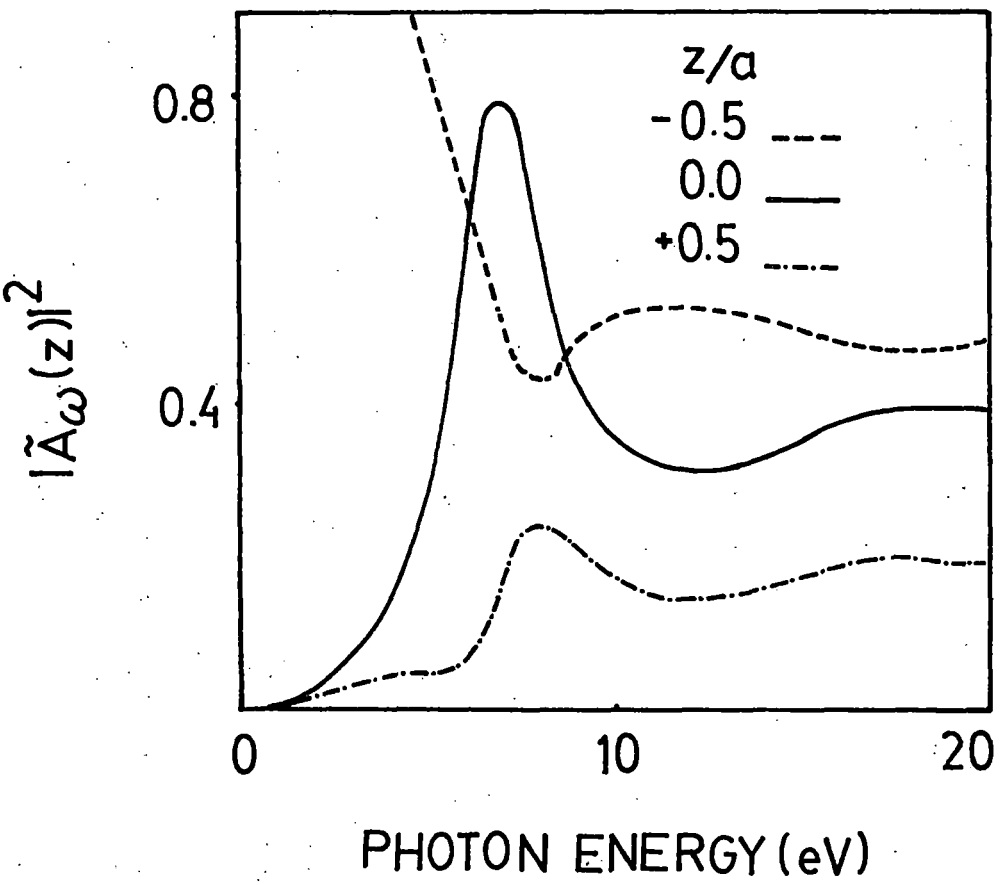

Figure 2.12

(vi) Silicon:

The presence of the surface states on the semiconductor surfaces was verified earlier by using the technique of angle integrated photoemission[32,33]. Moreover, the existence of the surface states was evident through the pinning of the Fermi level at the surface. In bulk semiconductors, the Fermi level shifts depending upon the doping level from the top of the valence band to the bottom of the conduction band. In contrast early angle integrated photoemission and work function measurements[34,35] showed that the Fermi level is pinned at the surface, almost independent of the doping level. Even though the existence of surface states on semiconductors was confirmed relatively early[36], little is known about these states compared to the surface states on metals.

Most semiconductor surfaces reconstruct. The best known example is that of Si(111) surface. A freshly cleaved surface structure can be prepared by the rapid quenching from a high temperature which stabilises the surface[37]. The Si(111) surface is only example of a variety of reconstructed semiconductor surfaces. Models for these have been developed mostly on the basis of dynamical LEED calculations. They clearly show the fundamental difference between a metal and semiconductor surfaces. For metals, reconstruction is the exception. The general behaviour is a few percent contraction of the surface

planes. In contrast semiconductors with their covalent bonding always exhibit reconstructed surfaces. The determination of the structure of semiconductor surfaces by calculating the position of surface states as a function of the structure and comparing to data has been the main objective of the angle resolved photoemission studies. Surface states on photoemission are in general s-p like unlike the case of metals, this does not imply that they are delocalised. Calculations shows that semiconductor surfaces are rather localised within certain bonds. Examples are the dangling bond structure surface states.

Since field calculations with respect to parameters like photon energy gives us the first hand informations about the photoemission cross-section, we have therefore calculated $|\tilde{A}_{\omega}(z)|^2$ against the photon energy also in the case of silicon. The plot of field square calculated against photon energy is shown in Fig. (2.13) for three different planes located at z/a=0.5(vacuum), 0.0(surface) and -0.5(bulk). We find that at the surface, there is a strong peak at 12 eV followed by a minimum at the plasmon energy 16 eV. The field then increases again but at 21 eV, it becomes very small. We note that this is the region where the dielectric function for silicon shows a resonance, as can be seen from the plots of real and imaginary parts of the dielectric function $\varepsilon(\omega)$ versus $\hbar\omega$ in Fig. (4.8). This behaviour is also reflected in the field data for the

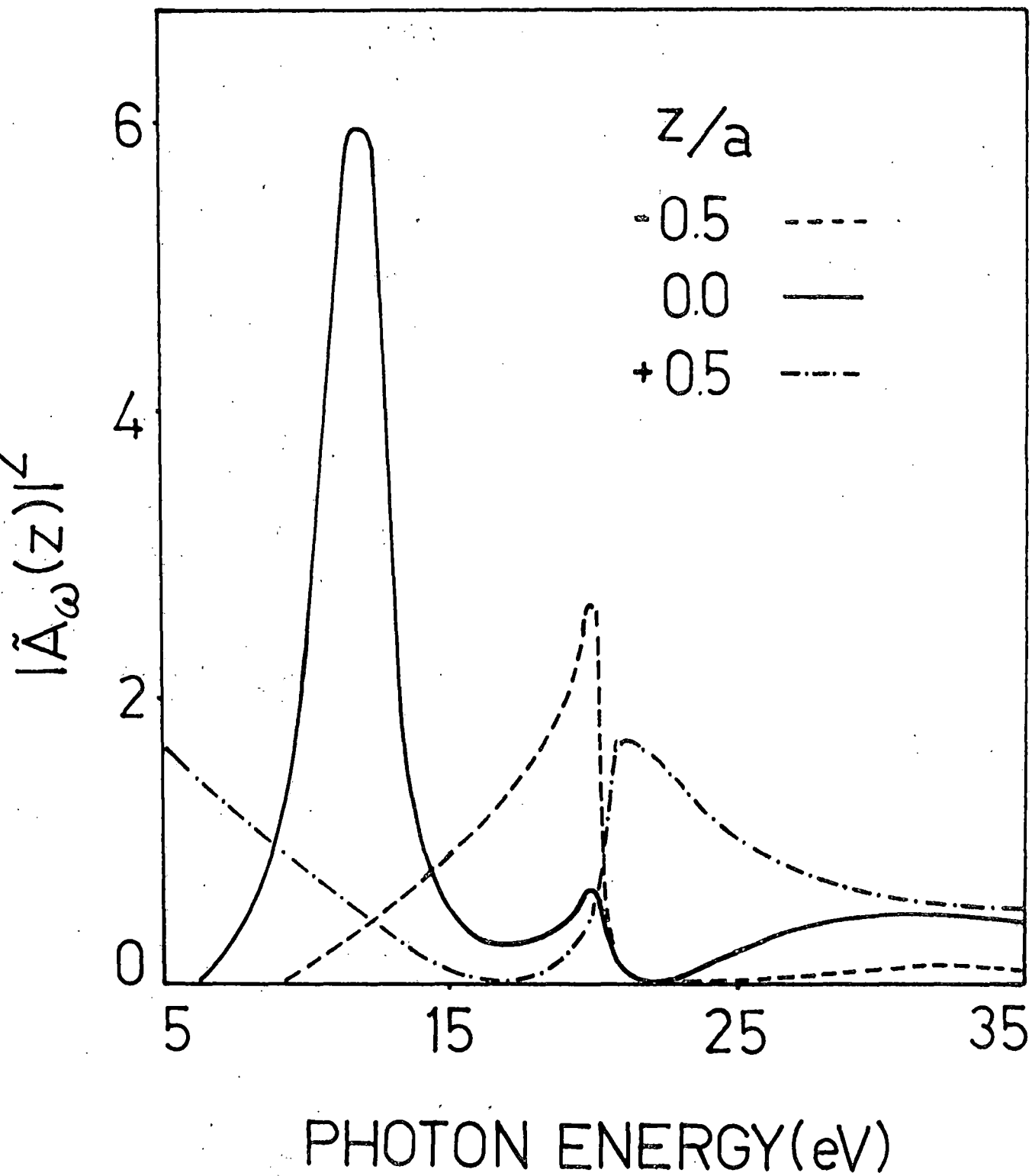

Figure 2.13

bulk-surface boundary (z/a=-0.5) which again becomes very small around 21 eV, although it does not show any minimum at the plasmon energy. The field on the vacuum-surface boundary (z/a=0.5) on the other hand shows a maximum at 21 eV and a minimum at the plasmon energy 16 eV - in direct contrast to the behaviour of the field in the bulk-surface boundary plane. This obviously points out that the variation of field in the surface region of a semiconductor is going to be quite important in photoemission calculations.

CHAPTER III

PHOTOEMISSION CALCULATIONS USING THE FREE ELECTRON MODEL

Photoelectric effect is of fundamental importance in physics as it is connected with the basic interaction of the electromagnetic field with the solid. Much of the current qualitative understanding of the bulk effects on photoemission is based on the free - electron (FE) model of the semi-infinite metal. In this simplest model, the surface barrier confining the electrons in the metal is represented by a step-function discontinuity in the potential. FE model has been applied in the theory of photoemission by Fowler[38], Mitchell[39] and others[5,10,40]. All these authors considered photoemission from free electron metals as an example of a pure surface effect.

In bulk photoemission, the necessary momentum is provided by the lattice and the surface induces the surface photoeffect as the incident photon carries too little momentum to be able to photoexcite electrons. The perpendicular component of the electromagnetic field undergoes a rapid spatial variation in the surface region of a metal and this is the main factor responsible for the cause of the surface photoemission. We will discuss here the photoemission from the free electron metals focusing mainly on aluminium.

The first unambiguous experimental evidence was contributions to the surface plasmon excitations due to surface roughness as seen by Endriz and Spicer[41]. Thereafter Flodström and Endriz[42] measured the ratio between the yields for p- and s-polarised light from aluminium at 5.4 eV and it could not be explained under the ordinary volume model of photoemission. Perhaps Feibelman[13] is the first one to calculate theoretically the photoyield treating the initial and final state wavefunctions as well as the electromagnetic field in the matrix element. He calculated the photoyield for photon energy below and above the plasmon energy for aluminium. Petersen and Hagstrom[9] were the first to obtain the absolute surface photoyield spectrum of aluminium by fully exploiting the properties of the synchrotron radiation. Then Levinson, Plummer and Feibelman[14] measured and calculated the normal cross-section for the surface state and the Fermi level of aluminium (100). The photoexcitation matrix element was calculated using the Lang-Kohn potential for the initial and final states as well as the dielectric response of the solid.

We shall calculate the photoemission cross-section from aluminium by using the golden rule formula (1.2), for which it is necessary to calculate $\langle \psi_f | H' | \psi_i \rangle$. We shall consider p-polarised radiation in the long wavelength limit, and we shall consider the z-component of $\vec{A}$ only. The relevant

expressions for the field are given by Bagchi and Kar[21]. The perturbation H′ due to the incident photon radiation in one dimension is given by

$$H' = \frac{e}{mc}\left[\tilde{A}_{\omega}(z)\,\frac{d}{dz} + \frac{1}{2}\,\frac{d}{dz}\,\tilde{A}_{\omega}(z)\right] \tag{3.1}$$

Photemission cross-section (PEC) was calculated by using the formula which may be derived from Eq. (1.2)[21]

$$\frac{d\sigma}{d\Omega} = \frac{k^2}{\omega}\,|\langle\psi_f|\tilde{A}_{\omega}(z)\,\frac{d}{dz} + \frac{1}{2}\,\frac{d}{dz}\,\tilde{A}_{\omega}(z)|\psi_i\rangle|^2 \tag{3.2}$$

To evaluate PEC in Eq. (3.2), we also need the initial state wavefunction ψ_i and the final state wavefunction ψ_f. Both ψ_i and ψ_f are calculated in the free electron approximation assuming a step like potential to be existing at the surface described by

$$V(z) = -V_o\theta(z) \tag{3.3}$$

which is shown in Fig. (3.1). In Eq. (3.3), we have $V_o=E_F+\phi$ where E_F is the Fermi level in the free electron model and ϕ is the work function. $\theta(z)$ is the step function described as

$$\theta(z) = \begin{cases} 0, & z<0 \\ 1, & z>0 \end{cases} \tag{3.4}$$

We have assumed the initial state wavefunction as

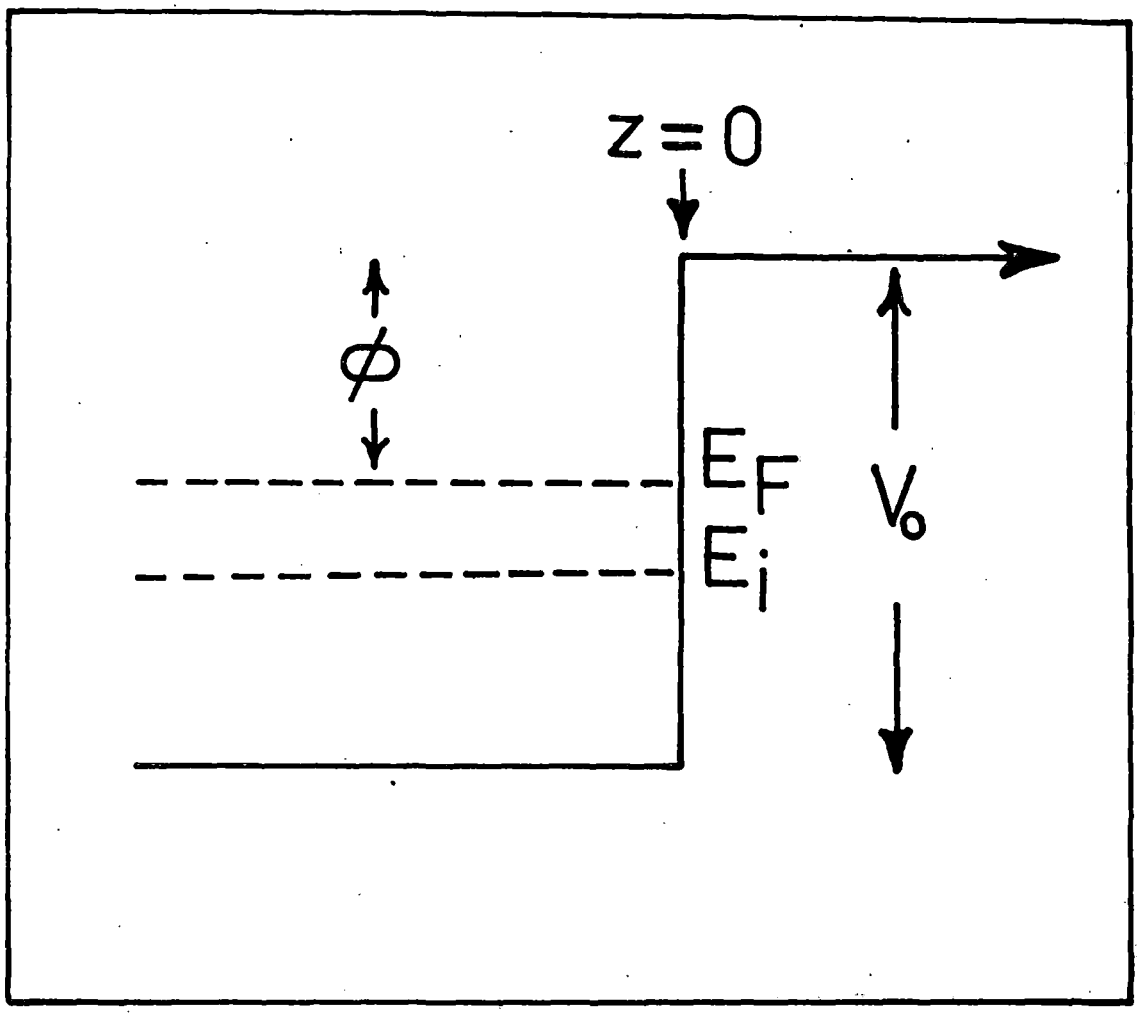

Figure 3.1

$$\psi_i(z) = \begin{cases} \sum A\, e^{i\vec{k}_{\parallel}\cdot\vec{r}_{\parallel}} \cdot (e^{ik_i z} + R\, e^{-ik_i z}), & z<0 \\ \sum A\, e^{i\vec{k}_{\parallel}\cdot\vec{r}_{\parallel}} \cdot T \cdot e^{-\varkappa z}, & z>0 \end{cases} \tag{3.5}$$

where A can be determined from the current normalisation and it turns out that $A = (m/2\pi\hbar^2 k_i)^{1/2}$.

Neglecting the transverse parts in Eq. (3.5), we can now write the initial state wavefunction as

$$\psi_i(z) = \begin{cases} \sum A\, (e^{ik_i} + R\, e^{-ik_i z}), & z<0 \\ \sum A\, T\, e^{-\varkappa z}, & z>0 \end{cases} \tag{3.6}$$

At z=0, the wavefunctions for the two regions can be written as

$$\psi_i(z)\Big|_{z\to 0^-} = A(1 + R)$$

$$\psi_i(z)\Big|_{z\to 0^+} = A\, T \tag{3.7}$$

The condition $\psi_i(z)\Big|_{z\to 0^-} = \psi_i(z)\Big|_{z\to 0^+}$ at the surface gives

$$1 + R = T \tag{3.8}$$

Now taking the derivatives of the initial state wavefunctions in the two regions, we have

$$\psi_i'(z) = Aik_i(e^{ik_i z} - R\, e^{-ik_i z}) \qquad \text{for } z < 0$$

$$\psi_i'(z) = -A\varkappa T\, e^{-\varkappa z}. \qquad \text{for } z > 0$$

At the surface(z=0), we have

$$\psi_i'(z)\Big|_{z\to 0^-} = Aik_i(1 - R)$$

and $$\psi_i'(z)\Big|_{z\to 0^+} = -A\varkappa T \quad .$$

But at the surface, using the condition

$$\psi_i'(z)\Big|_{z\to 0^-} = \psi'_i(z)\Big|_{z\to 0^+}$$

gives $$ik_i(1 - R) = -T \; . \qquad (3.9)$$

Solving Eqs. (3.8) and (3.9), we get

$$R = \frac{ik_i + \varkappa}{ik_i - \varkappa}$$

$$T = \frac{2ik_i}{ik_i - \varkappa} \qquad (3.10)$$

Putting the values of R and T from Eq. (3.10) in Eq. (3.6), we can write the initial state wavefunction for the free electron model as, following Bagchi and Kar[21]

$$\psi_i(z) = \begin{cases} \left(\frac{m}{2\pi\hbar^2 k_i}\right)^{1/2} \left[e^{ik_i z} + \frac{ik_i + \varkappa}{ik_i - \varkappa} e^{-ik_i z} \right] . e^{i\vec{k}_\parallel . \vec{r}_\parallel} , & z<0 \\ \left(\frac{m}{2\pi\hbar^2 k_i}\right)^{1/2} \frac{2ik_i}{ik_i - \varkappa} e^{-\varkappa z} . e^{i\vec{k}_\parallel . \vec{r}_\parallel} , & z>0 \end{cases} \tag{3.11}$$

where the parameters are described as follows:

$$k_i^2 = \frac{2mE_i}{\hbar^2} - \vec{k}_\parallel^2$$

$$\varkappa^2 = \frac{2m}{\hbar^2} (V_o - E_i) + \vec{k}_\parallel^2 . \tag{3.12}$$

$\vec{k}_\parallel$ and $\vec{r}_\parallel$ are the component of $\vec{k}$ and $\vec{r}$ in the x-y plane which is parallel to the surface. The final state wavefunction is the scattering state of the step potential V(z). This may be written as, following Bagchi and Kar [21]

$$\psi_f(z) = \begin{cases} \left(\frac{m}{2\pi\hbar^2 q}\right)^{1/2} \frac{2q}{q + k_f} e^{-\alpha|z|} e^{ik_f z} . e^{i\vec{k}_\parallel . \vec{r}_\parallel} , & z<0 \\ \left(\frac{m}{2\pi\hbar^2 q}\right)^{1/2} \left[e^{iqz} + \frac{q - k_f}{q + k_f} e^{-iqz} \right] e^{i\vec{k}_\parallel . \vec{r}_\parallel} , & z>0 \end{cases} \tag{3.13}$$

where $$k_f^2 = \frac{2m}{\hbar^2} E_f - k_{\parallel}^2$$

$$q^2 = \frac{2m}{\hbar^2} (E_f - V_o) - k_{\parallel}^2 \qquad (3.14)$$

and $E_f = E_i + \hbar\omega$. The matrix element for photoemission cross-section in Eq. (3.2) was evaluated by using the above expressions for the wavefunctions and the vector potential of Eq. (2.3). To ensure convergence of the integral for $z<0$, a convergence factor α was introduced which arises due to lifetime effects[12]. This is a standard procedure in low energy electron diffraction and photoemission calculations. We do it by introducing a factor $e^{-\alpha|z|}$ in the calculation of the matrix element for the region $z<0$. This is done to take into account the inelastic scattering of the electrons.

For surface state photoemission calculations, the initial state wavefunction ψ_i is replaced by a properly normalised Gaussian wavefunction as used by Bagchi and Kar[21] which is given by

$$\psi_i(z) = e^{i\vec{k}_{\parallel}\cdot\vec{r}_{\parallel}} \left(\frac{2\beta}{\pi a^2} \right)^{1/4} . e^{-\beta(z-z_o/a)^2} \qquad (3.15)$$

where β is a dimensionless parameter that describes the width of the Gaussian so that its full width at half maximum is given

by $\Delta=2a/\beta$. In Eq. (3.15), $\psi_i(z)$ is centred on the $z=z_o$ plane. The calculation of the photoemission cross-section for normal photoemission now reduces to the evaluation of the matrix element $\langle\psi_f|H'|\psi_i\rangle$. Rewriting Eq. (3.2), we have the formula for calculating the photoemission cross-section given by

$$\frac{d\sigma}{d\Omega} = \frac{k^2}{\omega}|I|^2 \tag{3.16}$$

where I is given by

$$\begin{aligned} I &= \int_{-\infty}^{\infty} \psi_f^*(z)\, H'\psi_i(z)dz \\ &= \int_{-\infty}^{-a/2} \psi_f^*\, \tilde{A}_\omega(z)\, \frac{d\psi_i}{dz}\, dz \;+\; \int_{-a/2}^{0} \psi_f^*\, \tilde{A}_\omega(z)\, \frac{d\psi_i}{dz}\, dz \\ &\quad + \frac{1}{2}\int_{-a/2}^{0} \psi_f^*\, \frac{d\tilde{A}_\omega(z)}{dz}\, \psi_i dz \;+\; \int_{0}^{a/2} \psi_f^*\, \tilde{A}_\omega(z)\, \frac{d\psi_i}{dz}\, dz \\ &\quad + \frac{1}{2}\int_{0}^{a/2} \psi_f^*\, \frac{d\tilde{A}_\omega(z)}{dz}\, \psi_i dz \;+\; \int_{a/2}^{\infty} \psi_f^*\, \tilde{A}_\omega(z)\, \frac{d\psi_i}{dz}\, dz \end{aligned} \tag{3.17}$$

Photoemission cross-section (PEC) was calculated from the band state (Fermi level) and surface state. The detailed evaluation

of the integral in Eq. (3.17) is shown in appendix I. The fortran program used for the numerical evaluation of integral I is given in appendix III. We have applied our results for calculating the normal photoemission from the Fermi level of aluminium for which the experimental data as well as the theoretical calculations using the jellium model is available. The data used are, as given by Ashcroft and Mermin[43], for work function ϕ=4.25 eV and initial state energy E_i=11.7 eV. Since the normal photoemission is considered, $\vec{k}_{\parallel}$=0 and θ_i is taken to be 45^{o} as in the experiment. The PEC results with a=10 a.u and α=0.35 is shown in Fig. (3.2). The calculated photocurrent results shows a peak at 11 eV, minimum at 15 eV and again a broad peak at 20.5 eV.

The origin of peak at 11 eV in the calculated spectrum was further investigated as shown in Fig. (3.3). Here $|\tilde{A}_{\omega}(z)|$ was plotted as a function of z in the surface region for photon energy at 20 eV, 11 eV and 15 eV respectively. It is seen that a strong peak occurs at 11 eV in the middle of the surface but at 15 eV and 20 eV, the plot does not show any peak in the surface region. As a further evidence of peak at 11 eV being surface related, we have also done calculations of photocurrent using free electron wavefunctions as in Eqs. (3.11) and (3.13) with fields as given by Fresnel refraction formula[44]. The plot shows a minimum at 12 eV and no peak at 11-12 eV. Above the

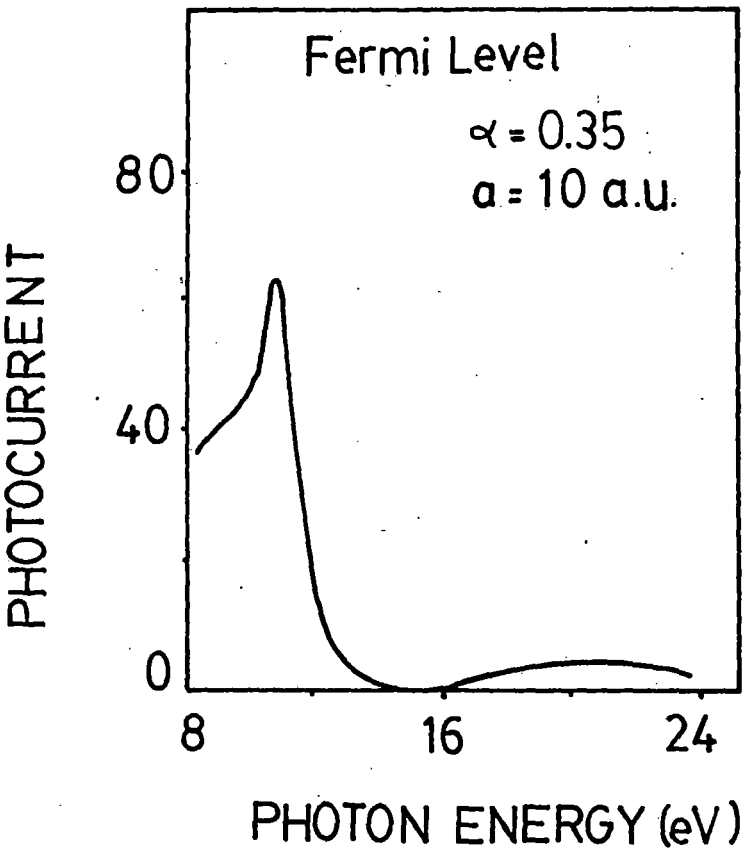
Fermi Level
α = 0.35
a = 10 a.u.
80
40
0
PHOTOCURRENT
8
16
24
PHOTON ENERGY (eV)

Figure 3.2

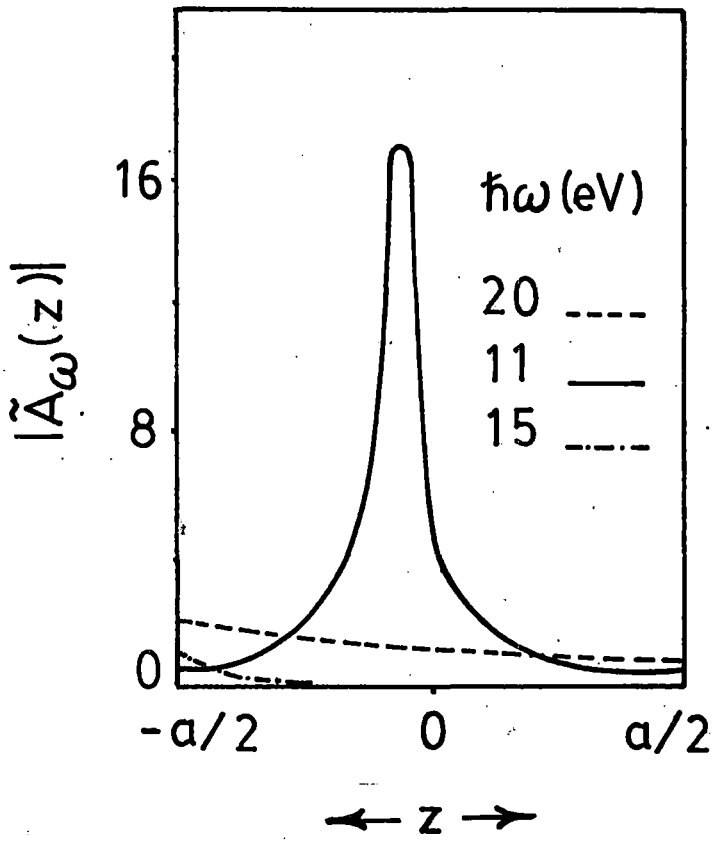

Figure 3.3

plasmon energy, the plot shows a peak (Fig. 3.4) which is more pronounced then that with the surface region included. Thus it is evident that the simple Fresnel refraction formula is inadequate in reproducing the surface photoemissive features and the inclusion of the surface in photoemission calculations is important.

The results of the surface state photoemission is shown in Fig. (3.5) for aluminium. We have considered the surface state energy to lie at 2.75 eV below the Fermi level[14]. The photocurrent is calculated for the surface widths 5 a.u and 10 a.u. The height of photocurrent peak is greater for the narrow surface width than the broad one. Also the calculated data showed a qualitative agreement with the experimental data of Levinson et al[14].

We find therefore that the frequency dependence of normal component of the electric field near the surface of metal has important consequences for the angle resolved photoemission from the bulk as well as from the surface of aluminium. The field component in the surface region decreases greatly near the plasma frequency and these features explains the observed decrease in normal photoemission from the metallic surface states near plasmon energy. We therefore conclude that the inclusion of refraction effects is essential in a complete angle resolved photoemission calculations.

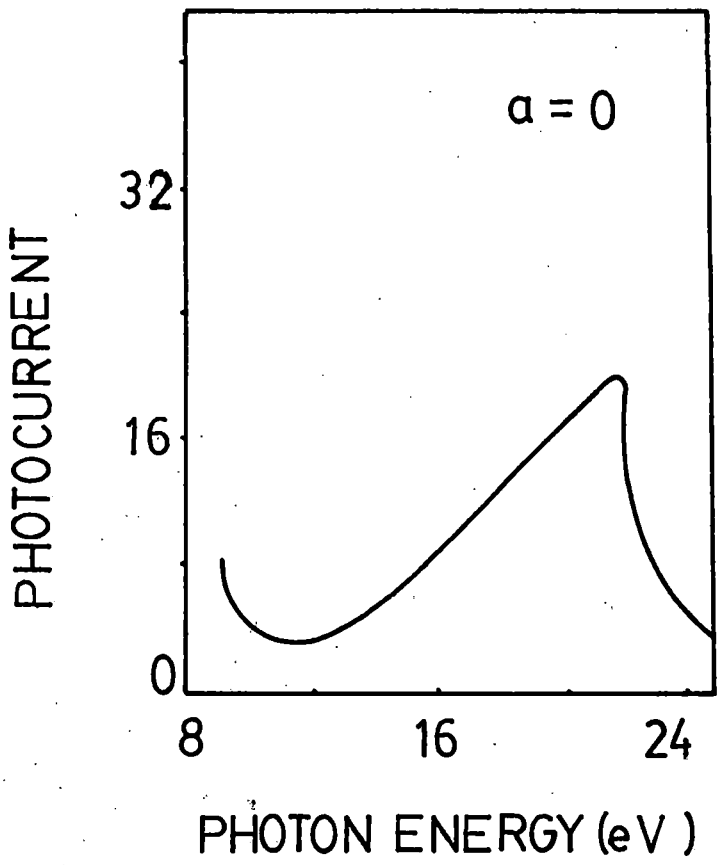

Figure 3.4

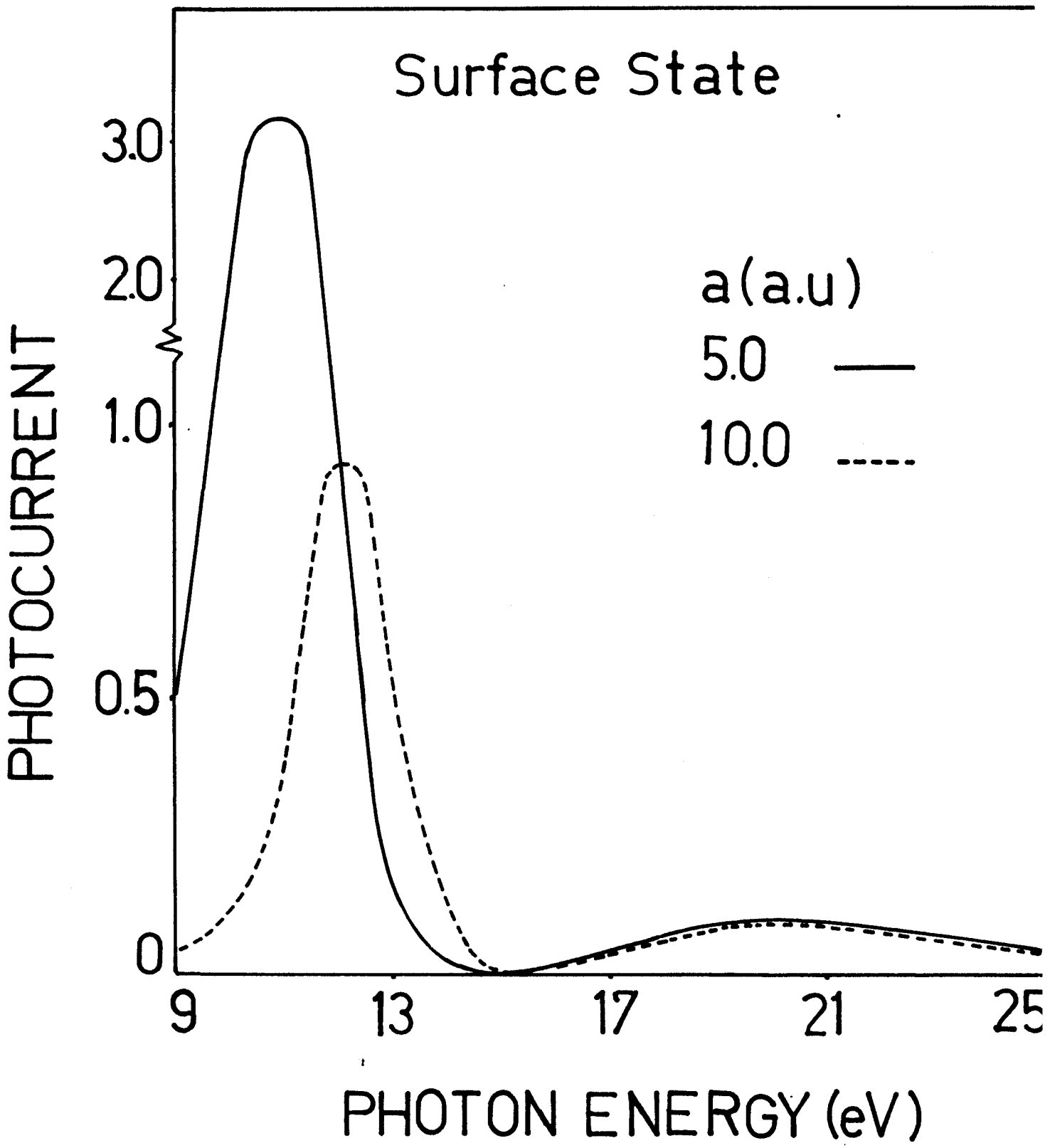
Surface State
3.0
2.0
1.0
0.5
0
PHOTOCURRENT
a(a.u)
5.0
10.0
9
13
17
21
25
PHOTON ENERGY (eV)

Figure 3.5

CHAPTER IV

PHOTOEMISSION CALCULATIONS USING KRONIG-PENNEY MODEL

In chapter III, we have discussed the photoemission calculations from the band states (Fermi level) and surface state of free electron solid like aluminium. Since aluminium is weakly bonded metal, we used a free electron initial state wavefunction ψ_i for the band state photoemission. ψ_i was formulated by way of normal matching of wavefunction at the boundary surface of the solid. The photocurrent was then computed by using the electromagnetic field developed by Bagchi and Kar[21].

To incorporate the band structure effects, a model calculation following Kronig and Penney potential was done as a first step. Kronig-Penney model has been used in connection with surface electronic states by several authors[45-48]. It has been seen that some surface related features come out, at least qualitatively, from these calculations. Schaich and Ashcroft[4] have calculated numerically the photoyield by using the modified form of the Kronig-Penney model. Band structure effects was also included in it. They used the wavefunction of Mitchell[39] for free electron gas in a semi-infinite box and considered the photon field vector $\tilde{A}_\omega(z)$ to remain constant.

However the numerical data as obtained by them in the case of potassium is quite realistic. This is evident for the nature of the photocurrent data obtained by them from various planes below the surface. Steslicka[49] had performed a detailed calculations of the surface states using the Kronig-Penney model both for the semi-infinite and the infinite crystal model. Eldib et al[50] had also applied the Kronig-Penney model to one dimensional crystal. He had calculated only the electronic energy bands for mono- and polyatomic crystals and compared his data with the one computed by using the linear combinations of atomic orbital (LCAO) methods.

In this chapter, we shall use the Kronig-Penney model to represent the crystal potential field by a linear array of rectangular well which would later be transformed into a chain of δ- function wells subject to the area of each well remaining constant as shown in Fig. (4.1). By using essentially the electromagnetic field as discussed in chapter-II, we will calculate the photoemission cross-section. The initial state wavefunction is obtained by matching at the surface. The relevant matrix element then can be written as

$$I = \langle \psi_f | H' | \psi_i \rangle = \int_{-\infty}^{\infty} \psi_f^*(z) H' \psi_i(z) dz$$

$$= \int_{-\infty}^{\infty} \psi_f^*(z) \left[\tilde{A}_\omega(z) \frac{d}{dz} + \frac{1}{2} \frac{d}{dz} \tilde{A}_\omega(z) \right] \psi_i(z) dz \qquad (4.1)$$

In Eq. (4.1) above, $\psi_f(z)$ the final state wavefunction, has the same form as given by Eq. (3.13).

To evaluate the initial state wavefunction $\psi_i(z)$, one generally solves the one-dimensional Schrödinger's equation which can be written as

$$\frac{d^2\psi(z)}{dz^2} + k_i^2\psi(z) = -\frac{2m}{\hbar^2} V(z)\psi(z) \qquad (4.2)$$

where $k_i^2=2mE/\hbar^2$ and $V(z)<0$. One can straight away replace the right hand side of Eq. (4.2) by Dirac δ- function and invoke the use of Green function technique as done by Davison and Levine[48] to calculate the electronic energy bands.

$\psi_i(z)$ is calculated[51] by proper matching of ψ and $d\psi/dz$ on the boundary plane defined by z=0 plane. Let $\phi(z|E)$ denote the Bloch wavefunction deep in the metal and $\phi^*(z|E)$ the time reversed version of $\phi(z|E)$. The eigenfunction in the semi-infinite metal (z<0) has been chosen to have the form as

$$\psi_i(z|E) = \phi(z|E) - P\,\phi^*(z|E) \qquad (4.3)$$

where P is the reflection coefficient which was evaluated by matching the wavefunction and the slope at z=0. We consider the potential V(z) as shown in Fig. (4.1) to be one dimensional

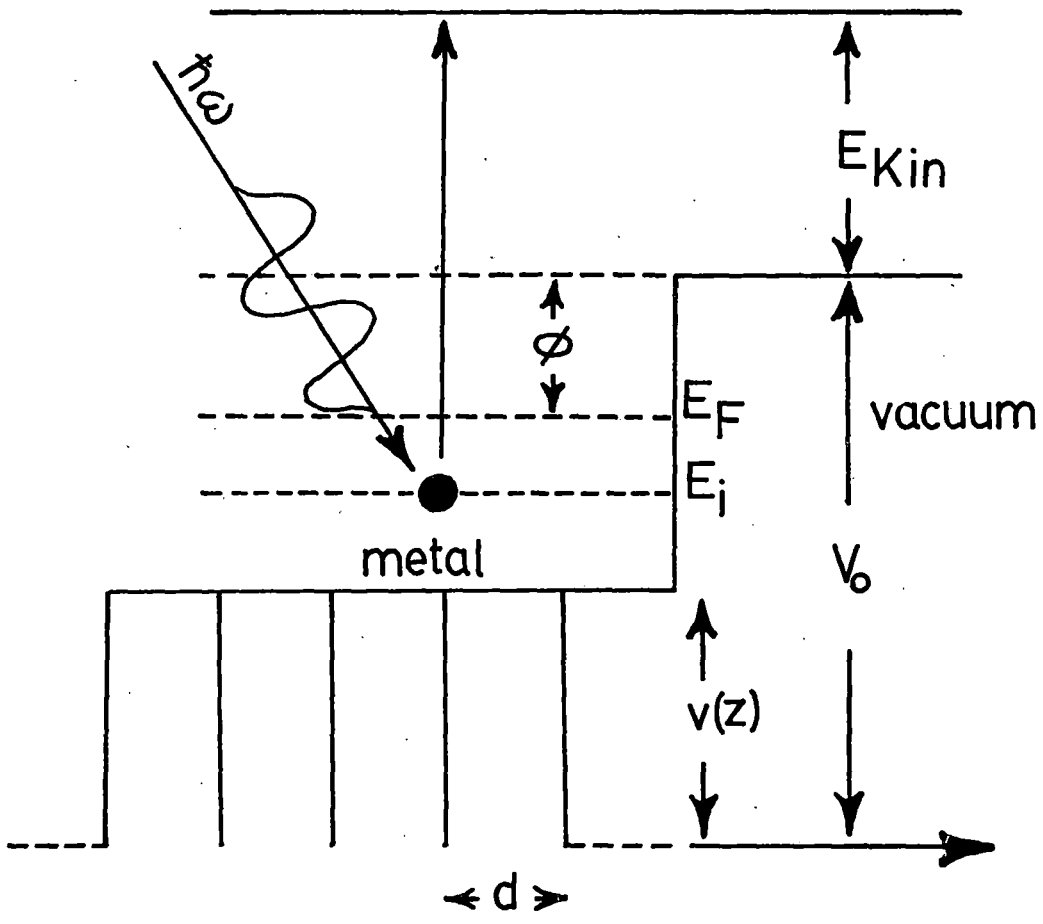

Figure 4.1

Kronig-Penney type described by

$$V(z) = \sum g\, \delta(z - (2n+1)\frac{d}{2}) \tag{4.4}$$

To find $\phi(z|E)$, let us consider an electron with initial state energy $E_i = \hbar^2 k_i^2/2m$ to be incident on the single barrier potential $v(z)$ of width d. Since $v(z)=0$ for $z \geq d/2$, the wavefunction $\phi(z)$ in these regions is described as

$$\phi(z) = \begin{cases} e^{ik_i z} + re^{-ik_i z}, & z \leq -d/2 \\ te^{ik_i z}, & z \geq d/2 \end{cases} \tag{4.5}$$

where r and t are the reflection and transmission coefficients through the potential barrier. For Kronig-Penney model, we have[52]

$$r = ie^{i\delta} \sin\delta$$

$$t = e^{i\delta}\cos\delta \tag{4.6}$$

where δ is the phase shift introduced in the transmitted wave the value of which is given by

$$\cot\delta = -\frac{\hbar k_i^2}{mg} \tag{4.7}$$

In Eq. (4.7), g is the strength of δ-potential which describes the bulk potential. Therefore now, Eq. (4.3) can be written in its final form, with the help of Eqs. (4.5) and (4.6), for the region within the solid ($z<0$) as

$$\psi_i(z|E) = (1-iPe^{-i\delta}\sin\delta)e^{ik_i z} - (P-ie^{i\delta}\sin\delta)e^{-ik_i z} \quad (4.8)$$

The initial state wavefunction outside the metal ($z>0$) is

$$\psi_i(z|E) = Te^{-\varkappa z} \quad (4.9)$$

where T is the transmission coefficient across the boundary plane and

$$\varkappa^2 = \frac{2m}{\hbar^2}(V_o - E_i). \quad (4.10)$$

V_o is the step potential at the surface which an electron encounters while transmitting through the boundary surface. By proper matching $\psi_i(z)$ in Eqs. (4.8) and (4.9) at the surface, we get

$$P = \frac{(\varkappa-ik_i) - (k_i-i\varkappa)e^{i\delta}\sin\delta}{(\varkappa-ik_i) + (k_i-i\varkappa)e^{-i\delta}\sin\delta} \quad (4.11)$$

$$T = \frac{2k_i \sin 2\delta}{(\varkappa - ik_i) + (k_i - i\varkappa)e^{-i\delta}\sin\delta} \qquad (4.12)$$

The proper evaluation of P and T with the appropriate numerical values for other factors enables one to write explicitly the initial state wavefunction ψ_i. The photoemission cross-section was calculated by using the formula

$$\frac{d\sigma}{d\Omega} = \frac{k^2}{\omega} |\langle \psi_f | H' | \psi_i \rangle|^2 \qquad (4.13)$$

The matrix element $I=\langle \psi_f | H' | \psi_i \rangle$ in Eq. (4.13) can be written as

$$I = \int_{-\infty}^{-a/2} \psi_f^* \tilde{A}_\omega(z) \frac{d\psi_i}{dz} dz + \int_{-a/2}^{0} \psi_f^* \tilde{A}_\omega(z) \frac{d\psi_i}{dz} dz$$

$$+\frac{1}{2} \int_{-a/2}^{0} \psi_f^* \frac{d\tilde{A}_\omega(z)}{dz} \psi_i \, dz + \int_{0}^{a/2} \psi_f^* \tilde{A}_\omega(z) \frac{d\psi_i}{dz} dz$$

$$+\frac{1}{2} \int_{0}^{a/2} \psi_f^* \frac{d\tilde{A}_\omega(z)}{dz} \psi_i \, dz + \int_{a/2}^{\infty} \psi_f^* \tilde{A}_\omega(z) \frac{d\psi_i}{dz} dz. \qquad (4.14)$$

The photocurrent was calculated numerically with the help of Eqs. (4.13) and (4.14). The detailed evaluation of the integrals in Eqs. (4.14) is shown in appendix II and the

fortran program in appendix IV. We have used a number of dielectric functions corresponding to different elements. The data for these were those given by Weaver[25] and Edwards[53]. Since it is a model calculations, we have chosen the following data (in atomic units) for all the solids:

$E_i = 0.43$

$\delta = -0.5753$

$g = 0.60$

$\theta_i = 45^o$

The results obtained with using the dielectric function $\varepsilon(\omega)$ for aluminium as given by Weaver[25] are shown in Figs. (4.2) and (4.3). The plots of photocurrent versus the photon energy for the surface region defined by $-a/2 \leq z \leq a/2$ having the surface width a=5 a.u and 10 a.u are shown in Figs. (4.2) and (4.3) respectively. For a=5 a.u, the current peaked at $\hbar\omega$=12 eV then it showed a minimum at $\hbar\omega$=15 eV which is close to the plasmon energy. There is a second peak in the photocurrent data which occurs at around 20 eV and is a broad one. For a=10 a.u (Fig. 4.3), we find a sharp peak at 11 eV and a broad one at 21 eV. The ratio of the two peak heights for a=10 a.u at 11 eV and 21 eV is about 3. These results are in qualitative agreement with the one obtained by using the free electron model[24]. However the peaks below the plasmon energy for the free electron case was much sharper compared to this model.

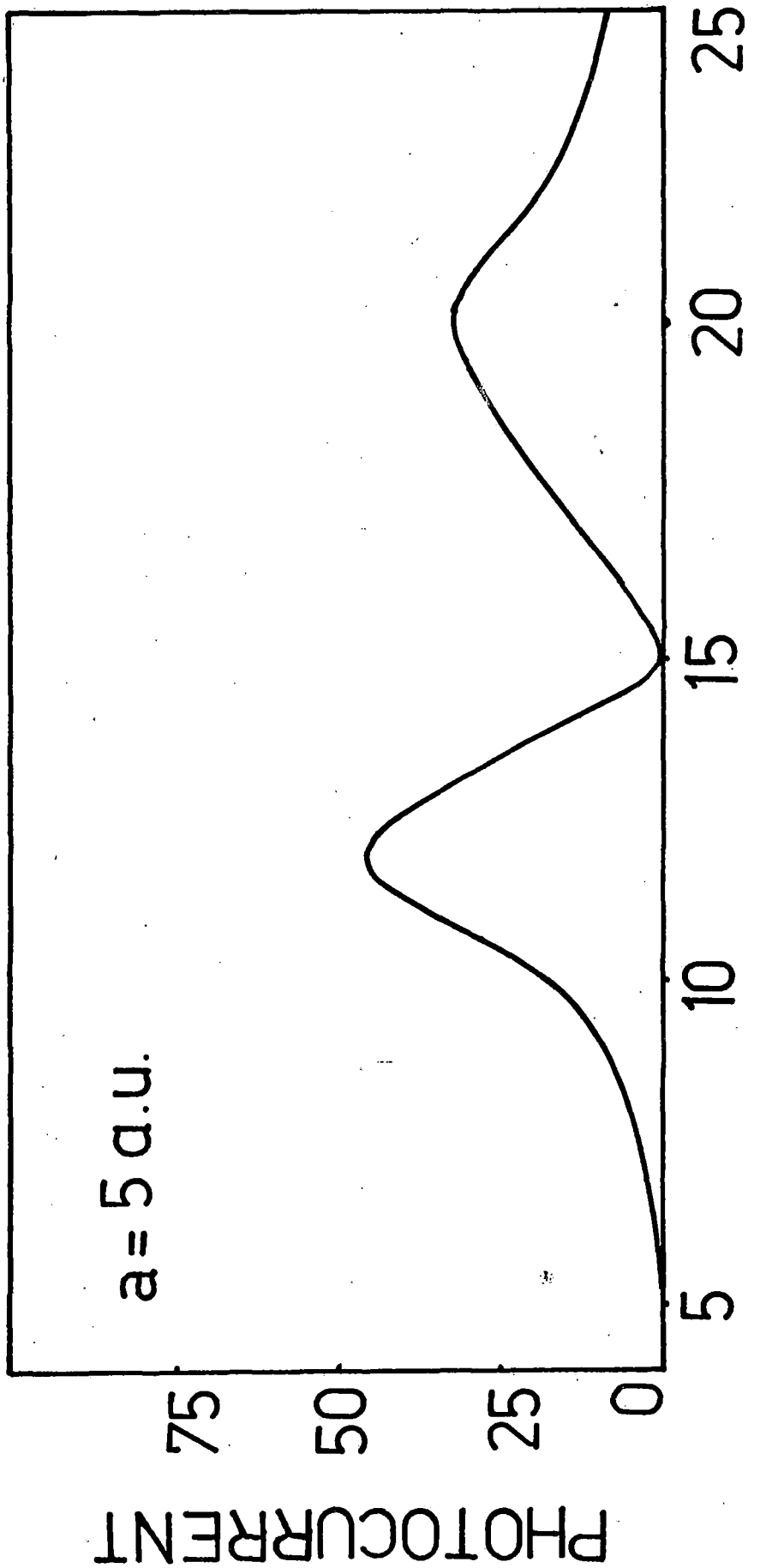

Figure 4.2

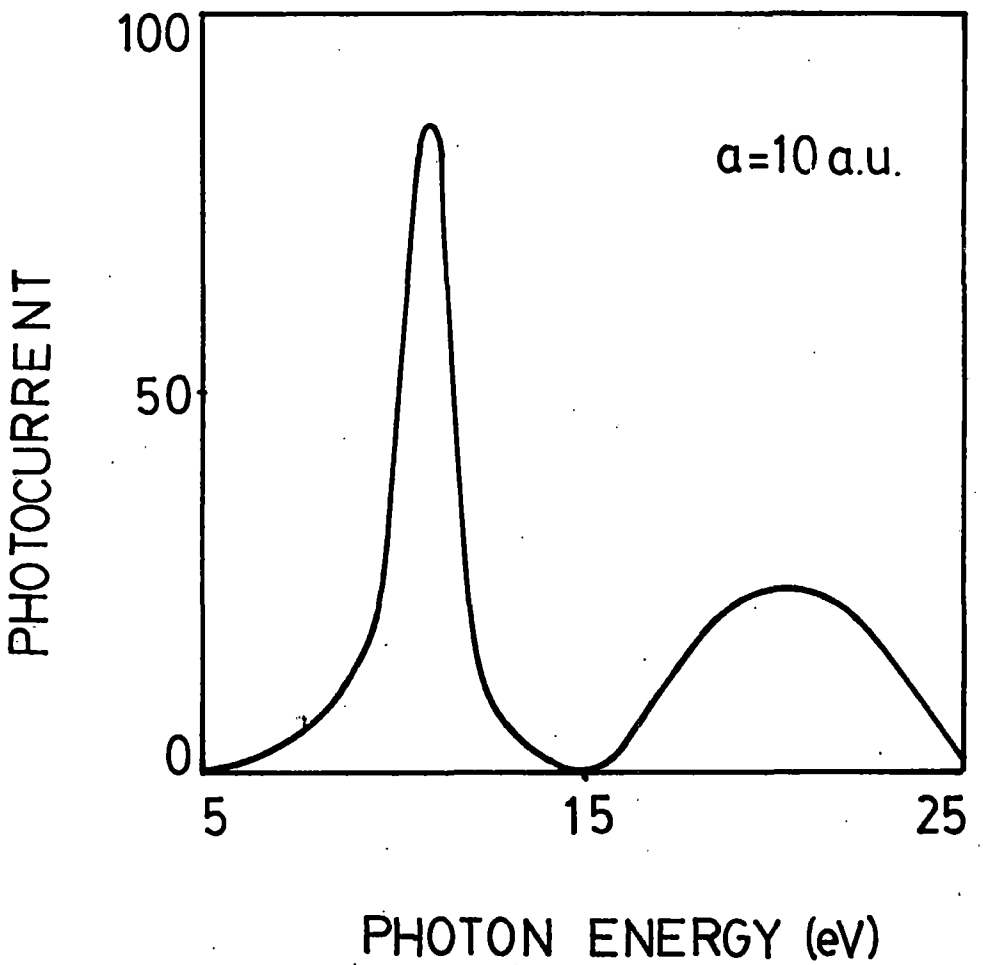

Figure 4.3

Interestingly, the results obtained with α=0.5 and a=10 a.u seem to be in better agreement with the experimental results than the free electron model. Fig. (4.4) shows the photocurrent data for aluminium with no surface region. In this case, there is no minimum at the plasmon energy and the behaviour is qualitatively different from the one obtained with the surface region. This clearly indicates the importance of including the surface region the conclusion which we also reached while doing the free electron model calculations.

We have also used[54] this model with the dielectric function of tungsten. The data used are those of Weaver[25]. We have kept the same Kronig-Penney parameters δ and g as before and we used the same E_i. The results for α=0.5 and a=10 a.u are shown in Fig. (4.5). As expected there is a minimum around the plasmon energy ($\hbar\omega_p$) which in this case is about 25 eV. There is a peak below $\hbar\omega_p$ and another broad one above it. In this respect the behaviour is similar to that obtained with aluminium dielectric functions. We also did a calculation without any surface region (Fig. 4.6) and again we find that the minimum at the plasmon energy is missing, rather there is a maximum at 27 eV. Experimental observations of photocurrent from the tungsten (100) surface state did show a minimum at $\hbar\omega_p$ and this supports our conclusion that the surface variation of the photon field is important in analysing this type of

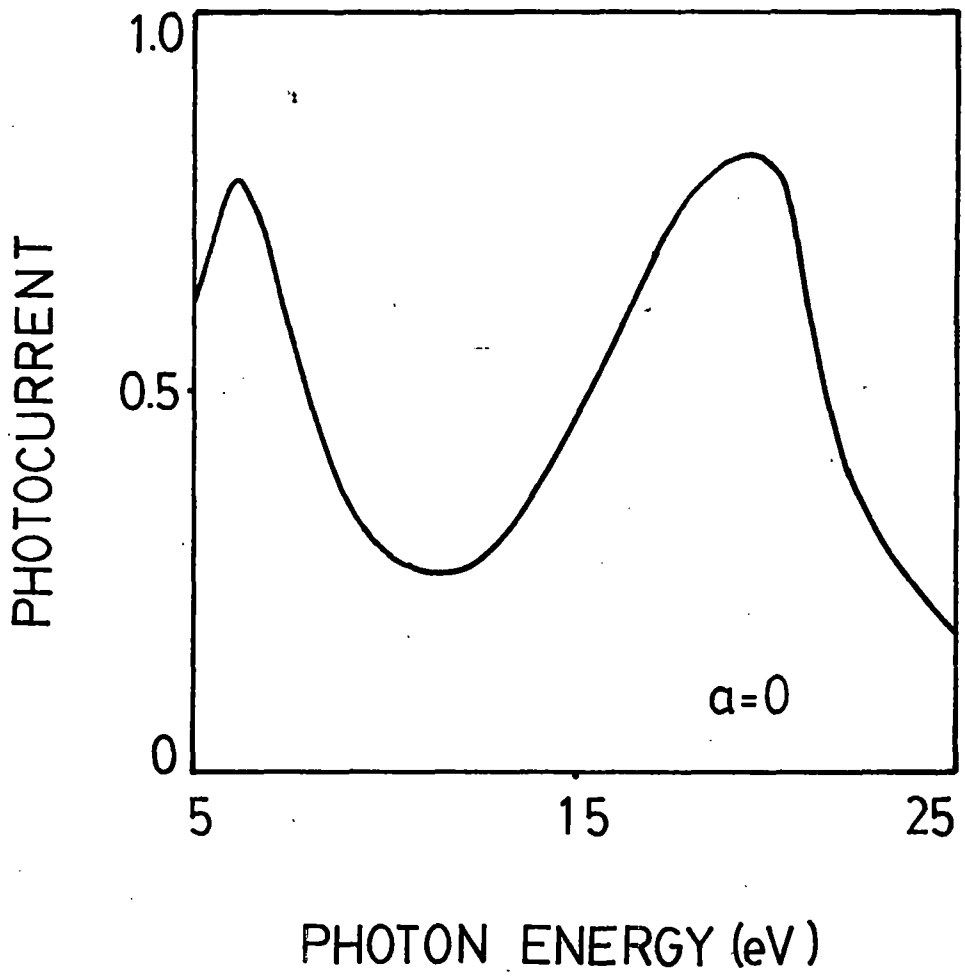

Figure 4.4

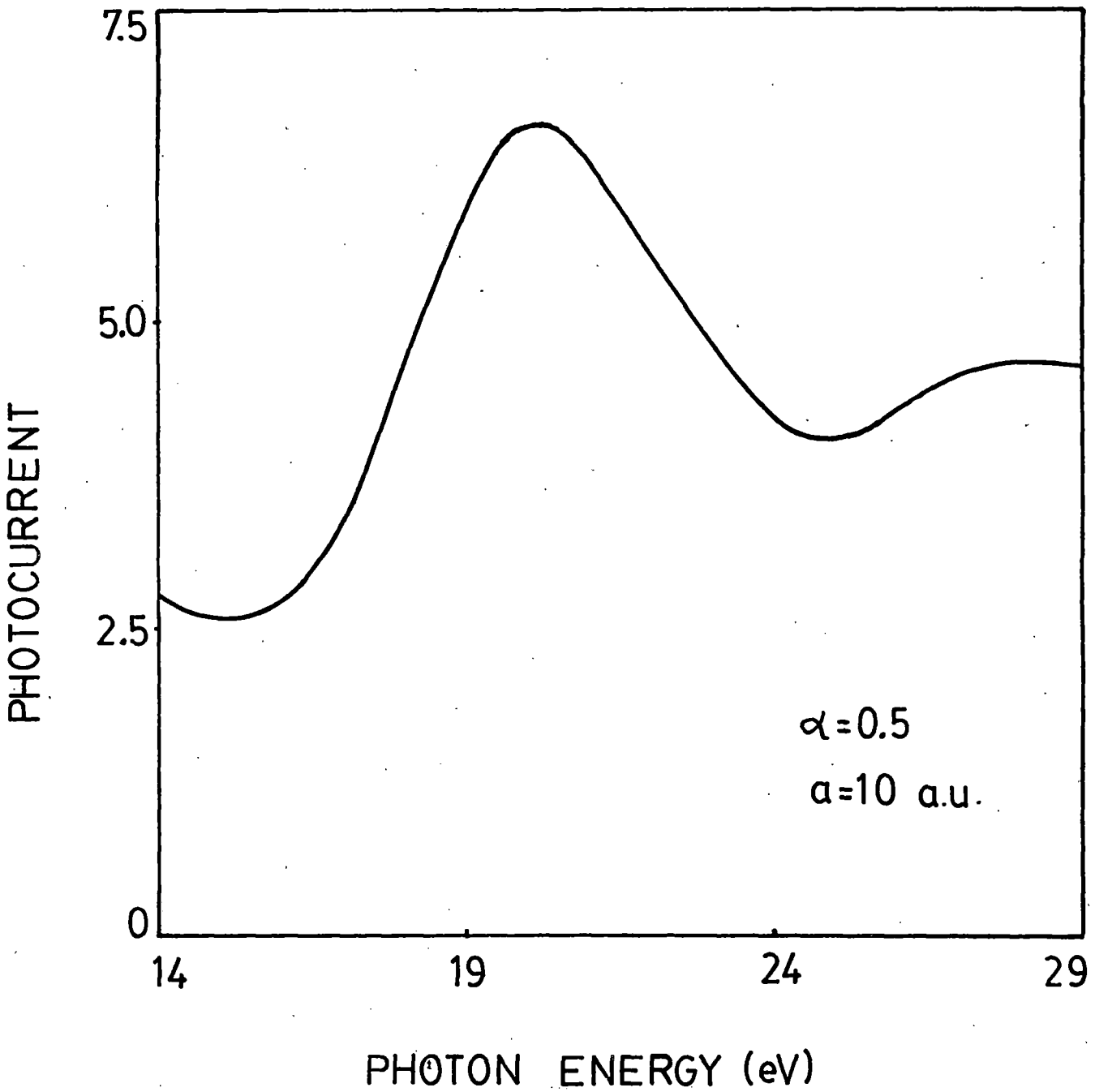

Figure 4.5

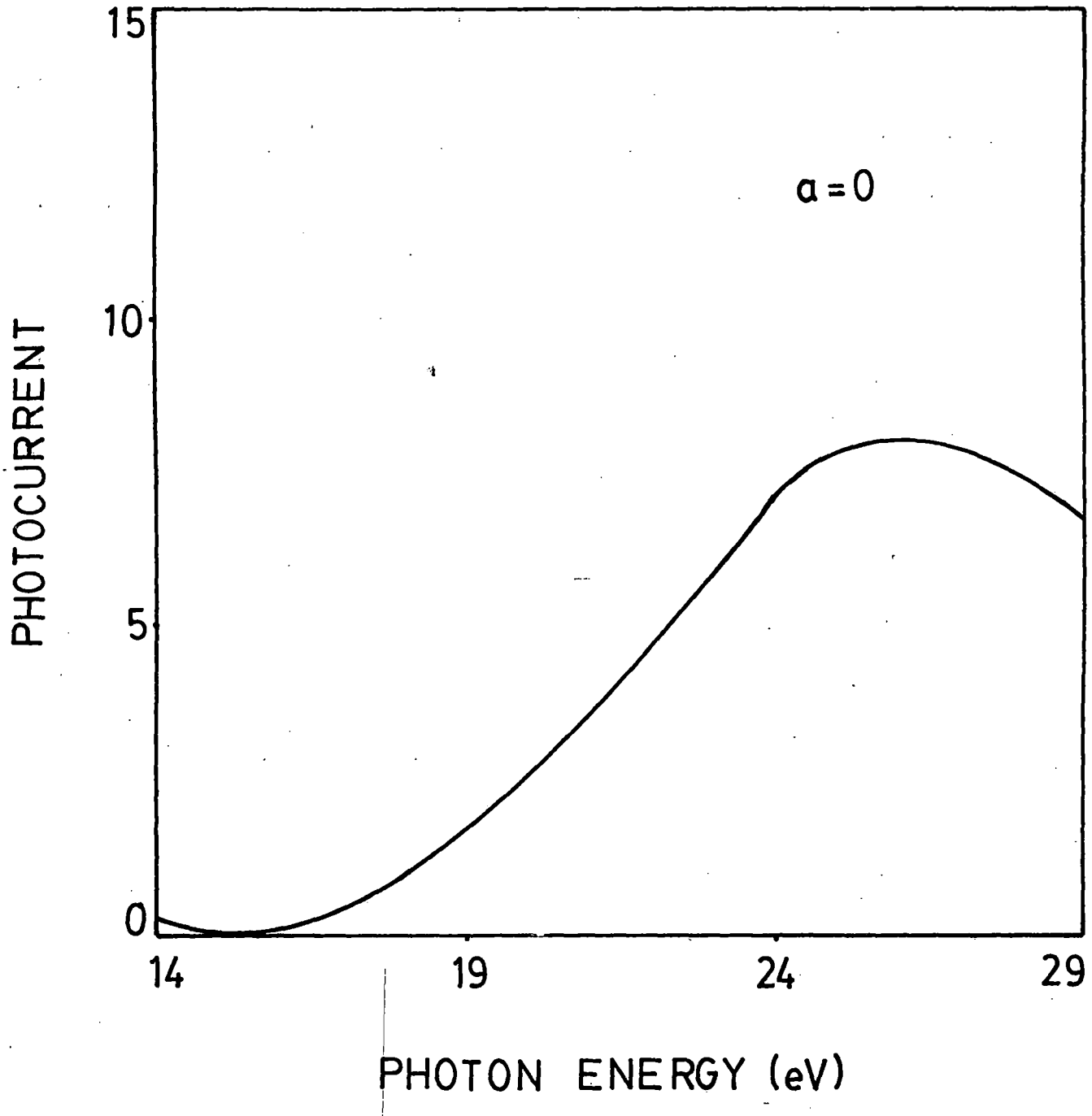

Figure 4.6

spectrum.

We have also used[54] this model in conjunction with the dielectric function $\varepsilon(\omega)$ for silicon as given by Edwards[53] which is a semiconductor and has somewhat different dielectric response. With the same Kronig-Penney parameters and the same E_i, the results for α=0.5 and a=10 a.u are shown in Fig. (4.7). As in other cases, there is a minimum at the plasmon energy around 16 eV. There is maximum below $\hbar\omega_p$ and the currrent rises also beyond $\hbar\omega_p$. But in this case, we see another minimum which is at 21 eV. The reason for this can be traced to the behaviour of $\varepsilon(\omega)$ for silicon which has a resonance in the region of 21 eV. This instability can be seen in Fig. (4.8) for $\varepsilon_1(\omega)$ and $\varepsilon_2(\omega)$ as a function of $\hbar\omega$. As a result of this, the fields inside the solid become vanishingly small (see Fig. 2.13) and consequently the photocurrent also shows a minimum. The photocurrent calculated with no surface region i.e., with Fresnel fields, as shown in (Fig. 4.9) shows no minimum at 16 eV or at 21 eV but it has a maximum at 21 eV. This again shows that the behaviour with and without the surface region is strikingly different.

We next changed the Kronig-Penney parameters g and δ with the new values being g=-0.1070 and δ=0.10, keeping everything else the same to see whether there is any marked change. We find that the behaviour is essentially the same as before which

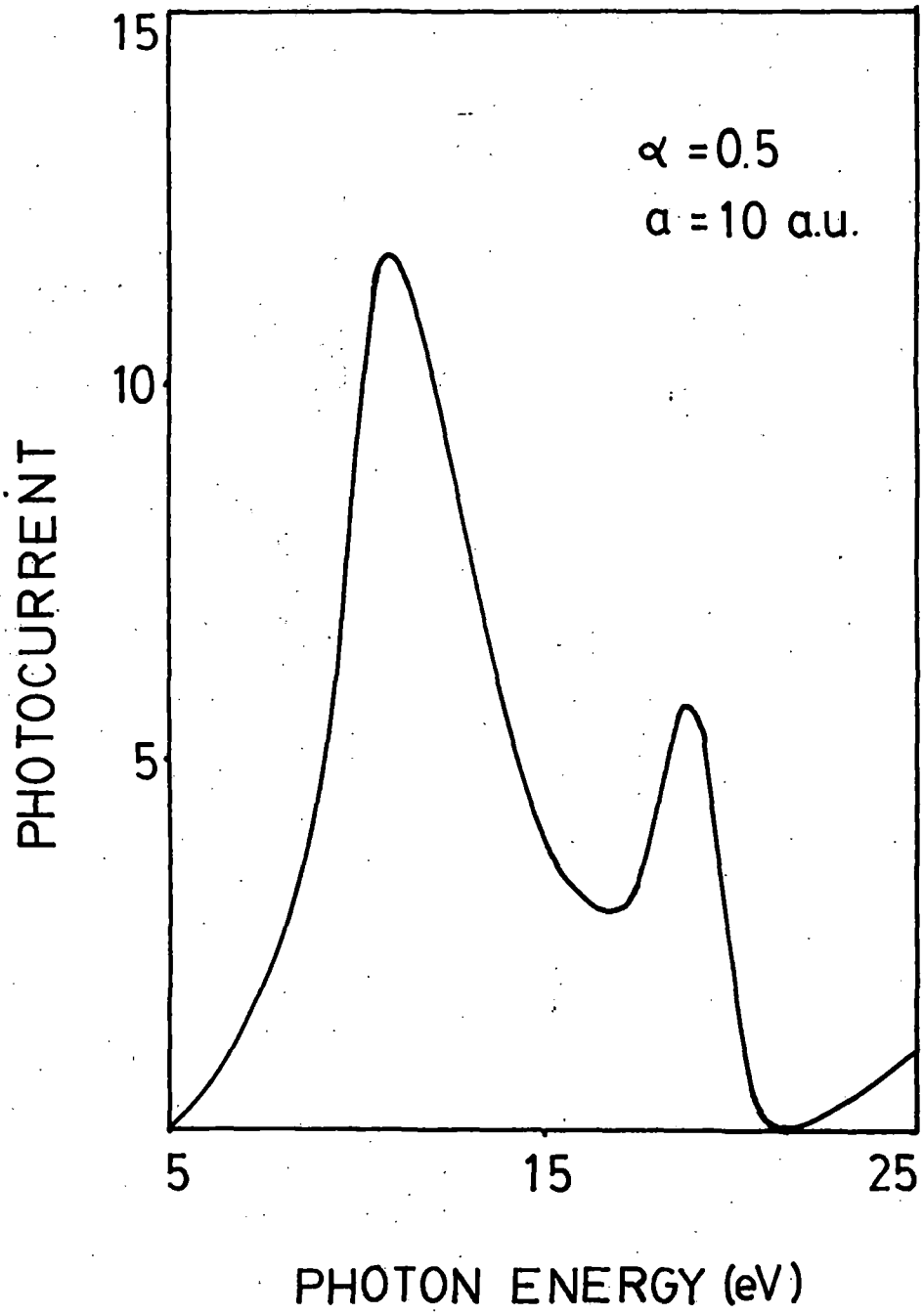

Figure 4.7

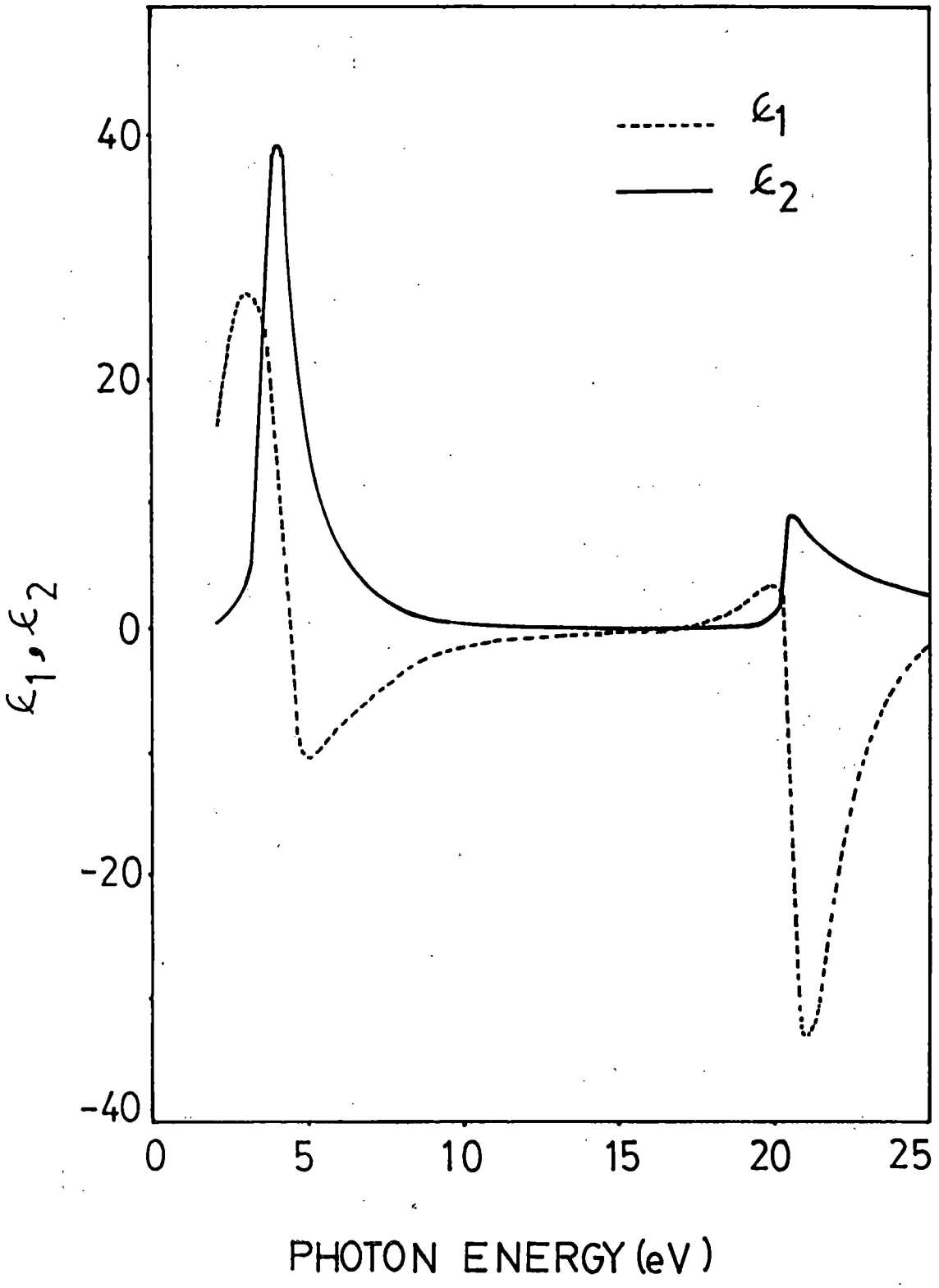

Figure 4.8

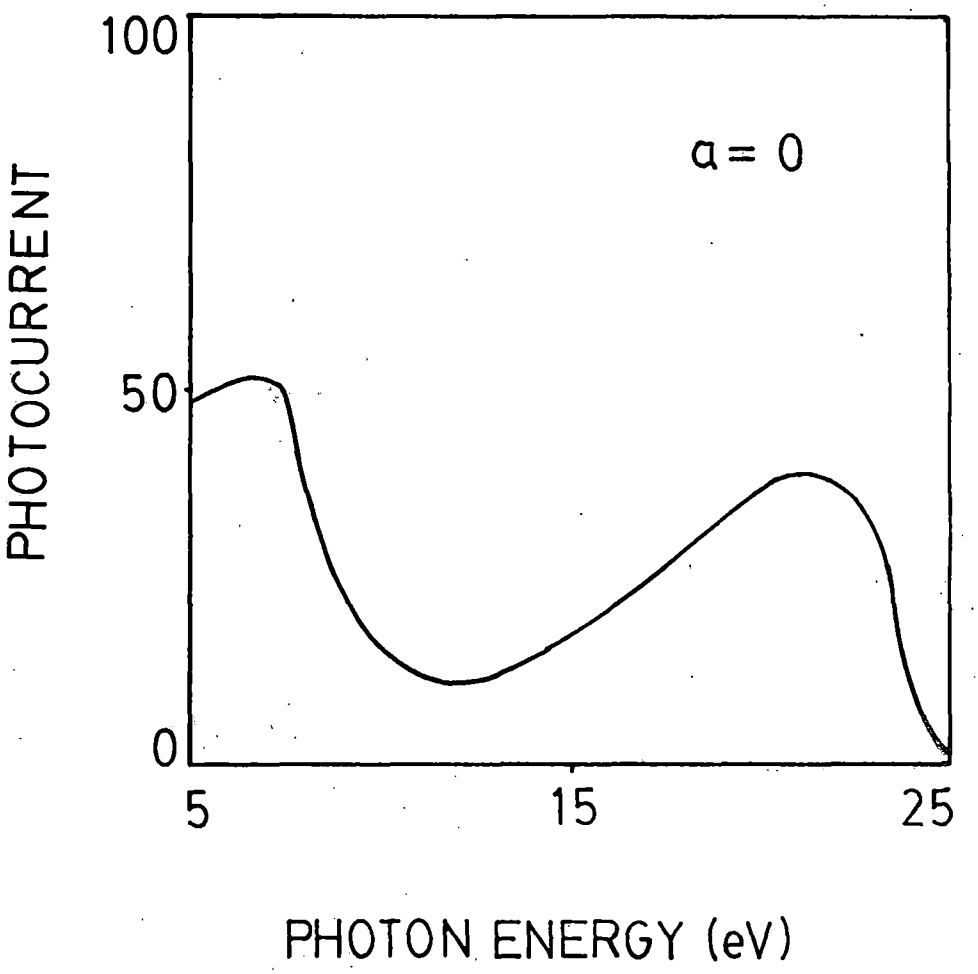

Figure 4.9

is shown in Fig. (4.10).

We have also used this model for calculating the photocurrent using the dielectric function $\varepsilon(\omega)$ of aluminium but with the surface region defined somewhat differently i.e., $-a \leq z \leq 0$ which is shown in Fig. (4.11). The parameters for the Kronig-Pennney model and the value of α and a are the same as used previously for Fig. (4.3) with the same E_i. The matrix element used for the photocurrent cross-section calculation may now be written as

$$I = \langle \psi_f | H' | \psi_i \rangle = \int_{-\infty}^{\infty} \psi_f^*(z) H' \psi_i(z) dz$$

$$= \int_{-\infty}^{-a} \psi_f^* \tilde{A}_\omega(z) \frac{d\psi_i}{dz} dz + \int_{-a}^{0} \psi_f^* \tilde{A}_\omega(z) \frac{d\psi_i}{dz} dz$$

$$+ \frac{1}{2} \int_{-a}^{0} \psi_f^* \frac{d\tilde{A}_\omega(z)}{dz} \psi_i dz + \int_{0}^{\infty} \psi_f^* \tilde{A}_\omega(z) \frac{d\psi_i}{dz} dz$$

There are now four terms as opposed to six terms for the previous case. The photocurrent computed for this case is shown in Fig. (4.12). The photocurrent shows a peak at photon energy 7 eV and a minimum near the plasmon energy of aluminium i.e.,15 eV. There is a second peak in the photocurrent at 20 eV. The ratio between the two peaks at 7 eV and 20 eV is 3 -comparable to the case of the surface region $-a/2 \leq z \leq a/2$. However, we

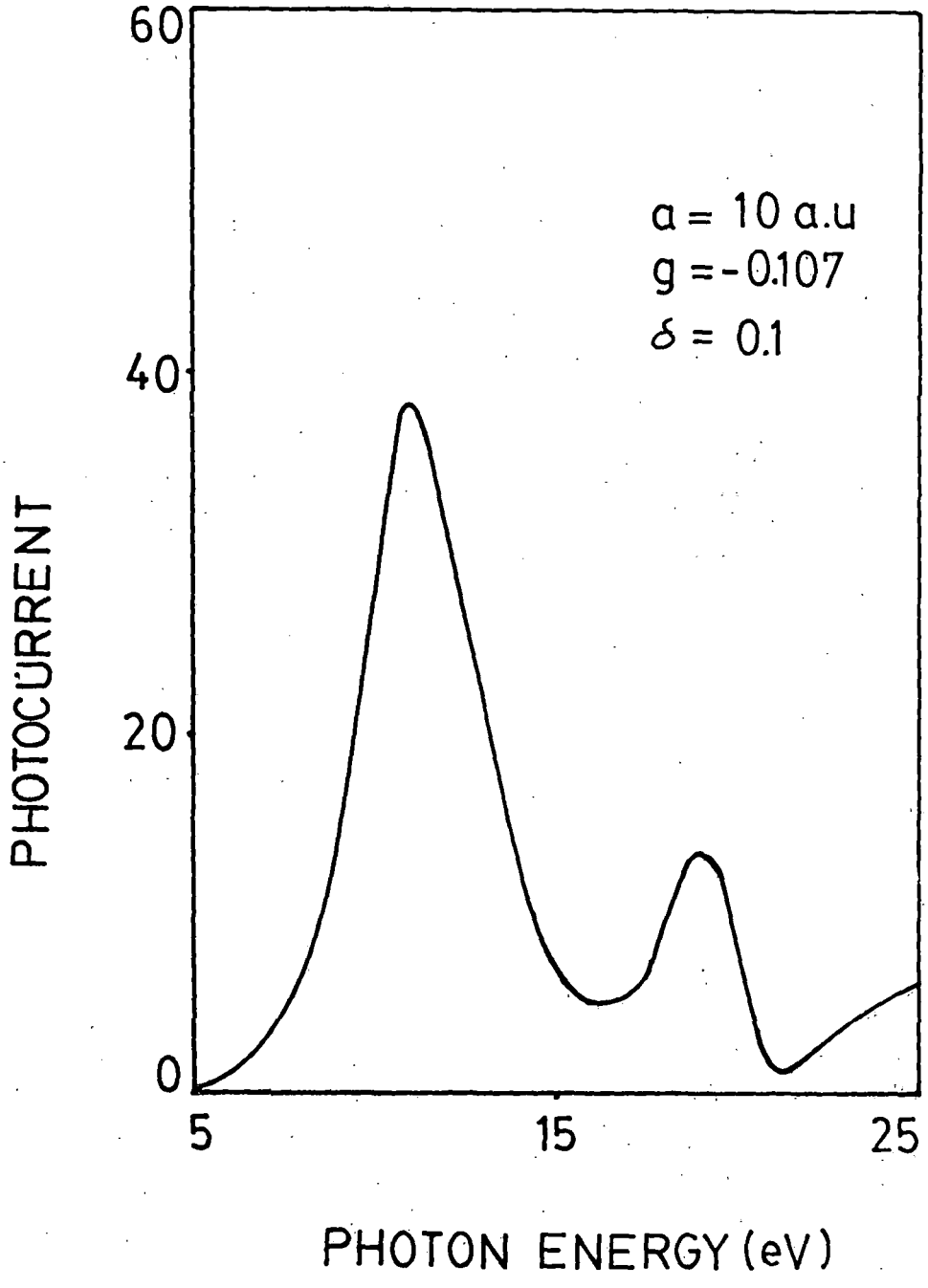
60
40
20
0
5
15
25
a = 10 a.u
g = -0.107
δ = 0.1
PHOTOCURRENT
PHOTON ENERGY (eV)

Figure 4.10

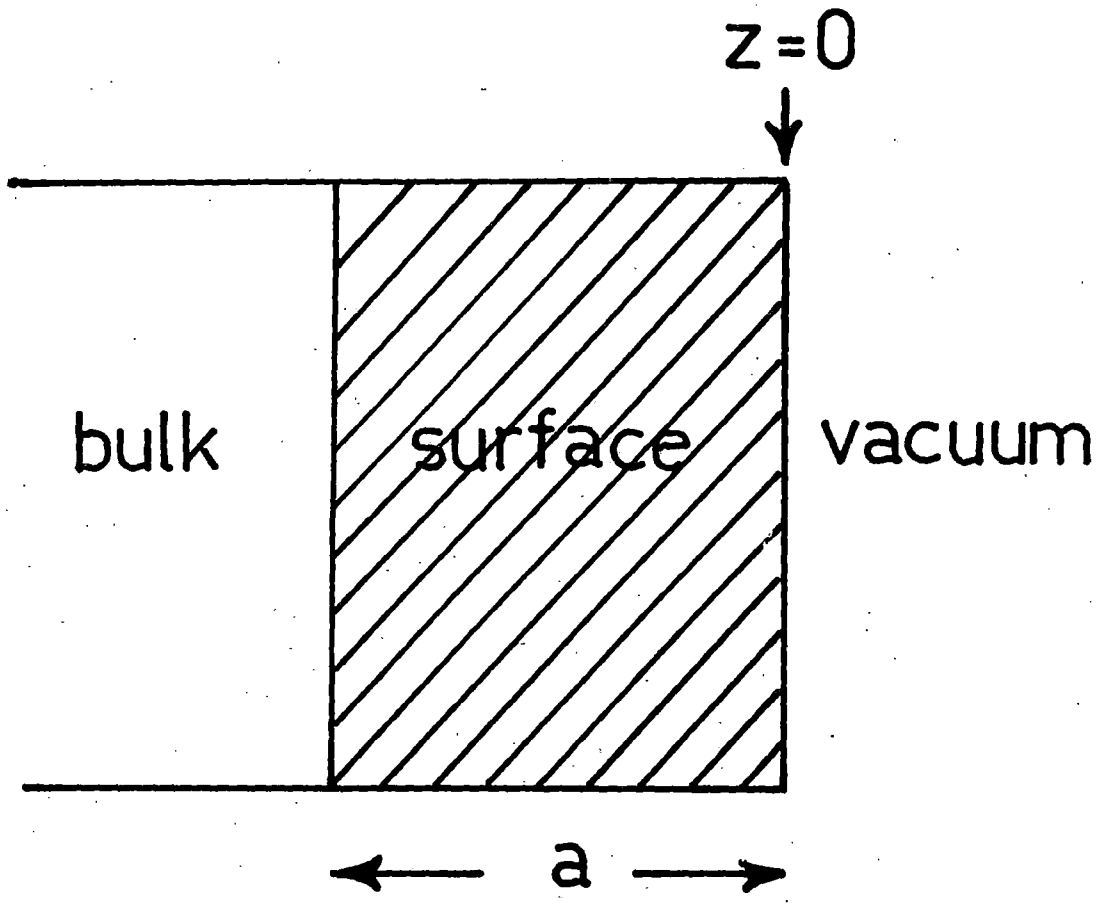

Figure 4.11 -

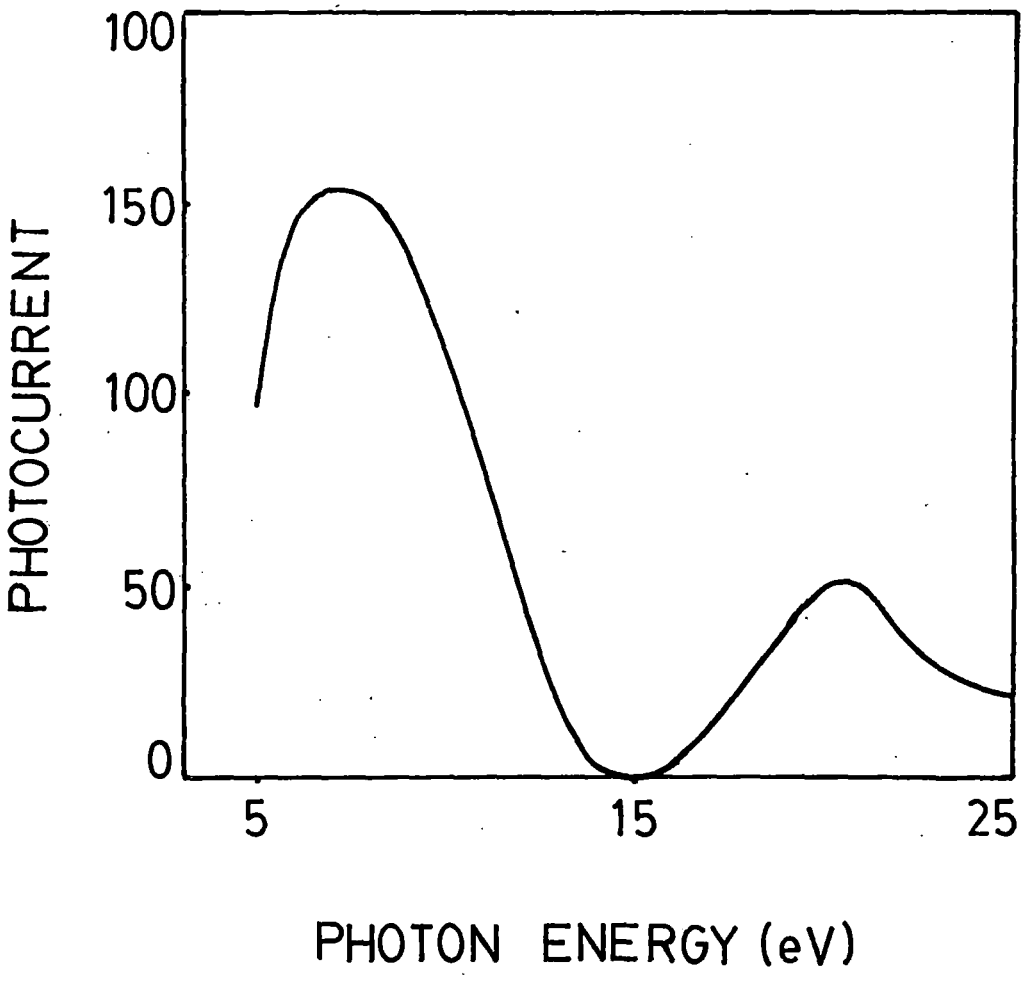

Figure 4.12

see that the peak before $\hbar\omega_p$ shifts in energy and becomes broader. We had calculated the photocurrent in this case also with a sharp surface and no surface region. The results are shown in Fig. (4.13). There is no minimum at the plasmon energy as in all the such cases.

A study of these cases shows that the surface variation of the photon field is important in calculating photoemission cross-section, since neglecting it fails to reproduce the minimum at the plasmon energy. We also see that using dielectric functions corresponding to different elements changes the results. All of these point to the fact that a full fledged photoemission calculation should include the correct variation of photon field near the surface.

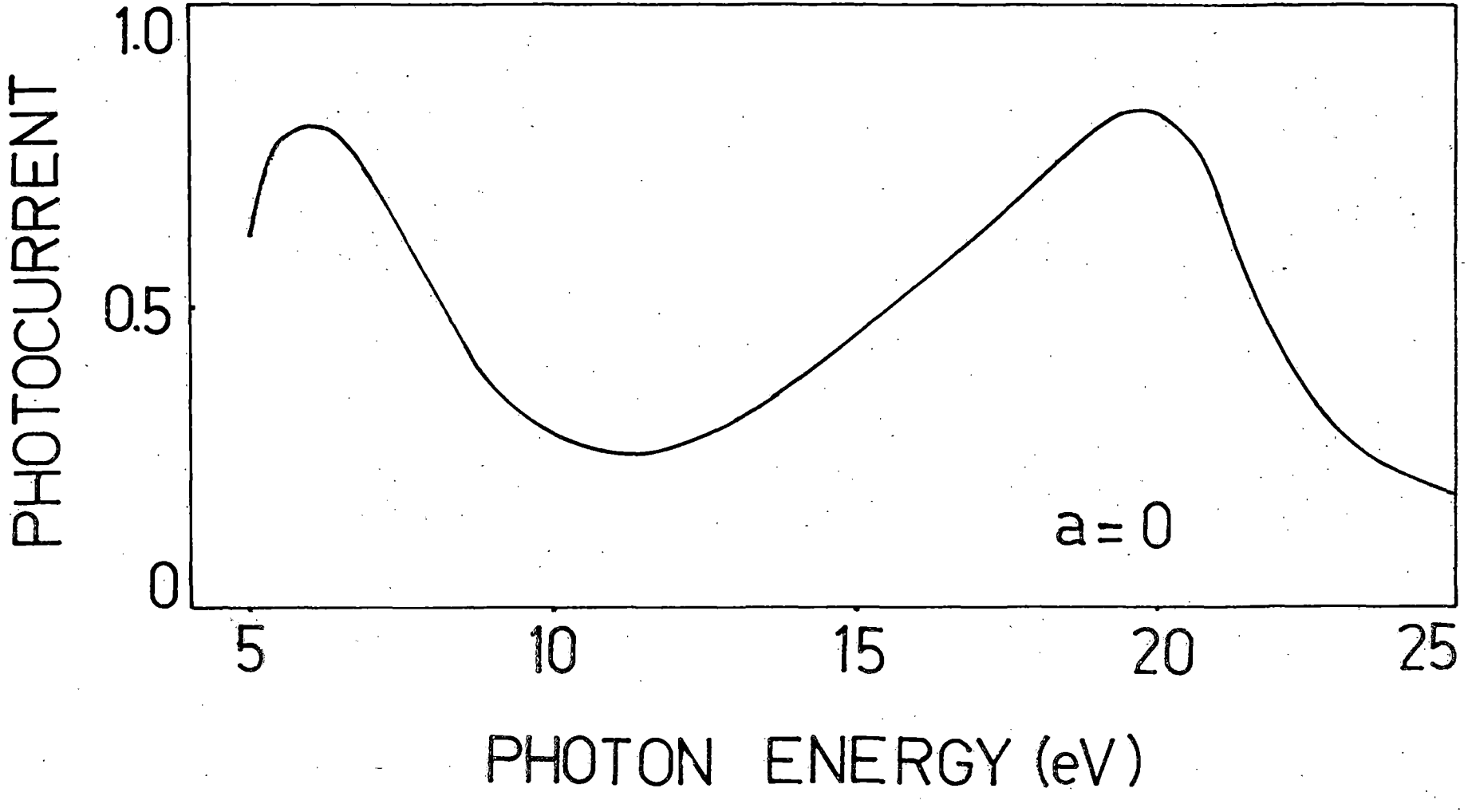

Figure 4.13

CHAPTER V

CONCLUSION

We have presented in this thesis the photoemission calculations by using a simple dielectric model as given by Bagchi and Kar[21]. We have calculated at first the variation of the electromagnetic field against the photon energy for planes located in the surface region. The solids for which the fields was calculated are the metals aluminium, silver, rhodium, molybdenum, palladium and the semiconductor silicon. In most cases we saw that instead of a monotonic behaviour, there was a lot of structure associated with the field variation, either as a function of energy or as a function of position.

We have next done a photoemission calculation with the photon field described as above and the initial and final state wavefunctions chosen to be free-electron wavefunctions in the presence of a surface. Since aluminium is a prototype free electron metal, numerical calculations were performed with the parameters appropriate for aluminium and the results compared with experimental data as well as previously calculated results. It was seen that qualitative agreement was obtained, even with this simple model.

As a first step towards including band structure effects, another model calculation was performed - this time considering

a Kronig - Penney model for the initial state wavefunction. As input for field calculation, the data for aluminium, tungsten and silicon were used, with the potential parameters kept the same. We could then see the influence of the optical parameters by comparing the results. As expected, the plasmon frequency has an important role in these calculations. It was seen that the photocurrent showed a peak at photon energy less than the plasmon energy and a minimum at the plasmon energy. Photocurrent calculations by using the same initial state and the final state wavefunctions was also done but with no surface region included. In this case the usual peak below the plasmon energy was not exhibited by the photocurrent data nor the minimum at the plasmon energy. This therefore led us to conclude that the inclusion of surface is important in photoemission calculations.

We have done photoemission calculations with simple models in this thesis. To include real band structure effects, we need a more realistic type of initial state wavefunction which in its true sense would be able to describe the actual configuration of the electronic states of the solids under investigation. However, we see that our calculations lead us to conclude that the spatial variation of electromagnetic field in the surface regions plays an important role during photoemission, which should be taken into account in more accurate photocurrent calculations.

REFERENCES

1 J. A. Appelbaum and D. R. Hamann, Phys. Rev., B6, 2166(1972).

2 G. P. Alldrege and L. Kliemann, Phys. Rev., B10, 559(1974)

3 G. D. Mahan, Phys. Rev. B2, 4332(1970), Phys. Rev. Lett., 24, 1066(1970).

4 W. L. Schaich and N. W. Ashcroft, Phys. Rev., B3, 2452(1971).

5 R. E. B. Makinson, Proc. R. Soc. London, A162, 367(1937).

6 T. Maniv and H. Metiv, Phys. Rev., B22, 4731(1980).

7 D. R. Penn, Phys. Rev. Lett., 28, 1041(1972).

8 J. G. Endriz, Phys. Rev., B7, 3464(1973).

9 H. Petersen and S. B. M. Hagstrom, Phys. Rev. Lett., 41, 1314(1978).

10 I. Adawi, Phys. Rev., 134, A788(1964).

11 A. Leibsch, Phys. Rev. Lett., 32, 1203(1973).

12 J. B. Pendry, Surf. Sci., 57, 679(1976).

13 P. J. Feibelman, Phys. Rev., B12, 1319(1975), Phys. Rev. Lett., 34, 1092(1975).

14 H. J. Levinson, E. W. Plummer and P. J. Feibelman, Phys. Rev. Lett., 43, 952(1979).

15 G. Mukhopadhayay and S. Lundqvist, Physica Scripta, 17, 69 (1978).

16 A. Bagchi, Phys. Rev., B5, 3060(1977).

17 K. L. Kliewer, Phys. Rev., B14, 1412(1976).

18 F. Forstman and H. Stenschke, Phys. Rev. Lett., 38, 1365(1977).

19 K. Kempa and F. Forstman, Surf. Sci., 129, 516(1983).

20 N. Barberan and J. E. Inglesfield, J. Phys., C14, 3114(1981).

21 A. Bagchi and N. Kar, Phys. Rev., B18, 5248(1978).

22 A. Bagchi, N. Kar and R. G. Barrera, Phys. Rev. Lett., 40, 803(1978).

23 R. K. Thapa and N. Kar, Indian J. Phys, 64A, 321(1990).

24 R. K. Thapa, P. Das and N. Kar, Eight Colloquium of Young Physicists, August 21 - 22, 1990, Saha Institute of Nuclear Physics, Calcutta published in Phys Teacher, 33, 221(1991).

25 J. H. Weaver, Handbook of Chemistry and Physics (Boca Raton, Florida, CRC Press, Ohio), 68-th edition, page E-377.

26 J. A . Appelbauam, Surface Physics of Materials, ed J. H. Blakely, Vol-I (Academic Press, New York) 1975, page 77.

27 R. K. Thapa, Indian J. Pure and Appld. Phys., 28, 357(1990).

28 R. K. Thapa, P. Das, N. Kar and R. A. Lal, Bull. Mat. Sci., 16, 29(1993).

29 C. N. Berguland and W. E. Spicer, Phys. Rev., 136A, 1044(1964).

30 S. -L. Weng, T. Gustaffson and E. W. Plummer, Phys. Rev. Lett., 39, 822(1978).

31 R. K. Thapa, N. Kar and R. A. Lal, Indian J. Pure and Appld. Phys., 29, 453(1991).

32 L. F. Wagner and W. E. Spicer, Phys. Rev. Lett., 28, 1381(1972).

33 D. E. Eastman and W. D. Grobman, Phys. Rev. Lett., 28, 1378(1972).

34 F. G. Allen and G. W. Gobelli, Phys. Rev., 150, 127(1962).

35 J. van Laar and J. J. Scheer, Surf. Sci., 8, 342(1967).

36 R. E. Schlier and H. E. Farnsworth, J. Chem. Phys., 30, 917(1959), W. Monch, Festhorperppproblem XIII, 241, Vieweg(1979).

37 H. D. Shih, F. Jona, D. W. Jepsen and P. M. Marcus, Phys. Rev. Lett., 37, 1622(1976).

38 R. H. Fowler, Proc. R. Soc., London, A118(1928).

39 K. Mitchell, Proc. R. Soc., London, A146, 443(1934).

40 Ig. Tamm and S. Schubin, Z. Phys, 68, 97(131).

41 J. G. Endriz and W. E. Spicer, Phys. Rev. Lett., 27, 570(1971).

42 S. A. Flosdström and J. G. Endriz, Phys. Rev. Lett., 31, 893(1973).

43 N. W. Ashcroft and N. D. Mermine, Solid State Physics (Holt, Reinhaert and Winston, New York, 1976) page 38.

44 P. Das, R. K. Thapa and N. Kar, Mod. Phys Lett., B5, 65(1991).

45 Ig. Tamm, Phys. Z. Souvjjet, 1, 733(1932)

46 A. W. Maue, Z. Physik, 94, 717(1935).

47 W. Shockley, Phys. Rev.,56, 317(1939).

48 S. G. Davison and J. D. Levine, Solid State Physics, 25, 2(1970).

49 M. Steslicka, Prog. Surf. Sci., 5, 157(1974).

50 A. M. Eldib, H. F. Hasson and M. A. Mohmad, J. Phys., C20, 3011(1987).

51 R. K. Thapa and N. Kar, Indian J. Pure and Appld. Phys., 26, 620(1988).

52 N. W. Ashcroft and N. D. Mermine, Solid State Physics (HRW International Editions, 1976), page 146.

53 D. F. Edwards, Handbook of Optical Constants of Solids, eds. E. P. Pallik (Orlando Academic Press, 1985) page 555.

54 R. K. Thapa, P. Das and N. Kar, International J. Mod. Phys., B, (Communicated).

APPENDIX I

CALCULATIONS OF PHOTOCURRENT BY USING THE FREE ELECTRON WAVEFUNCTIONS

We will derive here the complete formula used for the calculation of photoemission cross-section by using the free electron wavefunctions. Rewriting Eq. (3.2), the formula for the photocurrent cross-section can be written as

$$\frac{d\sigma}{d\Omega} = \frac{k^2}{\omega} |\langle \psi_f | H' | \psi_i \rangle|^2 = \frac{k^2}{\omega} |I|^2 \qquad (A-1)$$

The integral I in Eq. (A-1) can be written as

$$I = \int_{-\infty}^{+\infty} \psi_f^*(z) \left[\tilde{A}_\omega(z) \frac{d}{dz} + \frac{1}{2} \frac{d}{dz} \tilde{A}_\omega(z) \right] \psi_i(z)\, dz \qquad (A-2)$$

Since we are considering normal photoemission, the one electron initial state wavefunction $\psi_i(z)$ of Eq. (3.11) can be written as

$$\psi_i(z) = \begin{cases} \left(\frac{m}{2\pi\hbar^2 k_i}\right)^{1/2} \left[e^{ik_i z} + \frac{ik_i + \varkappa}{ik_i - \varkappa} e^{-ik_i z} \right], & z<0 \\ \left(\frac{m}{2\pi\hbar^2 k_i}\right)^{1/2} \frac{2ik_i}{ik_i - \varkappa} e^{-\varkappa z}, & z>0 \end{cases} \qquad (A-3)$$

where $k_i^2 = \frac{2mE_i}{\hbar^2}$, $\varkappa^2 = \frac{2m}{\hbar^2}(V_o - E_i)$. (A-4)

Similarly from Eq. (3.13), one dimensional final state wavefunction is given by

$$\psi_f(z) = \begin{cases} \left(\frac{m}{2\pi\hbar^2 q}\right)^{1/2} \frac{2q}{q + k_f} e^{-\alpha|z|} e^{ik_f z}, & z<0 \\ \left(\frac{m}{2\pi\hbar^2 q}\right)^{1/2} \left[e^{iqz} + \frac{q - k_f}{q + k_f} e^{-iqz} \right], & z>0 \end{cases} \qquad \text{(A-5)}$$

In Eq.(A-5) above, we have

$$k_f^2 = 2mE_f/\hbar^2, \qquad q^2 = (2m/\hbar^2)(E_f - V_o) \quad \text{and} \quad E_f = E_i + \hbar\omega.$$

Rewriting the photon field vector $\tilde{A}_\omega(z)$ from Eq.(2.5), we have

$$\tilde{A}_\omega(z) = \frac{E_\omega^z(z)}{E_o} =$$

$$\begin{cases} -\dfrac{\sin 2\theta_i}{\left[\varepsilon(\omega) - \sin^2\theta_i\right]^{1/2} + \varepsilon(\omega)\cos\theta_i}, & z \le -a/2 \\ -\dfrac{\sin 2\theta_i}{\frac{z}{a} + \frac{1}{2}\frac{1 + \varepsilon(\omega)}{1 - \varepsilon(\omega)}} \cdot \dfrac{\varepsilon(\omega)/[1 - \varepsilon(\omega)]}{\left[\varepsilon(\omega) - \sin^2\theta_i\right]^{1/2} + \varepsilon(\omega)\cos\theta_i}, & -a/2 \le z \le -a/2 \\ -\dfrac{\varepsilon(\omega)\sin 2\theta_i}{\left[\varepsilon(\omega) - \sin^2\theta_i\right]^{1/2} + \varepsilon(\omega)\cos\theta_i}, & z \ge a/2 \end{cases} \qquad \text{(A-6)}$$

For the surface region $-a/2 \leq z \leq a/2$, $\tilde{A}_\omega(z)$ is given by

$$\tilde{A}_\omega(z) = - A_1 \frac{\varepsilon(\omega)/[1 - \varepsilon(\omega)]}{\left(\frac{z}{a} + B_1 \right)}$$

where $$A_1 = \frac{\sin 2\theta_i}{[\varepsilon(\omega) - \sin^2\theta_i]^{1/2} + \varepsilon(\omega)\cos\theta_i},$$

and $$B_1 = \frac{1}{2} \frac{1 + \varepsilon(\omega)}{1 - \varepsilon(\omega)} .$$

For band state (Fermi level) photoemission calculations, integral I in Eq. (A-2) can be expanded as

$$I = \int_{-\infty}^{-a/2} \psi_f^* \tilde{A}_\omega(z) \frac{d\psi_i(z)}{dz} dz + \int_{-a/2}^{0} \psi_f^* \tilde{A}_\omega(z) \frac{d\psi_i(z)}{dz} dz$$

$$+ \frac{1}{2} \int_{-a/2}^{0} \psi_f^* \frac{d\tilde{A}_\omega(z)}{dz} \psi_i \, dz + \int_{0}^{a/2} \psi_f^* \tilde{A}_\omega(z) \frac{d\psi_i(z)}{dz} dz$$

$$+ \frac{1}{2} \int_{0}^{a/2} \psi_f^* \frac{d\tilde{A}_\omega(z)}{dz} \psi_i \, dz + \int_{a/2}^{\infty} \psi_f^* \tilde{A}_\omega(\omega) \frac{d\psi_i(z)}{dz} dz \qquad (A-7)$$

Using Eqs. (A-3), (A-5) and (A-6), the integrals in Eq. (A-7) can be written in the following way:

$$I_1 = \int_{-\infty}^{-a/2} \psi_f^* \tilde{A}_\omega(z) \frac{d\psi_i(z)}{dz} dz$$

$$= 2i\left(\frac{m}{2\pi\hbar^2}\right)\left(\frac{qk_i}{q+k_f}\right)^{1/2} A_1 \left[\frac{e^{-\alpha a/2}}{\alpha + ik_i - ik_f} e^{-i(k_i-k_f)a/2} - \frac{ik_i+\varkappa}{ik_i-\varkappa} \cdot \frac{e^{-\alpha a/2}}{\alpha - ik_i - ik_f} e^{-i(k_i+k_f)a/2}\right].$$

$$I_2 = \int_{-a/2}^{0} \psi_f^* \tilde{A}_\omega(z) \frac{d\psi_i(z)}{dz} dz$$

$$= 2i\left(\frac{m}{2\pi\hbar^2}\right)\left(\frac{qk_i}{q+k_f}\right)^{1/2} \frac{A_1\varepsilon(\omega)}{1-\varepsilon(\omega)} \left[\int_{-a/2}^{0} e^{\alpha z} \frac{e^{i(k_i-k_f)z}}{(\frac{z}{a}+B_1)} dz - \frac{ik_i+\varkappa}{ik-\varkappa} \int_{-a/2}^{0} e^{\alpha z} \frac{e^{-i(k_i+k_f)z}}{(\frac{z}{a}+B_1)} dz\right].$$

$$I_3 = \frac{1}{2}\int_{-a/2}^{0} \psi_f^* \frac{d\tilde{A}_\omega(z)}{dz} \psi_i dz$$

$$= -\left(\frac{m}{2\pi\hbar^2}\right)\left(\frac{q}{k_i}\right)^{1/2} \frac{A_1}{q+k_f} \frac{\varepsilon(\omega)}{[1-\varepsilon(\omega)]} \cdot \left[\int_{-a/2}^{0} \frac{e^{\alpha z} e^{i(k_i-k_f)z}}{(\frac{z}{a}+B_1)^2} dz + \frac{ik_i+\varkappa}{ik_i-\varkappa} \int_{-a/2}^{0} \frac{e^{\alpha z} e^{-i(k_i+k_f)z}}{(\frac{z}{a}+B_1)^2} dz\right]$$

$$I_4 = \int_0^{a/2} \psi_f^* \tilde{A}_\omega(z) \frac{d\psi_i(z)}{dz} dz$$

$$= -2i \left(\frac{m}{2\pi\hbar^2}\right)\left(\frac{k_i}{q}\right)^{1/2} \frac{\varkappa}{ik_i-\varkappa} \frac{A_1\varepsilon(\omega)}{[1-\varepsilon(\omega)]} \cdot$$

$$\left[\int_0^{a/2} \frac{e^{-iqz}\, e^{-\varkappa z}}{(\frac{z}{a}+A_1)}\, dz + \frac{q-k_f}{q+k_f} \int_0^{a/2} \frac{e^{iqz}\, e^{-\varkappa z}}{(\frac{z}{a}+B_1)}\, dz\right]$$

$$I_5 = \frac{1}{2}\int_0^{a/2} \psi_f^* \frac{d\tilde{A}_\omega(z)}{dz} \psi_i\, dz$$

$$= -i\left(\frac{m}{2\pi\hbar^2}\right)\left(\frac{k_i}{q}\right)^{1/2} \frac{A_1}{a(\varkappa-ik_i)} \frac{\varepsilon(\omega)}{[1-\varepsilon(\omega)]} \cdot$$

$$\left[\int_0^{a/2} \frac{e^{-iqz}\, e^{-\varkappa z}}{(\frac{z}{a}+B_1)^2}\, dz + \frac{q-k_f}{q+k_f} \int_0^{a/2} \frac{e^{iqz}\, e^{-\varkappa z}}{(\frac{z}{a}+B_1)^2}\, dz\right] .$$

$$I_6 = \int_{a/2}^{\infty} \psi_i^* \frac{d\psi_i(z)}{dz} \tilde{A}_\omega(z)\, dz$$

$$= 2i \left(\frac{m}{2\pi\hbar^2}\right)^{1/2} \left(\frac{k_i}{q}\right)^{1/2} \frac{\varkappa}{ik_i-\varkappa} A_1\varepsilon(\omega) .$$

$$\left[\frac{e^{-iqa/2}\, e^{-\varkappa a/2}}{iq+\varkappa} + \frac{q-k_f}{q+k_f} \frac{e^{iqa/2}\, e^{-\varkappa a/2}}{\varkappa - iq}\right]$$

In terms of I_1, I_2, I_3 ...., integral I in Eq. (A-7) can be written as

$$I = I_1+I_2+I_3+I_4+I_5+I_6 .$$

Therefore the photocurrent formula of Eq. (A-1) can be evaluated as

$$I = \frac{k^2}{\omega} |I_1+I_2+.....+I_6|^2 \qquad (A-8)$$

As the integrals I_2, I_3, I_4 and I_5 cannot be evaluated analytically, the integrals were calculated by numerical method. The fortran program developed for this is discussed in appendix III.

For the surface state photoemission calculations, the contributions of the integrals to photoemission calculations in the regions $-\infty$ to $-a/2$ and $a/2$ to ∞ is negligibly small. Therefore Eq. (A-7) can be written as

$$I = \int_{-a/2}^{0} \psi_f^* \tilde{A}_\omega(z) \frac{d\psi_i(z)}{dz} dz + \frac{1}{2} \int_{-a/2}^{0} \psi_f^* \frac{d\tilde{A}_\omega(z)}{dz} \psi_i \, dz$$
$$+ \int_{0}^{a/2} \psi_f^* \tilde{A}_\omega(z) \frac{d\psi_i(z)}{dz} dz + \frac{1}{2} \int_{0}^{a/2} \psi_f^* \frac{d\tilde{A}_\omega(z)}{dz} \psi_i \, dz \qquad (A-9)$$

Initial state wavefunction $\psi_i(z)$ was replaced by

$$\psi_i(z) = \left(\frac{2\beta}{\pi\hbar^2}\right)^{1/4} e^{-\beta(z-z_o/a)^2} \qquad (A-10)$$

where β describes the width of the Gaussian wavefunction (A-10) and z_o is the location of the nominal surface plane. For final state wavefunction $\psi_f(z)$ and $\tilde{A}_\omega(z)$, Eqs. (A-5) and (A-6) are used. Putting these in Eq. (A-9), each integral is computed as

follows:

$$I_1^s = \int_{-a/2}^{0} \psi_f^* \tilde{A}_\omega(z) \frac{d\psi_i(z)}{dz} dz$$

$$= -4\left(\frac{m}{2\pi\hbar^2}\right)^{1/2} \frac{\beta\varepsilon(\omega)A_1}{[1-\varepsilon(\omega)]} \frac{q^{1/2}}{q+k_f} \cdot$$

$$\int_{-a/2}^{0} e^{-\beta(z-z_o)^2} \frac{z-z_o}{(\frac{z}{a}+B_1)} (\cos k_f z - i\sin k_f z)\, dz.$$

$$I_2^s = \frac{1}{2} \int_{-a/2}^{0} \psi_f^* \frac{d\tilde{A}_\omega(z)}{dz} \psi_i\, dz$$

$$= -\left(\frac{m}{2\pi\hbar^2}\right)^{1/2} \frac{A_1\varepsilon(\omega)}{a[1-\varepsilon(\omega)]} \frac{q^{1/2}}{q+k_f} \int_{-a/2}^{0} \frac{e^{-\beta(z-z_o)^2} e^{-ik_f z}}{(\frac{z}{a}+B_1)^2} dz$$

$$I_3^s = \int_{0}^{a/2} \psi_f^* \tilde{A}_\omega(z) \frac{d\psi_i(z)}{dz} dz$$

$$= -4\left(\frac{m}{2\pi\hbar^2}\right)^{1/2} \frac{\beta A_1}{q^{1/2}} \frac{\varepsilon(\omega)}{[1-\varepsilon(\omega)]} \cdot$$

$$\int_{0}^{a/2} \left[e^{-iqz} + \frac{q-k_f}{q+k_f} e^{iqz} \right] \frac{z-z_o}{(\frac{z}{a}+B_1)} e^{-\beta(z-z_o)^2} dz$$

$$I_4^s = \frac{1}{2} \int_{0}^{a/2} \psi_f^* \frac{d\tilde{A}_\omega(z)}{dz} \psi_i\, dz$$

$$= \left(\frac{m}{2\pi\hbar^2 q}\right)^{1/2} \frac{A_1 \varepsilon(\omega)\beta}{a[1-\varepsilon(\omega)]} \cdot$$

$$\int_0^{a/2} \left[e^{-iqz} + \frac{q-k_f}{q+k_f} e^{iqz} \right] \frac{1}{\left(\frac{z}{a} + B_1\right)^2} e^{-\beta(z-z_o)^2} dz.$$

Photocurrent from the surface state can be calculated as

$$\frac{d\sigma}{d\Omega} = \frac{k^2}{\omega} \left| I_1^s + I_2^s + I_3^s + I_4^s \right|^2 \qquad \text{(A-11)}$$

Equation (A-11) was also evaluated by numerical method.

APPENDIX II

CALCULATIONS OF PHOTOCURRENT BY USING KRONIG - PENNEY POTENTIAL MODEL

We will derive here the working formula for calculating the photocurrent from the solids using Kronig -Penney potential model as described in chapter IV. The initial state wavefunction $\psi_i(z)$ derived by using the Kronig and Penney potential can be written written as

$$\psi_i(z) = \begin{cases} (1 - iPe^{-i\delta}\sin\delta)e^{ik_i z} - (P - ie^{i\delta}\sin\delta)e^{-ik_i z}, & z<0 \\ Te^{-\varkappa z}, & z>0 \end{cases} \qquad \text{(A-14)}$$

Here,

$$P = \frac{(\varkappa - ik_i) - (k_i - i\varkappa)e^{i\delta}\sin\delta}{(\varkappa - ik_i) + (k_i - i\varkappa)e^{-i\delta}\sin\delta}$$

$$T = \frac{2k_i \sin 2\delta}{(\varkappa - ik_i) + (k_i - i\varkappa)e^{-i\delta}\sin\delta}, \qquad k_i^2 = \frac{2mE_i}{\hbar^2},$$

$$\varkappa^2 = \frac{2m}{\hbar^2}(V_o - E_i) \quad \text{and} \quad \cot\delta = -\frac{\hbar^2 k_i}{mg}.$$

The final state wavefunction $\psi_f(z)$ of Eq. (A-5) and photon field vector potential of Eq. (A-6) is used for the evaluation of the integral I in Eq. (A-1). Using Eq. (A-14), the integrals in Eq. (A-9) can be written as follows:

$$I_1 = \int_{-\infty}^{-a/2} \psi_f^* \, \tilde{A}_\omega(z) \, \frac{d\psi_i}{dz} \, dz$$

$$= -2i \left[\frac{m}{2\pi\hbar^2}\right]^{1/2} \frac{k_i q^{1/2}}{q+k_f} A_1 \Big\{ (1 - P\sin^2\delta - iP\sin\delta\cos\delta) \cdot$$

$$\frac{e^{-\alpha a/2}}{(ik_i - ik_f + \alpha)} \left[\cos(k_i - k_f)\frac{a}{2} - i\sin(k_i - k_f)\frac{a}{2}\right] -$$

$$(P + \sin^2\delta - i\sin\delta\cos\delta) \frac{e^{-\alpha a/2}}{(ik_i + ik_f - \alpha)} \left[\cos(k_i + k_f)\frac{a}{2} + \right.$$

$$\left. i\sin(k_i + k_f)\frac{a}{2}\right] \Big\}.$$

$$I_2 = \int_{-a/2}^{0} \psi_f^* \, \tilde{A}_\omega(z) \, \frac{d\psi_i}{dz} \, dz$$

$$= -2i \left(\frac{m}{2\pi\hbar^2}\right)^{1/2} \frac{A_1 \varepsilon(\omega)}{[1-\varepsilon(\omega)]} \frac{k_i q^{1/2}}{q+k_f} \left\{(1-iPe^{-i\delta}\sin\delta.\right.$$

$$\int_{-a/2}^{0} \frac{e^{\alpha z}\, e^{i(k_i-k_f)z}}{(\frac{z}{a} + B_1)}\, dz + (P-ie^{i\delta}\sin\delta).$$

$$\left.\int_{-a/2}^{0} \frac{e^{\alpha z}\, e^{-i(k_i+k_f)z}}{(\frac{z}{a} + B_1)}\, dz \right\}.$$

$$I_3 = \frac{1}{2} \int_{-a/2}^{0} \psi_f^* \frac{d\tilde{A}_\omega(z)}{dz} \psi_i \, dz$$

$$= \left(\frac{m}{2\pi\hbar^2}\right)^{1/2} \frac{A_1 \varepsilon(\omega)}{a[1-\varepsilon(\omega)]} \frac{q^{1/2}}{q+k_f} \left\{(1-iPe^{-i\delta}\sin\delta.\right.$$

$$\int_{-a/2}^{0} \frac{e^{\alpha z}\, e^{i(k_i-k_f)z}}{(\frac{z}{a} + B_1)^2}\, dz - (P-ie^{i\delta}\sin\delta).$$

$$\left.\int_{-a/2}^{0} \frac{e^{\alpha z}\, e^{-i(k_i+k_f)z}}{(\frac{z}{a} + B_1)^2}\, dz \right\}.$$

$$I_4 = \int_{0}^{a/2} \psi_f^* \tilde{A}_\omega(z) \frac{d\psi_i}{dz}\, dz$$

$$= \left(\frac{m}{2\pi\hbar^2 q}\right)^{1/2} \frac{A_1 \varepsilon(\omega)}{a[1-\varepsilon(\omega)]} T \varkappa \left\{ \int_0^{a/2} \frac{e^{-(iq+\varkappa)z}}{(\frac{z}{a} + B_1)} dz \right.$$

$$\left. + \frac{q-k_f}{q+k_f} \int_0^{a/2} \frac{e^{(iq-\varkappa)z}}{(\frac{z}{a} + B_1)} dz \right\}$$

$$I_5 = \frac{1}{2} \int_0^{a/2} \psi_f^* \frac{d\tilde{A}_\omega(z)}{dz} \psi_i \, dz$$

$$= \frac{1}{2} \left(\frac{m}{2\pi\hbar^2 q}\right)^{1/2} \frac{A_1 \varepsilon(\omega)}{a[1-\varepsilon(\omega)]} T \left\{ \int_0^{a/2} \frac{e^{-(iq+\varkappa)z}}{(\frac{z}{a} + B_1)^2} dz \right.$$

$$\left. + \frac{q-k_f}{q+k_f} \int_0^{a/2} \frac{e^{(iq-\varkappa)z}}{(\frac{z}{a} + B_1)^2} dz \right\}$$

$$I_6 = \int_{a/2}^{\infty} \psi_f^* \tilde{A}_\omega(z) \frac{d\psi_i}{dz} dz$$

$$= \left(\frac{m}{2\pi\hbar^2 q}\right)^{1/2} \varkappa T A_1 \varepsilon(\omega) \left[\frac{e^{-(iq+\varkappa)z}}{iq+\varkappa} + \frac{q-k_f}{q+k_f} \frac{e^{(iq-\varkappa)a/2}}{\varkappa - iq} \right]$$

Substituting these integrals I_1, I_2, I_3,..I_6 in Eq. (A-1), the photocurrent from the solids was calculated by numerical method as some of these integrals cannot be evaluated analytically. This was done with the help of fortran program which is given in appendix IV.

APPENDIX III

```
C       MAIN PROGRAM  FOR  PHOTOEMISSION CALCULATION  USING
C       FREE ELECTRON WAVEFUNCTIONS
        COMPLEX A1,CI,T1,T2,T3,T4,T5,T6,EPS,B1
        COMMON/WAVE/AKI,AKP,AKF,AQ,A,ALPHA,CI
        CI=(0.,1.)
        READ (1,*) NP
        READ(1,*)WP,EI,THETA,A,ALPHA,VZ,NE
        WRITE(NP,4) WP,EI,THETA,A,ALPHA,VZ
        AKI=SQRT(2.*EI)
        AKP=SQRT(2.*(VZ-EI))
        DO 99 IE=1,NE
        READ(1,*) W,EPS1,EPS2
        AKF=SQRT(2.*(EI+W))
        AQ=SQRT(2.*(EI+W-VZ))
        WRITE(NP,2) W,AKI,AKP,AKF,AQ
        EPS=CMPLX(EPS1,EPS2)
        CALL REFRAC(W,WP,THETA,EPS,A1,B1)
        CALL TERM1 (A1,T1)
        CALL TERM2 (A1,B1,EPS,T2)
        CALL TERM3 (A1,B1,EPS,T3)
        CALL TERM4 (A1,EPS,T4)
        CALL TERM5 (A1,B1,EPS,T5)
        CALL TERM6 (A1,B1,EPS,T6)
        WRITE(NP,3) W,T1,T2,T3,T4,T5,T6
        CUR=CABS(T1+T2+T3+T4+T5+T6)
        CUR=CUR*CUR
        CUR=CUR*AKF*AKF/W
        WRITE(NP,5)W,EPS,CUR
  99    CONTINUE
  2     FORMAT(3X,5(E12.4,3X))
  3     FORMAT(1X,F7.3,12(2X,E10.3))
  4     FORMAT(15X,6F12.4)
  5     FORMAT(2X,'W=',F7.4,'EPS=',2F10.4,'CURRENT=',E12.4)
        STOP
        END
```

```
C
      SUBROUTINE TERM6(A1,B1,EPS,T6)
      COMPLEX A1,R1,R2,CI,T6,EPS,B1
      COMMON/WAVE/AKI,AKP,AKF,AQ,A,ALPHA,CI
      N=101
      CALL INT6(N,R1,R2,B1)
      Q=-0.5*SQRT(AKI/AQ)/A
      T6=R1+R2*(AQ-AKF)/(AQ+AKF)
      T6=T6*Q*A1*EPS/((-AKP+CI*AKI)*(1.-EPS))
      T6=CI*T6
      RETURN
      END
C
      SUBROUTINE TERM2(A1,B1,EPS,T2)
      COMPLEX A1,R1,R2,CI,T2,EPS,B1,Q
      COMMON/WAVE/AKI,AKP,AKF,AQ,A,ALPHA,CI
      N=201
      Q=0.5*SQRT(AKI*AQ)/(AQ+AKF)
      Q=Q*EPS/(1.-EPS)
      CALL INT2(N,R1,R2,B1)
      T2=R1-R2*(CI*AKI+AKP)/(CI*AKI-AKP)
      T2=CI*A1*Q*T2*2.
      RETURN
      END
C
      SUBROUTINE TERM3(A1,B1,EPS,T3)
      COMPLEX A1,R1,R2,CI,T3,EPS,B1,Q
      COMMON/WAVE/AKI,AKP,AKF,AQ,A,ALPHA,CI
      N=201
      CALL INT3(N,R1,R2,B1)
      Q=SQRT(AKI/AQ) *AKP*EPS/(1.-EPS)
      T3=R1+R2*(AQ-AKF)/(AQ+AKF)
      T3=-Q*T3*CI
      T3=T3*A1/(-AKP+CI*AKI)
      RETURN
      END
C
```

```
      SUBROUTINE TERM5(A1,B1,EPS,T5)
      COMPLEX A1,R1,R2,CI,T5,EPS,B1,Q
      COMMON/WAVE/AKI,AKP,AKF,AQ,A,ALPHA,CI
      N=101
      CALL INT5(N,R1,R2,B1)
      Q=-0.5*SQRT(AQ/AKI)*EPS/((AQ+AKF)*(1.-EPS))
      T5=R1+R2*(AKI*CI+AKP)/(CI*AKI-AKP)
      T5=T5*Q*A1/A
      RETURN
      END
C
      SUBROUTINE TERM1(A1,T1)
      COMPLEX A1,T1,C1,C2,CI
      COMMON/WAVE/AKI,AKP,AKF,AQ,A,ALPHA,CI
      Q=SQRT(AKI*AQ)
      Q=0.5*Q/(AQ+AKF)
      AH=0.5*A
      AH=AH*(AKI-AKF)
      C1=COS(AH)-CI*SIN(AH)
      C1=C1*EXP(-0.5*ALPHA*A)/(ALPHA+CI*(AKI-AKF))
      AG=0.5*(AKI+AKF)*A
      C2=COS(AG)+CI*SIN(AG)
      C2=C2*(CI*AKI+AKP)/(CI*AKI-AKP)
      C2=C2*EXP(-0.5*ALPHA*A)/(ALPHA-CI*(AKI+AKF))
      T1=2.*CI*A1*Q*(C1-C2)
      RETURN
      END
C
      SUBROUTINE REFRAC(W,WP,THETA,EPS,A1,B1)
      COMPLEX A1,CX,CSQRT,CMPLX,EPS,B1
      S2=SIN(2.*THETA)
      S1=SIN(THETA)
      C1=COS(THETA)
C     EPS=1.-(WP/W)**2
      B1=0.5*(1.+EPS)/(1.-EPS)
      CX=EPS-S1*S1
      CX=CSQRT(CX)
      A1=-S2/(CX+EPS*C1)
      RETURN
      END
```

```
C
      SUBROUTINE INT2(N,R1,R2,B1)
      COMPLEX R1,R2,CI,CMPLX,Z1,Z2,B1
      COMMON/WAVE/AKI,AKP,AKF,AQ,A,ALPHA,CI
      R1=CMPLX(0.,0.)
      R2=CMPLX(0.,0.)
      D=0.5*A/FLOAT(N-1)
      X=-0.5*A
      I=0
    2 I=I+1
      IF (I.GT.N)GO TO 10
      E=EXP(ALPHA*X)
      Z1=(COS((AKI-AKF)*X)+CI*SIN((AKI-AKF)*X))/(B1+X/A)
      Z2=(COS((AKI+AKF)*X)-CI*SIN((AKI+AKF)*X))/(B1+X/A)
      Z1=E*Z1
      Z2=E*Z2
      R1=R1+Z1
      R2=R2+Z1
      IF (I.EQ.1) R1=R1-0.5*Z1
      IF(I.EQ.N) R1=R1-0.5*Z1
      IF(I.EQ.1) R2=R2-0.5*Z2
      IF(I.EQ.N) R2=R2-0.5*Z2
      X=X+D
      GO TO 2
   10 R1=R1*D
      R2=R2*D
      RETURN
      END
C
      SUBROUTINE TERM4(A1,EPS,T4)
      COMPLEX A1,R1,R2,CI,T4,EPS,Q
      COMMON/WAVE/AKI,AKP,AKF,AQ,A,ALPHA,CI
      Q=SQRT(AKI/AQ)*AKP*EPS
      R1=EXP(-0.5*AKP*A)*(COS(0.5*AQ*A)-CI*SIN(0.5*AQ*A))
      R1=R1/(AKP+CI*AQ)
      R2=EXP(-0.5*AKP*A)*(COS(0.5*AQ*A)+CI*SIN(0.5*AQ*A))
      R2=R2*(AQ-AKF)/((AQ+AKF)*(AKP-CI*AQ))
      T4=CI*Q*A1*(R1+R2)/(-AKP+CI*AKI)
      T4=-T4
      RETURN
      END
C
```

```
      SUBROUTINE INT3(N,R1,R2,B1)
      COMPLEX R1,R2,CI,CMPLX,Z1,Z2,B1
      COMMON/WAVE/AKI,AKP,AKF,AQ,A,ALPHA,CI
      R1=CMPLX(0.,0.)
      R2=CMPLX(0.,0.)
      D=0.5*A/FLOAT(N-1)
      X=0.0
      I=0
    2 I=I+1
      IF(I.GT.N) GO TO 10
      Z1=EXP(-AKP*X)*(COS(AQ*X)-CI*SIN(AQ*X))/(B1+X/A)
      Z2=EXP(-AKP*X)*(COS(AQ*X)+CI*SIN(AQ*X))/(B1+X/A)
      R1=R1+Z1
      R2=R2+Z2
      IF (I.EQ.1)R1=R1-0.5*Z1
      IF(I.EQ.N) R1=R1-0.5*Z1
      IF(I.EQ.N)R2=R1-0.5*Z2
      IF(I.EQ.N) R2=R2-0.5*Z2
      X=X+D
      GO TO 2
   10 R1=R1*D
      R2=R2*D
      RETURN
      END
C
```

```
      SUBROUTINE INT6(N,R1,R2,B1)
      COMPLEX R1,R2,CI,CMPLX,Z1,Z2,B1,B
      COMMON/WAVE/AKI,AKP,AKF,AQ,A,ALPHA,CI
      R1=CMPLX(0.,0.)
      R2=CMPLX(0.,0.)
      D=0.5*A/FLOAT(N-1)
      X=0.0
      I=0
    2 I=I+1
      IF (I.GT.N) GO TO 10
      C=COS(AQ*X)
      S=SIN(AQ*X)
      E=EXP(-AKP*X)
      B=(B1+X/A)**2
      Z1=E*(C-CI*S)/B
      Z2=E*(C+CI*S)/B
      R1=R1+Z1
      R2=R2+Z2
      IF (I.EQ.1) R1=R1-0.5*Z1
      IF (I.EQ.N) R1=R1-0.5*Z1
      IF((I.EQ.1).OR.(I.EQ.N))R2=R2-0.5*Z2
      X=X+D
      GO TO 2
   10 R1=R1*D
      R2=R2*D
      RETURN
      END
C
```

```
      SUBROUTINE INT5(N,R1,R2,B1)
      COMPLEX R1,R2,CMPLX,Z1,Z2,CI,B1
      COMMON/WAVE/AKI,AKP,AKF,AQ,A,ALPHA,CI
      R1=CMPLX(0.,0.)
      R2=CMPLX(0.,0.)
      D=0.5*A/FLOAT(N-1)
      X=-0.5*A
      I=0
    2 I=I+1
      IF(I.GT.N) GO TO 10
      C=COS((AKI-AKF)*X)
      S=SIN((AKI-AKF)*X)
      CP=COS((AKI+AKF)*X)
      SP=SIN((AKI+AKF)*X)
      E=EXP(ALPHA*X)
      Z1=(C+CI*S)/((B1+X/A)**2)
      Z2=(CP-CI*SP)/((B1+X/A)**2)
      Z1=E*Z1
      Z2=E*Z2
      R1=R1+Z1
      R2=R2+Z2
      IF((I.EQ.1).OR.(I.EQ.N)) R1=R1-0.5*Z1
      IF((I.EQ.1).OR.(I.EQ.N)) R2=R2-0.5*Z2
      X=X+D
      GO TO 2
   10 R1=R1*D
      R2=R2*D
      RETURN
      END
```

APPENDIX IV

```
C       MAIN PROGRAM FOR PHOTOEMISSION CALCULATIONS USING
C       KRONIG-PENNEY MODEL POTENTIAL
C       THIS PROGRAM HAS THE SURFACE THICKNESS Z=-A/2 TO +A/2
        COMPLEX AQ,AKP,EPS
        COMPLEX A1,CI,T1,T2,T3,T4,T5,T6,B1,ASP,AST,SP1,SP2,SPA,SPB
        COMMON AKI,AKP,AKF,AQ,AG,A,ALPHA,CI,DELTA,ASP
        CI = (0.,1.)
        READ (1,*) NP
C       WRITE (1,*) 'WP,EI,THETA,A,ALPHA,DELTA,AG,VZ,NE'
        READ (1,*) WP,EI,THETA,A,ALPHA,VZ,DELTA,AG,NE
C       READ (1,*) W,EPS1,EPS2
        WRITE (NP,2) WP,EI,THETA,A,ALPHA,VZ,DELTA,AG,NE
        AKI = SQRT(2.*EI)
        AKP = SQRT(2.*(VZ-EI))
        SP1 = AKP-CI*AKI
        SP2 = AKI-CI*AKP
        SPA = (COS(DELTA)+CI*SIN(DELTA))*SIN(DELTA)
        SPB = (COS(DELTA)-CI*SIN(DELTA))*SIN(DELTA)
        ASP = (SP1-SP2*SPA)/(SP1+SP2*SPB)
        AST = 2.*AKI*SIN(2.*DELTA)/(SP1+SP2*SPB)
        DO 90 IE=1,NE
C       WRITE (1,*) 'W,EPS1,EPS2'
        READ (1,*) W,EPS1,EPS2
        AKF = SQRT(2.*(EI+W))
        AQ = SQRT(2.*(EI+W-VZ))
        WRITE (NP,3) W,AKI,AKF,AG,DELTA,AKP,ASP,AST,AQ
        EPS = CMPLX (EPS1,EPS2)
        CALL REFRAC (W,WP,THETA,EPS,A1,B1)
        CALL TERM1 (A1,B1,APA,APB,EPS,T1)
        CALL TERM2 (A1,B1,EPS,T2)
        CALL TERM3 (A1,B1,EPS,T3)
        CALL TERM4 (A1,B1,EPS,AST,T4)
        CALL TERM5 (A1,B1,EPS,T5)
        CALL TERM6 (A1,B1,EPS,T6)
        WRITE (NP,4) W,T1,T2,T3,T4,T5,T6
        XINT= CABS(T1+T2+T3+T4+T5+T6)
        XCUR= XINT*XINT
        CUR= (XCUR*AKF*AKF)/W
        WRITE (NP,5) W,EPS,CUR
   90   CONTINUE
    3   FORMAT (1X,5(2X,F6.4), 8(E9.2,2X))
    4   FORMAT (1X,F7.3,12(2X,E10.3))
    2   FORMAT (2X,8F9.4,I4)
    5   FORMAT (2X,'W=',F7.4,3X,'EPS=',2F10.4,5X,'CURRENT='E12.4)
C       WRITE (NP,*) R.K.THAPA, P. U. COLLEGE, AIZAWL, MIZORAM
        STOP
        END

C
```

```
      SUBROUTINE TERM1 (A1,B1,APA,APB,EPS,T1)
      COMPLEX A1,T1,C1,C2,CI,ASP,AST,SPA,SPB,APA,APB,Q,AQ,AKP,EPS
      COMMON AKI,AKP,AKF,AQ,AG,A,ALPHA,CI,DELTA,ASP
      Q = AKI*(SQRT(AQ))
      Q = Q/(AQ+AKF)
      AH = 0.5*(AKI-AKF)*A
      APA = 1.-ASP*(SIN(DELTA))**2 -CI*ASP*SIN(DELTA)*COS(DELTA)
      C1 = APA*(COS(AH)-CI* SIN(AH))
      C1 = C1*EXP(-0.5*ALPHA*A)/(CI*(AKI-AKF)+ALPHA)
      AD = 0.5*(AKI+AKF)*A
      APB = ASP+(SIN(DELTA))**2 -CI*(SIN(DELTA)*COS(DELTA))
      C2 = APB * (COS(AD)+CI*SIN(AD))
      C2 = C2*EXP(-0.5*ALPHA*A)/(CI*(AKI+AKF)-ALPHA)
      T1 =-2.*CI*A1*Q*(C1-C2)
C     WRITE (6,91)AG,A,T1
C91   FORMAT(2X,'TERM1 COMPUTED',2F10.2,2E14.4,/)
      RETURN
      END

C

      SUBROUTINE TERM2(A1,B1,EPS,T2)
      COMPLEX A1,R1,R2,CI,T2,EPS,B1,Q,ASP,SPA,SPB,APA,APB,AQ,AKP
      COMMON AKI,AKP,AKF,AQ,AG,A,ALPHA,CI,DELTA,ASP
      N=201
      Q = -AKI*(SQRT(AQ))/(AQ+AKF)
      Q = Q*EPS/(1.-EPS)
      APA = 1.- ASP*(SIN(DELTA))**2 - CI*ASP*SIN(DELTA)*COS(DELTA)
      APB = ASP + (SIN(DELTA))**2 -CI*(SIN(DELTA)*COS(DELTA))
      CALL INT2 (N,R1,R2,B1)
      T2 = R1 *APA-R2*APB
      T2 = CI*A1*Q*T2*2.
C     WRITE (6,91)AG
C 91  FORMAT(3X,'TERM2 COMPUTED',F10.2,/)
      RETURN
      END
```

```
C
      SUBROUTINE INT2 (N,R1,R2,B1)
      COMPLEX R1,R2,CI,CMPLX,Z1,Z2,B1,AQ,AKP,EPS
      COMMON AKI,AKP,AKF,AQ,AG,A,ALPHA,CI,DELTA,ASP
      R1 = CMPLX (0.,0.)
      R2 = CMPLX (0.,0.)
      D = 0.5*A/FLOAT(N-1)
      X = -0.5*A
      I = 0
    2 I = I+1
      IF (I.GT.N) GO TO 10
      E = EXP(ALPHA*X)
      Z1 = (COS(AKI-AKF)*X + CI* SIN(AKI-AKF)*X)/(B1+X/A)
      Z2 = (COS(AKI-AKF)*X - CI* SIN(AKI-AKF)*X)/(B1+X/A)
      Z1 = E*Z1
      Z2 = E*Z2
      R1 = R1+Z1
      R2 = R2+Z2
      IF (I.EQ.1) R1 = R1-0.5*Z1
      IF (I.EQ.N) R1 = R1-0.5*Z1
      IF (I.EQ.1) R2 = R2-0.5*Z2
      IF (I.EQ.N) R2 = R2-0.5*Z2
      X = X+D
      GO TO 2
   10 R1=R1*D
C     WRITE(6,91)AG
C91   FORMAT(4X,'INTEGRAL-2 COMPUTED',F10.2,/)
      RETURN
      END

C

      SUBROUTINE TERM3 (A1,B1,EPS,T3)
      COMPLEX A1,R1,R2,CI,T3,B1,EPS,APA,APB,Q,AQ,AKP
      COMMON AKI,AKP,AKF,AQ,AG,A,ALPHA,CI,DELTA,ASP
      N = 201
      CALL INT3 (N,R1,R2,B1)
      Q =  (SQRT(AQ)*EPS)/((AQ+AKF)*(1.-EPS))*A
      APA = 1. -ASP*(SIN(DELTA))**2 -CI*ASP*SIN(DELTA)*COS(DELTA)
      APB = ASP + (SIN(DELTA))**2 -CI*(SIN(DELTA)*COS(DELTA))
      T3 =R1*APA - R2*APB
      T3 =T3*Q*A1
C     WRITE (6,91)AG
C 91  FORMAT(5X,'TERM3 COMPUTED',F10.2,/)
      RETURN
      END
```

```
C
      SUBROUTINE INT3 (N,R1,R2,B1)
      COMPLEX R1,R2,CMPLX,Z1,Z2,B1,EPS,APA,APB,CI,AQ,AKP
      COMMON AKI,AKP,AKF,AQ,AG,A,ALPHA,CI,DELTA,ASP
      R1 = CMPLX(0.,0.)
      R2 = CMPLX(0.,0.)
      D = 0.5*A/FLOAT(N-1)
      X=-0.5*A
      I=0
    2 I=I+1
      IF (I.GT.N) GO TO 10
      C = COS(AKI-AKF)*X
      S = SIN(AKI-AKF)*X
      CP=COS(AKI+AKF)*X
      SP=SIN(AKI+AKF)*X
      E=EXP(ALPHA*X)
      Z1=(C+CI*S)/((B1+X/A)**2.)
      Z2=(CP-CI*SP)/((B1+X/A)**2.)
      Z1=E*Z1
      Z2=E*Z2
      R1=R1+Z1
      R2=R2+Z2
      IF (I.EQ.1) R1=R1-0.5*Z1
      IF (I.EQ.N) R1=R1-0.5*Z1
      IF (I.EQ.1) R2=R2-0.5*Z2
      IF (I.EQ.N) R2=R2-0.5*Z2
      X=X+D
      GO TO 2
   10 R1=R1*D
      R2=R2*D
C     WRITE (6,91)AG
C91   FORMAT(6X,'INTEGRAL-3 COMPUTED',F10.2,/)
      RETURN
      END

C

      SUBROUTINE REFRAC (W,WP,THETA,EPS,A1,B1)
      COMPLEX A1,CX,CSQRT,EPS,B1,CMPLX
      S2=SIN (2.*THETA)
      S1=SIN(THETA)
      C1=COS(THETA)
C     EPS=1.-(WP/W)**2.
      B1=0.5*(1.+EPS)/(1.-EPS)
      CX=EPS-S1*S1
      CX=CSQRT(CX)
      A1=-S2/(CX+EPS*C1)
      RETURN
      END
```

```
C
      SUBROUTINE TERM4 (A1,B1,EPS,AST,T4)
      COMPLEX A1,R1,R2,T4,EPS,B1,Q,AQ,AKP
      COMMON AKI,AKP,AKF,AQ,AG,A,ALPHA,CI,DELTA,ASP
      N=201
      CALL INT4(N,R1,R2,B1)
      Q=(AKP*AST*EPS)/(SQRT(AQ)*(1.-EPS))
      T4=R1+R2*(AQ-AKF)/(AQ+AKF)
      T4=-Q*T4*A1
      RETURN
      END

C
      SUBROUTINE INT4(N,R1,R2,B1)
      COMPLEX R1,R2,CI,CMPLX,Z1,Z2,B1,AQ,AKP,EPS
      COMMON AKI,AKP,AKF,AQ,AG,A,ALPHA,CI,DELTA,ASP
      R1=CMPLX(0.,0.)
      R2=CMPLX(0.,0.)
      D =0.5*A/FLOAT(N-1)
      X=0.0
      I=0
    2 I=I+1
      IF (I.GT.N) GO TO 10
      Z1=EXP(-AKP*X)*(COS(AQ*X)-CI*SIN(AQ*X))/(B1+X/A)
      Z2=EXP(-AKP*X)*(COS(AQ*X)+CI*SIN(AQ*X))/(B1+X/A)
      R1=R1+Z1
      R2=R2+Z2
      IF (I.EQ.1)R1=R1-0.5*Z1
      IF (I.EQ.N)R1=R1-0.5*Z1
      IF (I.EQ.1)R2=R2-0.5*Z2
      IF (I.EQ.N)R2=R2-0.5*Z2
      X=X+D
      GO TO 2
   10 R1=R1*D
      R2=R2*D
      RETURN
      END

C
      SUBROUTINE TERM5(A1,B1,EPS,T5)
      COMPLEX A1,R1,R2,CI,T5,EPS,B1,AQ,AST,AKP
      COMMON AKI,AKP,AKF,AQ,AG,A,ALPHA,CI,DELTA,ASP
      N=201
      CALL INT5(N,R1,R2,B1)
      Q=(0.5*AST*EPS)/(A*(1.-EPS)*SQRT(AQ))
      T5=R1+R2*(AQ-AKF)/(AQ+AKF)
      T5=T5*Q*A1
      RETURN
      END
```

```
C
      SUBROUTINE INT5(N,R1,R2,B1)
      COMPLEX R1,R2,CI,CMPLX,Z1,Z2,B1,B,AQ,AKP,EPS
      COMMON AKI,AKP,AKF,AQ,AG,A,ALPHA,CI,DELTA,ASP
      R1=CMPLX(0.,0.)
      R2=CMPLX(0.,0.)
      D=0.5*A/FLOAT(N-1)
      X=0.0
      I=0
    2 I=I+1
      IF(I.GT.N) GO TO 10
      C=COS(AQ*X)
      S=SIN(AQ*X)
      E=EXP(-AKP*X)
      B=(B1+X/A)**2
      Z1=E*(C-CI*S)/B
      Z2=E*(C+CI*S)/B
      R1=R1+Z1
      R2=R2+Z2
      IF(I.EQ.1) R1=R1-0.5*Z1
      IF(I.EQ.N) R1=R1-0.5*Z1
      IF(I.EQ.1) R2=R2-0.5*Z2
      IF(I.EQ.N) R2=R2-0.5*Z2
      X=X+D
      GO TO 2
   10 R1=R1*D
      R2=R2*D
      RETURN
      END

C
      SUBROUTINE TERM6(A1,B1,EPS,T6)
      COMPLEX A1,R1,R2,CI,T6,EPS,Q,AQ,AKP
      COMMON AKI,AKP,AKF,AQ,AG,A,ALPHA,CI,DELTA,ASP
      Q= (AKP*AST*EPS)/(SQRT(AQ))
      R1=EXP(-0.5*AKP*A)*(COS(0.5*AQ*A)-CI*SIN(0.5*AQ*A))
      R1=R1/(AKP+CI*AQ)
      R2=EXP(-0.5*AKP*A)*(COS(0.5*AQ*A)+CI*SIN(0.5*AQ*A))
      R2=R2*(AQ-AKF)/(AQ+AKF)
      T6=Q*A1*(R1+R2)
      RETURN
      END
```